

**Development and Evaluation of a Data Acquisition Camera
Technique to Measure Opening Loads Caused by Plasticity-Induced
Crack Closure during Fatigue Crack Growth**

A Thesis

Presented in Partial Fulfillment of the Requirements for the

Degree of Master of Science

with a

Major in Mechanical Engineering

in the

College of Graduate Studies

University of Idaho

by

Jacob S. Middleton

Major Professor: Gabriel Potirniche, Ph.D.

Committee Members: Robert Stephens, Ph.D.; Vibhav Durgesh, Ph.D.; Michael Maughan, Ph.D.

Department Administrator: Gabriel Potirniche, Ph.D.

August 2020

Authorization to Submit Thesis

This thesis of Jacob S. Middleton, submitted for the degree of Master of Science with a Major in Mechanical Engineering and titled "Development and Evaluation of a Data Acquisition Camera Technique to Measure Opening Loads Caused by Plasticity-Induced Crack Closure during Fatigue Crack Growth," has been reviewed in final form. Permission, as indicated by the signatures and dates below, is now granted to submit final copies to the College of Graduate Studies for approval.

Major Professor: _____ Date: _____
Gabriel Potirniche, Ph.D.

Committee Members: _____ Date: _____
Robert Stephens, Ph.D.

_____ Date: _____
Vibhav Durgesh, Ph.D.

_____ Date: _____
Michael Maughan, Ph.D.

Department

Administrator: _____ Date: _____
Gabriel Potirniche, Ph.D.

Abstract

This document describes the experimental approach used to identify crack-tip opening loads due to the plasticity-induced crack closure under fatigue loading conditions using a data acquisition camera (DAC) and DaVis, an advanced data analysis software. The primary pieces of equipment used in the experimental work are as follows: (1) a loading frame, which uses hydraulics to supply and control a cycling load applied to a compact tension (CT) specimen, (2) the DAC itself, set up on a stable tripod to collect the images required for specimen analysis by this method, and (3) a computer equipped with the DaVis software, used to analyze and process the images collected by the DAC. The DAC was used to collect images of the crack closing and opening during fatigue loading. The goal was to determine the exact instant of crack-tip opening during loading and unloading. Images were collected in series for each applied cycle, with separate data sets collected for the loading and unloading portion of each cycle. Data was collected at three ΔK levels, i.e., 10, 15, and 20 MPa $\cdot\sqrt{m}$, to identify changes in opening load as the crack increased in length. Using the DaVis software, the images collected were used to compute crack opening displacements, from which it could be determined whether or not the crack was open or closed at a given point in the cycle. As expected, the data collected indicated that opening load changes with increasing ΔK value. The computed opening load values were consistent with those computed using other methods, as will be laid out in this paper.

Acknowledgements

I would like to acknowledge the following people for their help and encouragement on this project:

Dr. Gabriel Potirniche, for advising and guidance in the execution of this project, and for insight into research methods

Dr. Robert Stephens, for guidance in the experimental approach and lab work

Dr. Vibhav Durgesh, for guidance in the use of the DAC and analysis software

Mr. Rodrigo Padilla, for help in acquiring the data displayed in this thesis, and support with the software

Mr. Colin Burkhalter, for insight and help with the machinery in the lab, and with initial specimen analysis

Table of Contents

Authorization to Submit Thesis	ii
Abstract.....	iii
Acknowledgements	iv
Table of Contents.....	v
List of Tables	vii
List of Figures	viii
Chapter 1. Introduction	1
Chapter 2. Background	4
2.1 Mathematical Background and ASTM Standards	4
2.2 Existing Work	6
2.3 Advancements	7
Chapter 3. Methods.....	8
3.1 Specimen	8
3.2 Test Matrix.....	8
3.3 Data Collection.....	9
3.3.1 DAC Settings and Photograph Approach	9
3.3.2 Camera and Specimen Setup.....	9
3.3.3 Data Analysis.....	11
Chapter 4. Results.....	16
4.1 $\Delta K=10$ MPa $\sqrt{\text{m}}$	16
4.1.1 Cycle 1.....	16
4.1.2 Cycle 2.....	23
4.1.3 Cycle 3.....	30
4.2 $\Delta K=15$ MPa $\sqrt{\text{m}}$	37
4.2.1 Cycle 1.....	37
4.2.2 Cycle 2.....	44
4.2.3 Cycle 3.....	51
4.3 $\Delta K=20$ MPa $\sqrt{\text{m}}$	58
4.3.1 Cycle 1.....	58
4.3.2 Cycle 2.....	65
4.3.3 Cycle 3.....	72
Chapter 5. Analysis & Verification	79

5.1 Compliance Curves	79
5.2 Method Comparison	82
Chapter 6. Discussion.....	86
Chapter 7. Conclusion.....	89
References	91

List of Tables

Table 1.1: Nippon Steel Alloy 709 Chemical Composition.....	2
Table 1.2: Nippon Steel Alloy 709 Tensile Properties at Room Temperature	2
Table 1.3: Nippon Steel Alloy 709 Coefficient of Linear Thermal Expansion.....	2
Table 1.4: Nippon Steel Alloy 709 Modulus of Elasticity (GPa).....	2
Table 3.1: Specimen Dimensions.....	8
Table 3.2: Selected Specimen Information.....	8
Table 3.3: Test Matrix.....	8
Table 5.1: Identified Opening Loads and Average Opening Loads for all Data Sets at each ΔK Level and for each Loading Cycle.....	79

List of Figures

Figure 2.1: ASTM standard diagram of a CT specimen.....	4
Figure 2.2: Representation of opening and effective K values.....	6
Figure 2.3: Back face strain gage application.....	6
Figure 3.1: Photograph of the DAC used in this project.....	10
Figure 3.2: Basic specimen setup and area of interest diagram.....	11
Figure 3.3: Base image of the region of interest with the notch and crack line.....	12
Figure 3.4: Base image, with contrast activated in DaVis software.....	13
Figure 3.5: An image from the $\Delta K=10$ MPa $\cdot\sqrt{m}$, with the refined displacement observation method in effect.....	14
Figure 4.1: Series of colored images showing progression of $\Delta K=10$ MPa $\cdot\sqrt{m}$ Cycle 1 from minimum to maximum load.....	19
Figure 4.2: Half of the crack opening displacement (COD) evolution during the loading in cycle 1, $\Delta K=10$ MPa $\cdot\sqrt{m}$	20
Figure 4.3: Crack tip focus for approximate opening load range identification, $\Delta K=10$ MPa $\cdot\sqrt{m}$, Cycle 1.....	21
Figure 4.4: Variation of the crack tip opening displacement as a function of applied load during cycle 1, $\Delta K=10$ MPa $\cdot\sqrt{m}$	22
Figure 4.5: Series of colored images showing progression of $\Delta K=10$ MPa $\cdot\sqrt{m}$ Cycle 2 from minimum to maximum load.....	26
Figure 4.6: Half of the crack opening displacement (COD) evolution during the loading in cycle 2, $\Delta K=10$ MPa $\cdot\sqrt{m}$	27
Figure 4.7: Crack tip focus for approximate opening load range identification, $\Delta K=10$ MPa $\cdot\sqrt{m}$, Cycle 2.....	28
Figure 4.8: Variation of the crack tip opening displacement as a function of applied load during cycle 2, $\Delta K=10$ MPa $\cdot\sqrt{m}$	29

Figure 4.9: Series of colored images showing progression of $\Delta K=10$ MPa $\cdot\sqrt{m}$ Cycle 3 from minimum to maximum load.....	33
Figure 4.10: Half of the crack opening displacement (COD) evolution during the loading in cycle 3, $\Delta K=10$ MPa $\cdot\sqrt{m}$	34
Figure 4.11: Crack tip focus for approximate opening load range identification, $\Delta K=10$ MPa $\cdot\sqrt{m}$, Cycle 3.....	35
Figure 4.12: Variation of the crack tip opening displacement as a function of applied load during cycle 3, $\Delta K=10$ MPa $\cdot\sqrt{m}$	36
Figure 4.13: Series of colored images showing progression of $\Delta K=15$ MPa $\cdot\sqrt{m}$ Cycle 1 from minimum to maximum load.....	40
Figure 4.14: Half of the crack opening displacement (COD) evolution during the loading in cycle 1, $\Delta K=15$ MPa $\cdot\sqrt{m}$	41
Figure 4.15: Crack tip focus for approximate opening load range identification, $\Delta K=15$ MPa $\cdot\sqrt{m}$, Cycle 1.....	42
Figure 4.16: Variation of the crack tip opening displacement as a function of applied load during cycle 1, $\Delta K=15$ MPa $\cdot\sqrt{m}$	43
Figure 4.17: Series of colored images showing progression of $\Delta K=15$ MPa $\cdot\sqrt{m}$ Cycle 2 from minimum to maximum load.....	47
Figure 4.18: Half of the crack opening displacement (COD) evolution during the loading in cycle 2, $\Delta K=15$ MPa $\cdot\sqrt{m}$	48
Figure 4.19: Crack tip focus for approximate opening load range identification, $\Delta K=15$ MPa $\cdot\sqrt{m}$, Cycle 2.....	49
Figure 4.20: Variation of the crack tip opening displacement as a function of applied load during cycle 2, $\Delta K=15$ MPa $\cdot\sqrt{m}$	50
Figure 4.21: Series of colored images showing progression of $\Delta K=15$ MPa $\cdot\sqrt{m}$ Cycle 3 from minimum to maximum load.....	54

Figure 4.22: Half of the crack opening displacement (COD) evolution during the loading in cycle 3, $\Delta K=15 \text{ MPa}\cdot\sqrt{\text{m}}$	55
Figure 4.23: Crack tip focus for approximate opening load range identification, $\Delta K=15 \text{ MPa}\cdot\sqrt{\text{m}}$, Cycle 3.....	56
Figure 4.24: Variation of the crack tip opening displacement as a function of applied load during cycle 3, $\Delta K=15 \text{ MPa}\cdot\sqrt{\text{m}}$	57
Figure 4.25: Series of colored images showing progression of $\Delta K=20 \text{ MPa}\cdot\sqrt{\text{m}}$ Cycle 1 from minimum to maximum load.....	61
Figure 4.26: Half of the crack opening displacement (COD) evolution during the loading in cycle 1, $\Delta K=20 \text{ MPa}\cdot\sqrt{\text{m}}$	62
Figure 4.27: Crack tip focus for approximate opening load range identification, $\Delta K=20 \text{ MPa}\cdot\sqrt{\text{m}}$, Cycle 1.....	63
Figure 4.28: Variation of the crack tip opening displacement as a function of applied load during cycle 1, $\Delta K=20 \text{ MPa}\cdot\sqrt{\text{m}}$	64
Figure 4.29: Series of colored images showing progression of $\Delta K=20 \text{ MPa}\cdot\sqrt{\text{m}}$ Cycle 2 from minimum to maximum load.....	68
Figure 4.30: Half of the crack opening displacement (COD) evolution during the loading in cycle 2, $\Delta K=20 \text{ MPa}\cdot\sqrt{\text{m}}$	69
Figure 4.31: Crack tip focus for approximate opening load range identification, $\Delta K=20 \text{ MPa}\cdot\sqrt{\text{m}}$, Cycle 2.....	70
Figure 4.32: Variation of the crack tip opening displacement as a function of applied load during cycle 2, $\Delta K=20 \text{ MPa}\cdot\sqrt{\text{m}}$	71
Figure 4.33: Series of colored images showing progression of $\Delta K=20 \text{ MPa}\cdot\sqrt{\text{m}}$ Cycle 3 from minimum to maximum load.....	75
Figure 4.34: Half of the crack opening displacement (COD) evolution during the loading in cycle 3, $\Delta K=20 \text{ MPa}\cdot\sqrt{\text{m}}$	76

Figure 4.35: Crack tip focus for approximate opening load range identification, $\Delta K=20 \text{ MPa}\cdot\sqrt{\text{m}}$, Cycle 3.....	77
Figure 4.36: Variation of the crack tip opening displacement as a function of applied load during cycle 3, $\Delta K=20 \text{ MPa}\cdot\sqrt{\text{m}}$	78
Figure 5.1: Load-displacement compliance curve measured at the load line using a clip gage for $\Delta K = 10 \text{ MPa}\cdot\sqrt{\text{m}}$	80
Figure 5.2: Load-displacement compliance curve measured at the load line using a clip gage for $\Delta K = 15 \text{ MPa}\cdot\sqrt{\text{m}}$	81
Figure 5.3: Load-displacement compliance curve measured at the load line using a clip gage for $\Delta K = 20 \text{ MPa}\cdot\sqrt{\text{m}}$	82
Figure 5.4: Comparison of the compliance curves obtained from the analytical, clip gage, and DAC COD methods for $\Delta K=15 \text{ MPa}\cdot\sqrt{\text{m}}$	84
Figure 5.5: Comparison of the compliance curves obtained from the analytical, clip gage, and DAC COD methods for $\Delta K=20 \text{ MPa}\cdot\sqrt{\text{m}}$	85

Chapter 1. Introduction

A data acquisition camera, or DAC, is an advanced instrument capable of recording data rapidly and with high resolution. This allows for high precision analysis of a variety of processes, in which minute changes to the subject can be observed, based on the settings and capability of the camera. Non-intrusive methods such as DAC techniques will aid in crack growth measurement in hostile environments, as will be the case in future work using this method with the material in question in this project, the Ni-Cr austenitic stainless steel known as Alloy 709.

Data acquisition cameras have been in use for a very long time and for a variety of purposes. One particularly noteworthy earlier use of the technology was on the Apollo 11 mission, in which two data acquisition cameras were sent on the mission for data collection, and one of them was used to record Neil Armstrong on the moon [1]. Another example of use for DAC technology is in biomechanics. The cameras in this application are reinforced and placed in crash sleds for data collection [2]. Interestingly, DAC technology has also been used for automotive research, in traffic tracking applications [3]. Data acquisition cameras also find use in Particle Image Velocimetry (PIV). In this process, particles are inserted into a flow of fluid to be studied, and the cameras are used to study the fluid by tracking and recording the trajectories of the particles within it [4]. The use of cameras to track points in a fluid flow data set is similar to how they were used in this project to track the motion of individual points on the surface of fracture specimens, using Digital Image Correlation (DIC), which will be discussed later.

The compact tension specimens used in this study were made of Alloy 709. Alloy 709 (Fe-25Ni-20Cr based austenitic steel), developed as NF709 by Nippon Steel in Tokyo, Japan, is a high performance steel used in structural applications at high temperatures in sodium-cooled fast reactors (SFR). The material is stabilized with an austenitic structure, the close packed nature of which improves its ability to resist creep, as opposed to the more loosely packed BCC ferritic phase [5]. Austenitic stainless steels are known to be capable of exhibiting, at high temperatures and prolonged times, enhanced oxidation and corrosion resistance (due to the high chromium content), creep strength, stability (due to the high nickel content), sodium compatibility, and weldability [6].

In the downselection process by which the Department of Energy (DOE) arrived at Alloy 709 as a material of interest for this application, its creep properties in particular were noted, as well as

oxidation resistance and good weldability. A DOE document also noted that the material exhibits solution hardening and precipitate hardening as strengthening mechanisms [7].

The datasheet from Nippon Steel outlines a selection of properties for Alloy 709, as shown in the tables below [8].

Table 1.1: Nippon Steel Alloy 709 Chemical Composition [8]
[Mass %]

Specification	C	Si	Mn	P	S	Cr	Ni	Nb	N	W	V
Vb TÜV 554/2 09.2009	-	-	-	-	-	17.0	8.00	0.25	0.10	1.50	0.20
	0.05	1.00	2.00	0.040	0.030	20.0	11.0	0.50	0.25	2.60	0.50
TP347W	-	-	-	-	-	17.0	8.00	0.25	0.10	1.50	0.20
	0.05	1.00	2.00	0.040	0.030	20.0	11.0	0.50	0.25	2.60	0.50

Table 1.2: Nippon Steel Alloy 709 Tensile Properties at Room Temperature [8]

Specification	Proof stress [MPa]		Tensile strength [MPa]	Elongation [%]
	0.2%	1.0%		
Vb TÜV 563/2 09.2009	≥270	-	≥640	≥30
TP31MoCbN	≥270	-	≥640	≥30

Table 1.3: Nippon Steel Alloy 709 Coefficient of Linear Thermal Expansion [8]

R.T.-300	R.T.-400	R.T.-500	R.T.-600	R.T.-700	R.T.-800
16.8	17.1	17.4	17.6	18.0	18.5

Table 1.4: Nippon Steel Alloy 709 Modulus of Elasticity (GPa) [8]

Temperature (°C)	R.T.	100	200	300	400	500	600	700	800
	193.1	118.0	181.1	176.5	169.6	162.7	155.8	148.9	140.1

Alloy 709 is of particular interest in sodium-cooled fast reactors. Sodium-fueled fast reactors are considered to be Generation IV reactors, a group of designs formed to attempt to overcome challenges centered around conservation, safety, and economics [9]. The technology is still very much in development, and that includes identifying and studying ideal structural materials, such as Alloy 709. Scientists in South Korea are seeking to develop and implement a prototype SFR by 2028 to reduce the amount of waste produced by their power system, which currently includes a number

of nuclear reactors of less than ideal efficiency when it comes to waste production [10]. In an SFR, structural materials will be exposed to elevated temperatures, severely corrosive environments and enhanced levels of radiation, all of which are extremely hard on most materials. The operating temperature of an SFR is around 550 degrees Celsius, and the expected lifespan of the reactor is sixty or more years [11]. Therefore, it is important for the structural materials used to be able to withstand the extreme conditions for an extended period of time.

With that in mind, and given the significant impact a structural failure could have in a nuclear reactor, it is important to evaluate the viability of materials for such applications. This is where the DAC comes into play. Where many methods may struggle to gather reliable data at the extreme conditions necessary to simulate service in an SFR, the separation of a DAC from the testing environment theoretically allows it to gather images just as it would under more ordinary conditions.

Therefore, the goal of this project is to lay out a method for using a DAC to acquire crack opening displacement data during fatigue crack growth with precision, and demonstrate the viability of said method relative to other known methods of data acquisition and analysis. Comparisons will be made to data collected and analysis made by other methods, to confirm similar results under baseline conditions, and provide a foundation for the assertion that a DAC can be used to collect high quality crack growth data.

Chapter 2. Background

2.1 Mathematical Background and ASTM Standards

The American Society for Testing and Materials (ASTM) has developed a number of standards relevant to crack growth in metals. Two such standards are ASTM E647: Standard Test Method for Measurement of Fatigue Crack Growth Rates, and ASTM 1290: Test Method for determining Critical Crack Tip opening displacement (CTOD) from which the linear elastic fracture toughness (K_{IC}) can be determined. E647 defines guidelines for the design of compact tension (CT) specimens [13]. The standard also describes the load shedding method used to reach a desired starting stress intensity factor range (ΔK) in a specimen, which was the method used in preparing the specimen for this project. Standard E647 also presents the drawing and associated dimensions for the CT specimen, as shown in Figure 2.1:

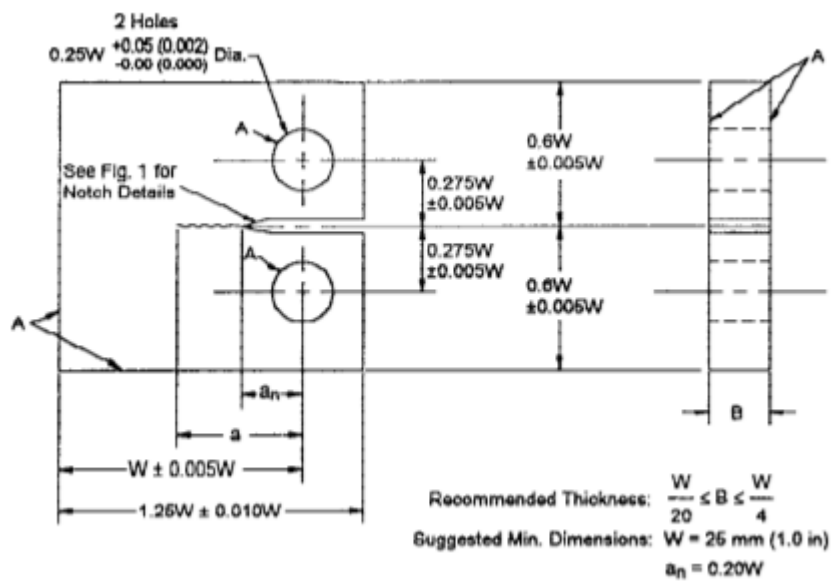


Figure 2.1: ASTM standard diagram of a CT specimen [13].

The specimen used in this project followed the same general design as shown in Figure 2.1, with the notable exception of the presence of teeth at the load line (between the two holes for mounting on the load frame) to facilitate the fitting of a clip gage extensometer.

Standard E1290 defines a test method which determines critical crack tip opening displacement (CTOD) values, and is specifically applied to notched specimens [12]. The method utilizes compliance curves, which compare the force applied to a specimen with the resulting displacement, in this case

recorded by a clip gage extensometer at the load line of the specimen. Among other methods, compliance curves can be used to identify an opening load value for a fracture process, by identifying the load value corresponding to the inflection point of the force-displacement curve, the point at which the curve transitions from being curved to being straight.

The main crack growth equation used in this project was the Paris-Erdogan power law [14]. The model uses ΔK as the input variable, and its basic form is given in Equation 2.1.

$$\frac{da}{dN} = A'(\Delta K)^{n'} \quad (2.1)$$

To account for the influence of plasticity-induced crack closure at the crack tip, the value of ΔK is replaced by ΔK_{eff} resulting in Equation 2.2.

$$\frac{da}{dN} = A(\Delta K_{eff})^n \quad (2.2)$$

In the above equations, A , A' , n , and n' are material constants. The effective stress intensity factor range, ΔK_{eff} , is defined as the difference between the maximum K value and the K value at opening, as shown in Equation 2.3.

$$\Delta K_{eff} = K_{max} - K_{op} \quad (2.3)$$

From ASTM E2760: Standard Test Method for Measurement of Fatigue Crack Growth Rates [21], both K_{op} and K_{max} can be calculated using Equation 2.4.

$$K = \frac{P}{(B \cdot B_N)^{1/2} \cdot W^{1/2}} \cdot F(a/W) \quad (2.4)$$

where P_{op} or P_{max} should be inserted for the load P in order to calculate the corresponding K factor. In the equation above, B is the specimen thickness, B_N is the specimen groove thickness (since there is no groove in this specimen, in this case $B = B_N$), W is the specimen width, and the geometrical factor $F(a/W)$ is given by Equation 2.5 [19], where a is the crack length.

$$F(a/W) = \left[\frac{2 + \frac{a}{W}}{\left(1 - \frac{a}{W}\right)^{3/2}} \right] \left(0.886 + 4.64 \left(\frac{a}{W}\right) - 13.32 \left(\frac{a}{W}\right)^2 + 14.72 \left(\frac{a}{W}\right)^3 - 5.6 \left(\frac{a}{W}\right)^4 \right) \quad (2.5)$$

Figure 2.2 shows the various ΔK values over the course of a cycle, providing a visualization of how K values are related to the opening load values sought in this project [22].

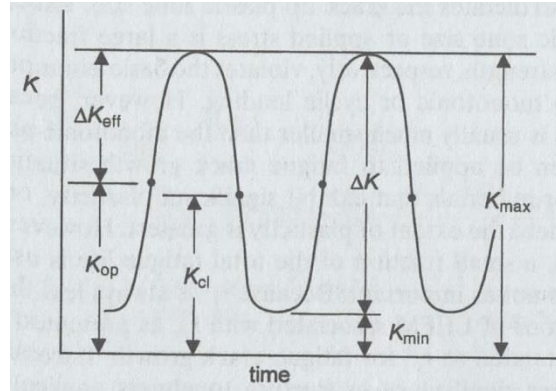


Figure 2.2: Representation of opening and effective K values [22]

2.2 Existing Work

Several methods have been used to evaluate crack opening and crack growth rates during fatigue loading over the years. Experimental methods have used measurement methods such as clip gage extensometers or back-face strain gages, while computational methods have resorted to finite element analysis (FEA), or strip-yield modeling. Extensometers in this context are simple two-pronged devices, in which the prongs are inserted in the specimen notch positioned at the load line, and used to measure the crack opening displacement at that point based on deflection of the prongs [15]. Some extensometers are designed to be used in high temperature tests, and other less standard conditions. Another experimental method uses back-face strain gages to measure the correlation between the strain reported by the instrument, and the crack tip opening displacement (CTOD). Figure 2.3, from a NASA paper on the subject, illustrates the application of a back-face strain gage to a four-point flexure specimen [16].

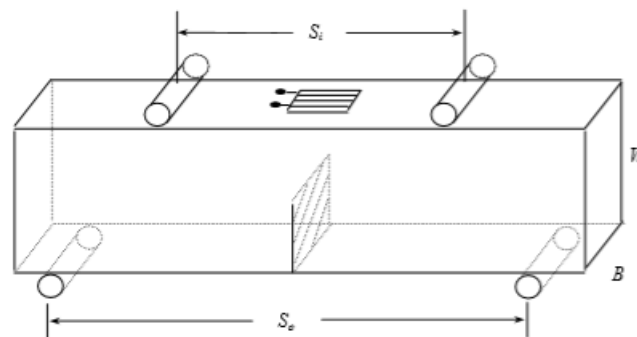


Figure 2.3: Back face strain gage application [16]

In terms of analytical approaches, FEA can be used to model fracture specimens, with loads and conditions being applied to simulate a wide variety of scenarios and observe how the specimen behaves. The strip-yield model, first introduced by Dugdale in 1960 and initially applied to through cracks in plates of infinite thickness, is another analytical model. The model assumes that the plastic deformation is concentrated in a strip in front of the crack. By utilizing this assumption and adding boundary conditions, this model replaces the elastic-plastic problem with an analytically solvable elastic problem. This allows for key equations of stress intensity factors and crack opening displacements to be used to solve for the crack-tip opening load and compute the crack growth rate during a fatigue cycle [17].

G. Potirniche developed a strip yield method for the analysis creep-fatigue crack growth rate (CFCG) in materials at elevated temperatures [18]. Additionally, work was done by J. Ramirez on the development of FEA models to simulate the impact of CFCG hold time on opening load. Ramirez's work focused in part on Alloy 709 [19]. While most research has focused only on fatigue crack growth loading at room temperature, future work should consider using the experimental techniques laid out in this document to measure opening load data during CFCG, for comparison to existing work with CFCG cycles.

2.3 Advancements

While the existing methods for fracture analysis are popular and have been used extensively over the years, they do suffer from a number of shortcomings that can be overcome by refining the DAC method. Primarily for the mentioned experimental methods, the clip gage extensometer and the back-face strain gage, the presence of extreme conditions in the testing environment can interfere with any measurements obtained under those conditions. As previously mentioned, the separation of the DAC from the testing environment allows it to operate without these concerns. Analytical methods such as FEA and the strip-yield model can produce excellent results, but need reliable experimental measurements to back them up. The ability of the DAC to produce high quality data of a specimen under extreme conditions makes it ideally suited to supporting the analytical methods, if it can be shown to be reliable itself.

Chapter 3. Methods

3.1 Specimen

The specimen used was a compact tension (CT) specimen made of Alloy 709. The schematic of the specimen was presented in Figure 2.1. The specimen dimensions and crack growth test conditions are given in Tables 3.1 and 3.2, respectively.

Table 3.1: Specimen Dimensions

Width (W)	Thickness (B)	Notch Length
50.8 mm	12.75 mm	13.1 mm

The table below gives additional specimen information of note. Precrack information refers to the process prior to data collection, in which the specimen was cycled to prepare it for testing at the initial ΔK level.

Table 3.2: Selected Specimen Information

Modulus of Elasticity (GPa)	Precrack Crack Length (mm)	Precrack Cycles	Final Crack Length (mm)	Final Cycles
193.1	16	112,368	35.5	6,632,407

3.2 Test Matrix

Table 3.3 lays out the testing conditions used in this project. Additional conditions and specimens were planned, but ultimately had to be moved to future work due to unexpected circumstances. The R value is a ratio of minimum to maximum load ($R = F_{min}/F_{max}$), and fatigue crack growth (FCG) refers to a situation when the crack grows during a cycle type in which the load immediately begins descending back to its minimum value after hitting its maximum, with no hold time.

Table 3.3: Test Matrix

Specimen	R	Temperature	$\sim F_{max}$ (N)	Load Condition
1	0.1	Room	3000	Fatigue Crack Growth (FCG)

3.3 Data Collection

This section will discuss the data collection and analysis procedure for this technique.

3.3.1 DAC Settings and Photograph Approach

The data acquisition camera was equipped with a high powered lens, and set with an exposure value of 17,000 μ s. Additionally, the camera software was set to not throttle data collection. The approach used in image collection was to have two persons in the lab, one running the camera, and the other at the controls of the load frame. Each individual would initiate their system simultaneously, in an effort to synchronize the beginning of data collection with the beginning of the period of interest. Fatigue cycles were split in half, such that data would be collected on the climb to the peak of the cycle, then the cycle would be held at that point, and a separate set of data would then be collected for the descent from the peak value to the minimum value. With a recorded final data collection rate of 8.5 frames per second, and a cycle frequency of 0.1 Hz, roughly 42-43 images would be collected for each of these 5 second load or unload periods.

3.3.2 Camera and Specimen Setup

The DAC method requires very careful and purposeful setup of the camera to function properly. The camera must be positioned at the desired distance from the specimen in such a way that it is not only perfectly stable, as vibrations during image collection will skew results, but also such that it is perpendicular to the specimen, with the camera facing the area of interest as directly as possible. Lighting must be positioned and adjusted to fully light the area of interest near the crack plane and always have the crack tip in sight. In this experiment, a flexible lamp was fixed to the load frame and its two bulbs were positioned to provide light on the specimen surface. For clarity, it is sometimes better to ensure that the light strikes the specimen from an angle, rather than head on, to make the contour easier to identify. An image of the DAC used in this project is included below.



Figure 3.1: Photograph of the DAC used in this project.

The specimen was inserted into the load frame, and scored using sandpaper to create a field of marks to be identified in the image analysis software DaVis. Scoring for earlier tests was done outside of the load frame, but as the crack increased in length, scoring was applied to ensure the scored speckle pattern continued as far as needed to track the movement of the fracture as loads were applied and removed. Once the specimen was fixed in the load frame, a clip gage extensometer was inserted into the notch at the load line, to generate reference data for use in validating the DAC method, as well as for machine control purposes. Figure 3.2 shows a schematic of the specimen setup and critical area of interest.

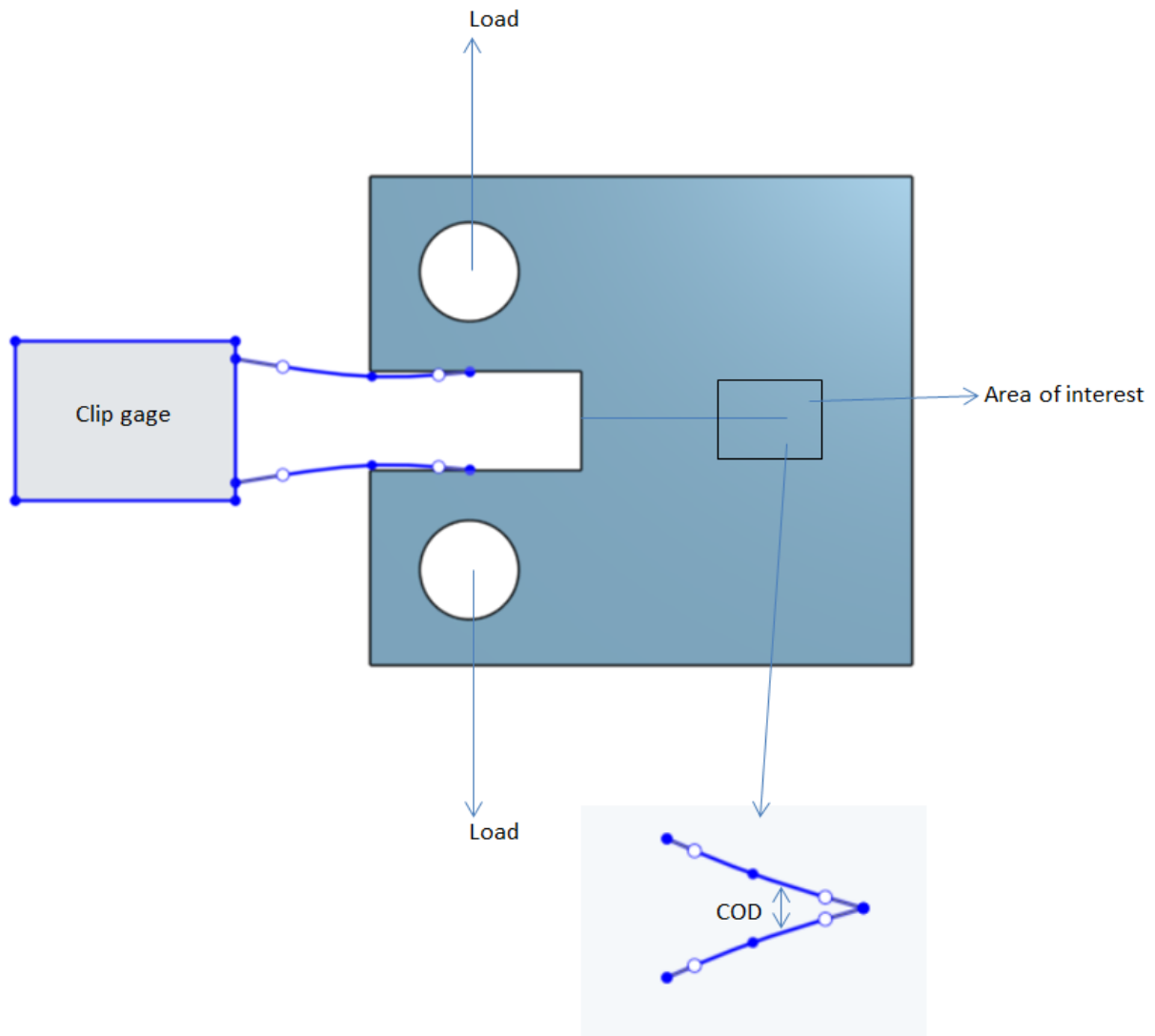


Figure 3.2: Basic specimen setup and area of interest diagram

The specimen was loaded in FCG cycles with a triangular shape, loading up to a maximum load of approximately 3,000 N, then unloading to a minimum load target of approximately 300 N. There was some overshoot on either end of the cycle, with actual minimum and maximum values existing a bit above or below the targeted minimum and maximum values. This was reflected in the data analysis process.

3.3.3 Data Analysis

Images collected in the lab were loaded into the DaVis analysis software. The sets of roughly 42 images for each cycle were independently analyzed, with the software focusing on squares of 64 by 64 pixels, and doing multiple passes at 87% overlap, to identify movement in the speckle pattern

identified on the specimen images. The software utilizes Digital Image Correlation (DIC) to overlay and compare images in series to identify and track changes. The overlap setting represents the thoroughness of the analysis. The following series of figures illustrates the progression from image as collected, to fully processed image ready for analysis.

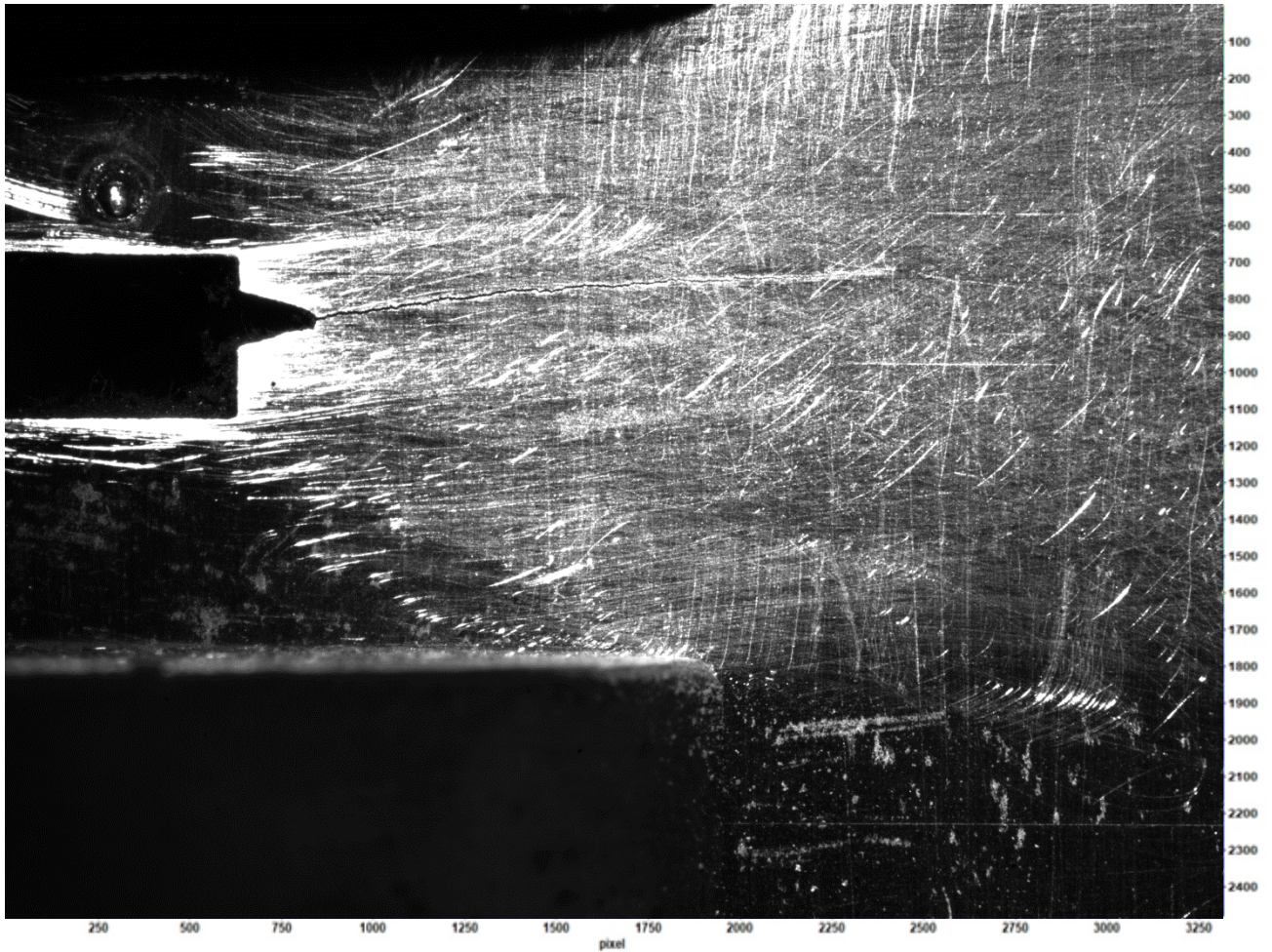


Figure 3.3: Base image of the region of interest with the notch and crack line. X and y scales were added to the image, and values are in pixels.

Figure 3.3 demonstrates the unprocessed form in which images are collected in the lab using the DIC. This image was collected at a point of maximum load during preliminary testing of the system.

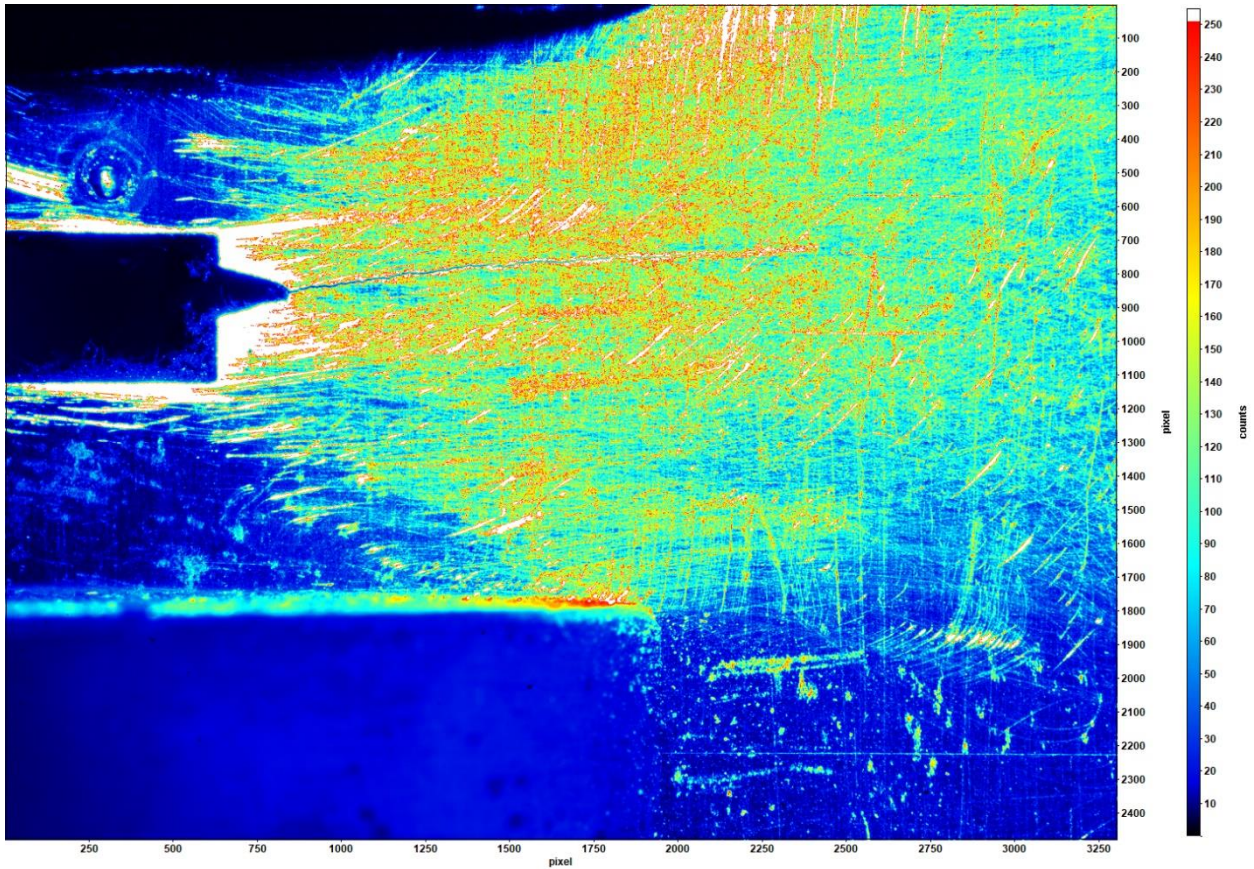


Figure 3.4: Base image, with contrast activated in DaVis software.

Figure 3.4 is the same image as the one in Figure 3.3, but processed to a basic level in the DaVis software. The software allows for contrast to be enabled, highlighting the speckle patterns that the software depends on to track changes in a data set. Images such as this were used to develop the earliest data sets used in this project. In the software, x (horizontal) and y (vertical) coordinates on the image are given for the cursor location on the screen. By carefully documenting y coordinates at either side of the visible crack for a given x value, a set of data was developed, and then differences in displacements between the top and bottom halves of the crack plane were calculated manually to calculate the crack opening displacement (COD), before being entered into a program written in Matlab for further processing and plotting.

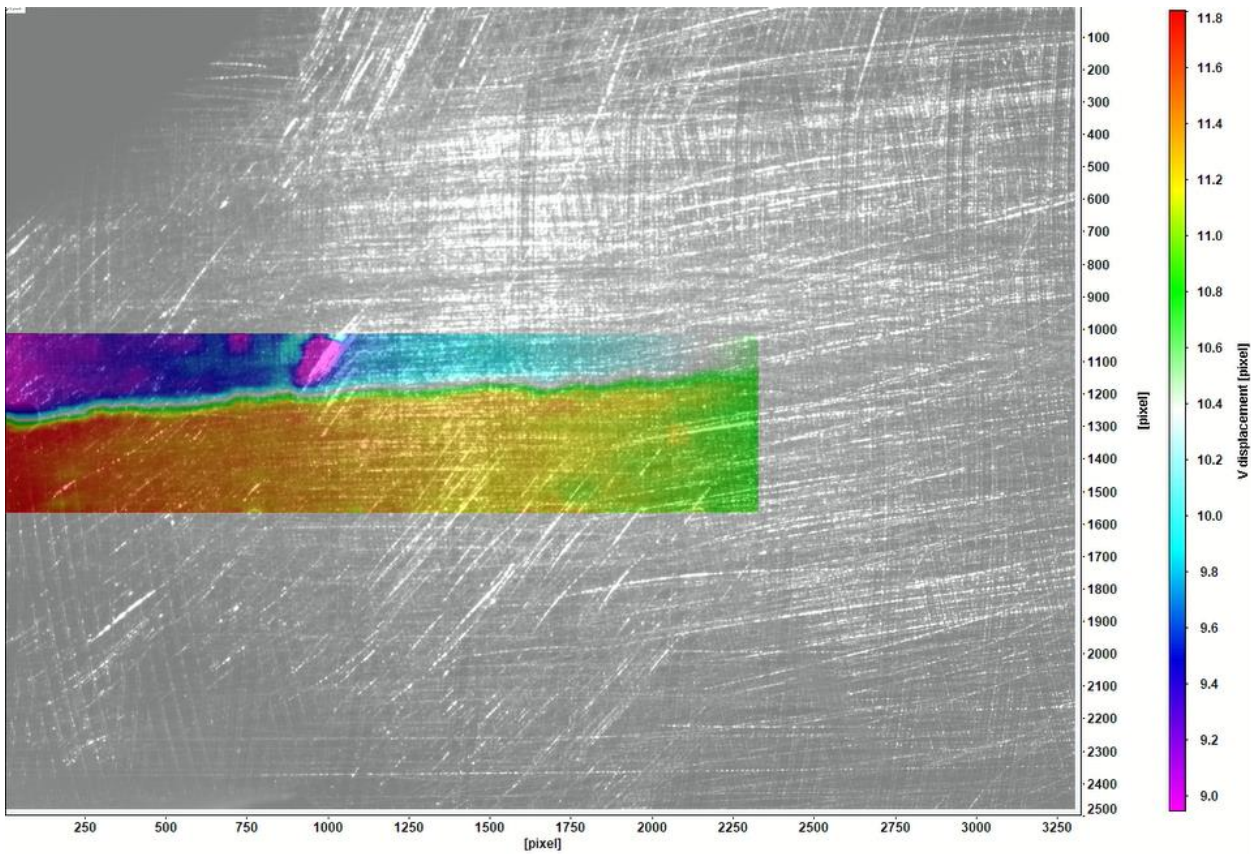


Figure 3.5: An image from the $\Delta K=10$ MPa $\sqrt{\text{m}}$ data set, with the refined displacement observation method in effect. The color scheme indicates the magnitude of the vertical displacement of each pixel. The conversion value for this image is approximately 174 pixels/mm. Therefore, with a pixel x coordinate of about 2250, the crack tip is about 13 mm from the notch.

Figure 3.5 is an image from later tests at the same ΔK level as Figures 3.4 and 3.3. As usage of the tools and software progressed, it was determined that a better method for tracking displacement of given points along the crack plane would be to develop images such as the one shown in Figure 3.4, and then identify the displacement of a given point on the x axis based on its color, per the scale on the right hand side of the figure. By observing the displacements of points above and below the crack plane at a given x coordinate, COD at that point can be identified. Differences in color between the upper and lower portions of the crack plane region represent the crack being open at that point. A similar color above and below the crack plane indicated that the crack was closed, or that the region of the material is uncracked. During the taking of the pictures, the position of the physical crack tip was known at all times. The image shown in Figure 3.5 corresponds to the maximum load level for the specimen. A mask is defined in the DaVis software to restrict the data collection to only the

region of interest, i.e. near the crack plane and including the crack tip and notch region. The image shown in Figure 3.5 is the typical picture taken for the bulk of analysis in this project.

Given the increasing length of the crack, it was determined that it would be ideal for efficiency to take fewer data points by hand. Fortunately, in analyzing the displacement of a given point over time, consistent patterns developed in which the motion of a given point could be mapped to either a linear or quadratic fit fairly accurately, allowing a more developed data set to be produced from a smaller collection of data points. With this in mind, the current method is to collect a set of displacement data points for the top and bottom of the crack plane at a given x value over the length of the climb from minimum to maximum load. These data points are then first plotted on their own, to identify an ideal fit curve approach, and then fit curves were developed for the displacement of each top and bottom point at the selected x values. X values were spaced 250 pixels apart until the crack tip, which may not be quite 250 pixels from the previous point. Pixels were converted into millimeters by identifying known dimensions in the images, generally the notch width, and using those as references for conversion. Pixel to mm conversion did vary between data sets, as the camera had to be adjusted when the crack progressed, to ensure it all was visible in the images.

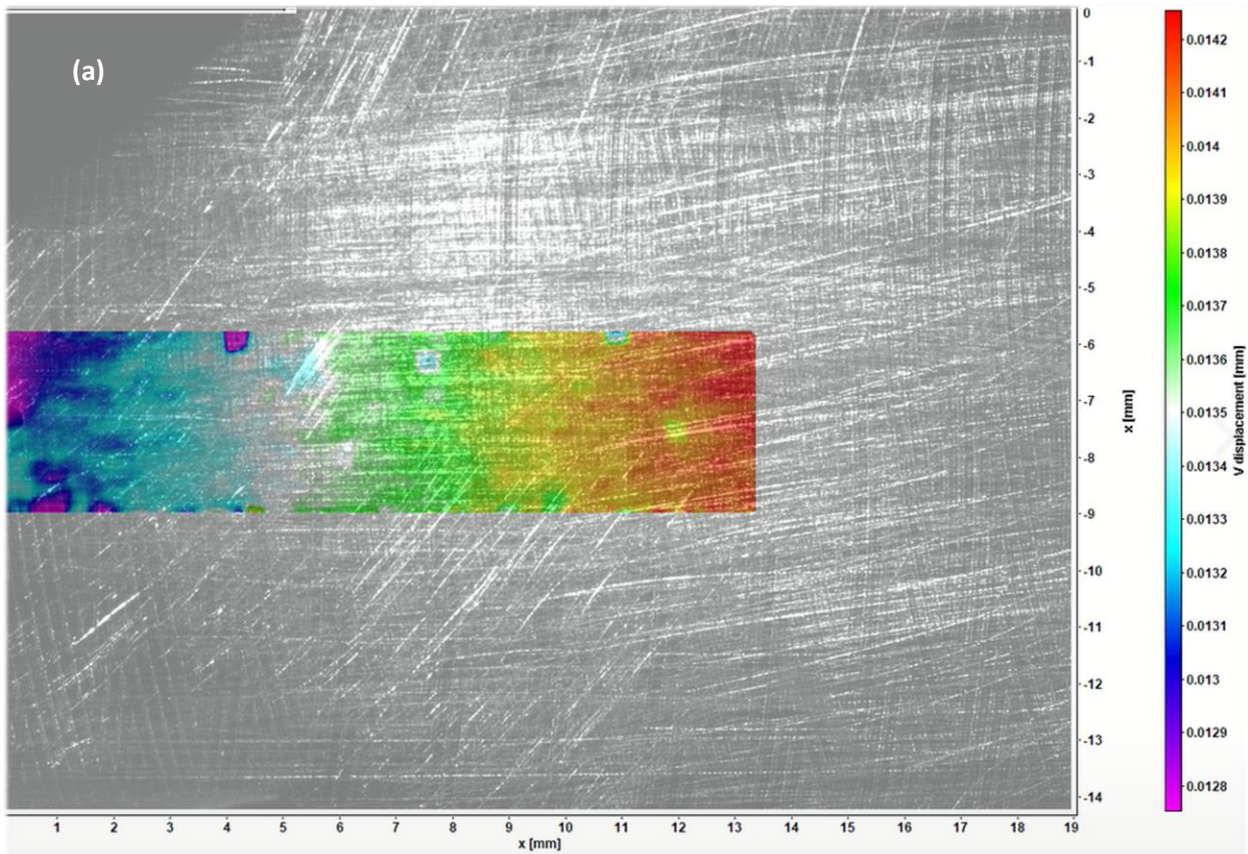
To process the data further, the difference between the fit curves was determined for each selected point along the x-axis, and the equations resulting from that process were arranged arrays. From those arrays, curves could then be plotted to show the rough progression of the crack shape with increasing load. The intended purpose of these plots is to show a range in which the opening load of the crack exists, by identifying the last curve that does not end above the x-axis, and the first curve that does. To further validate the opening loads represented in these plots, displacement values of the identified crack tip were plotted independently against the applied load. With these plots, by identifying the x-intercept of the curves within the minimum to maximum load range, a more exact opening load approximation could be determined.

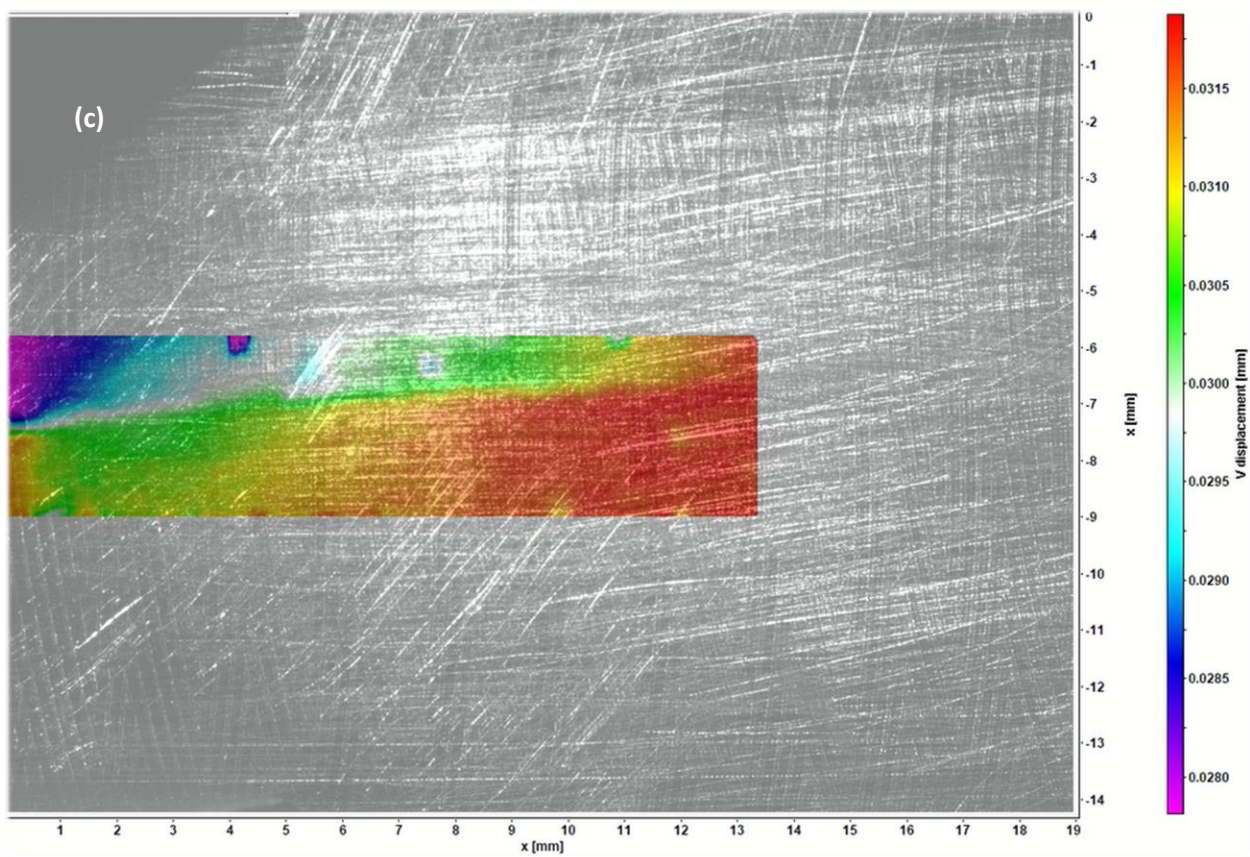
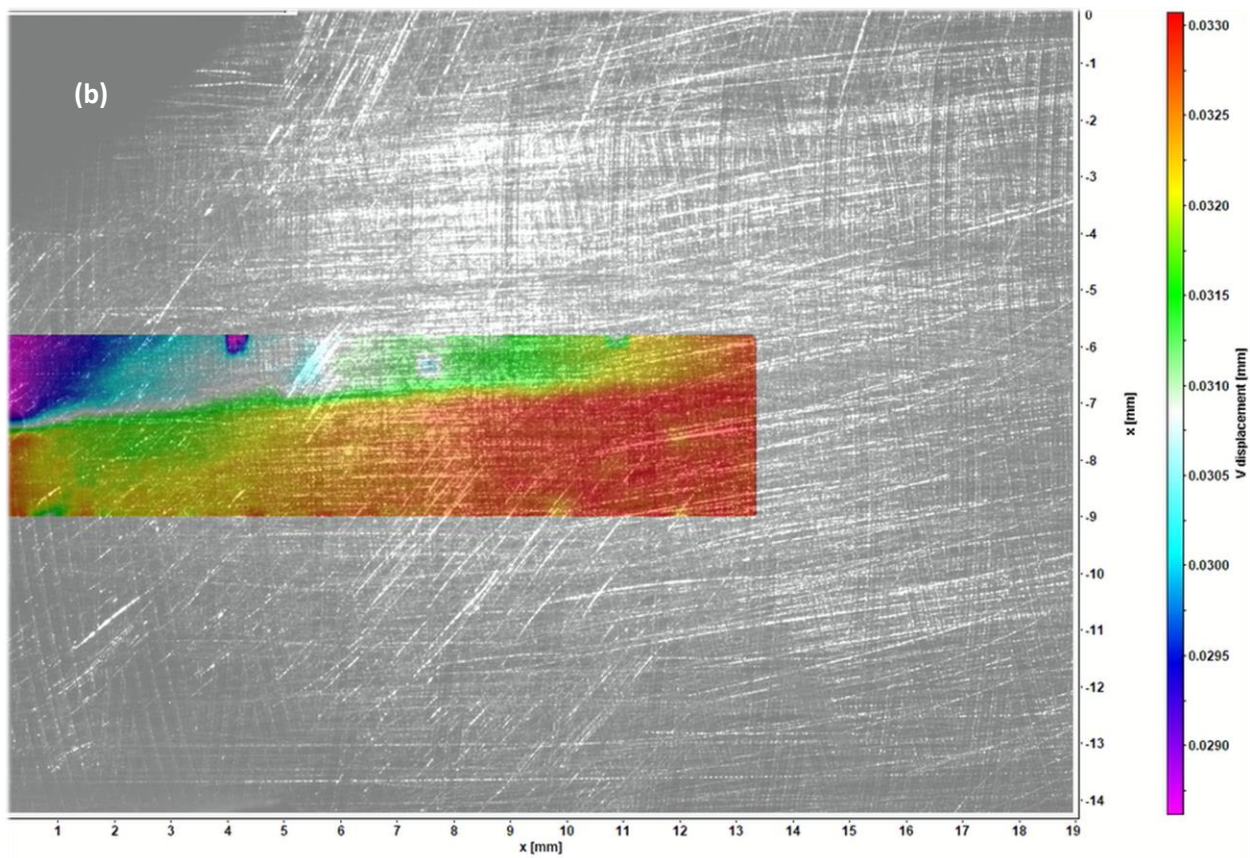
Chapter 4. Results

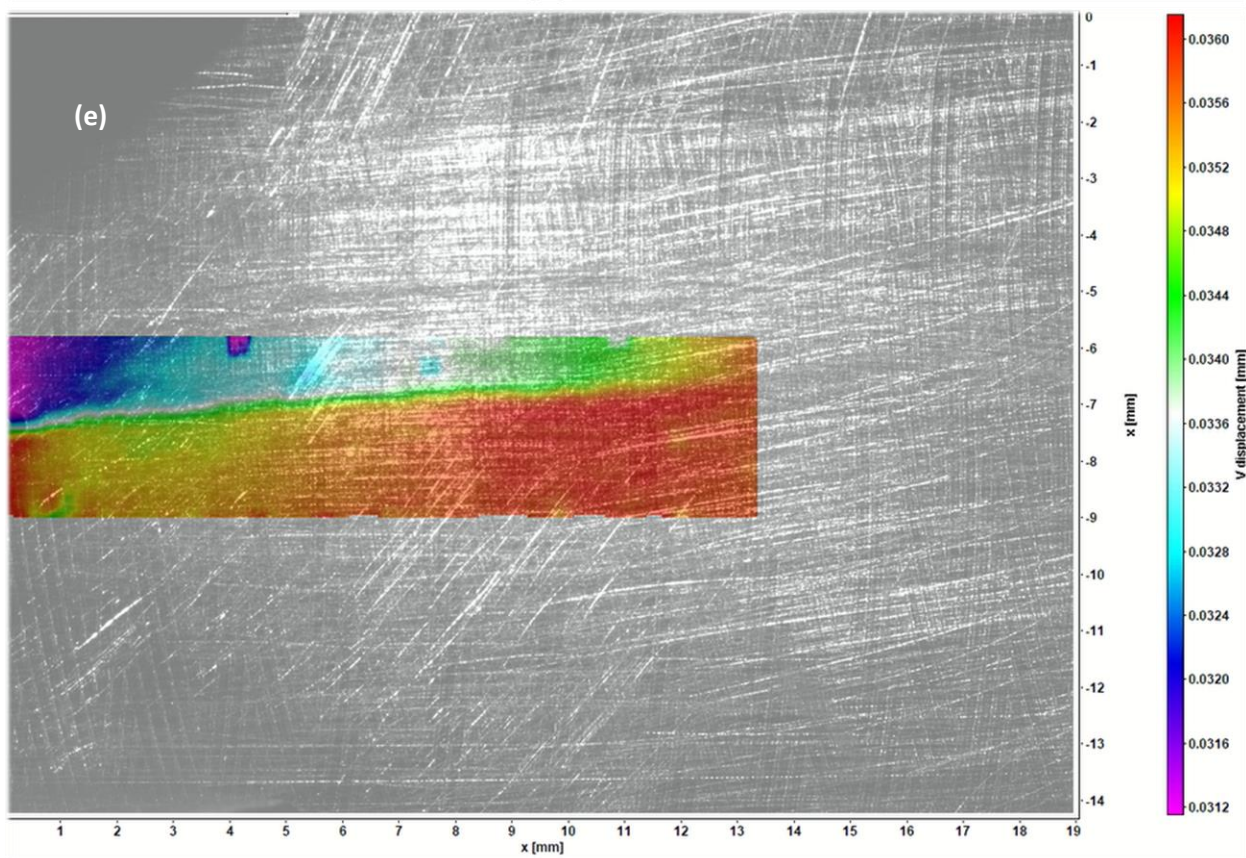
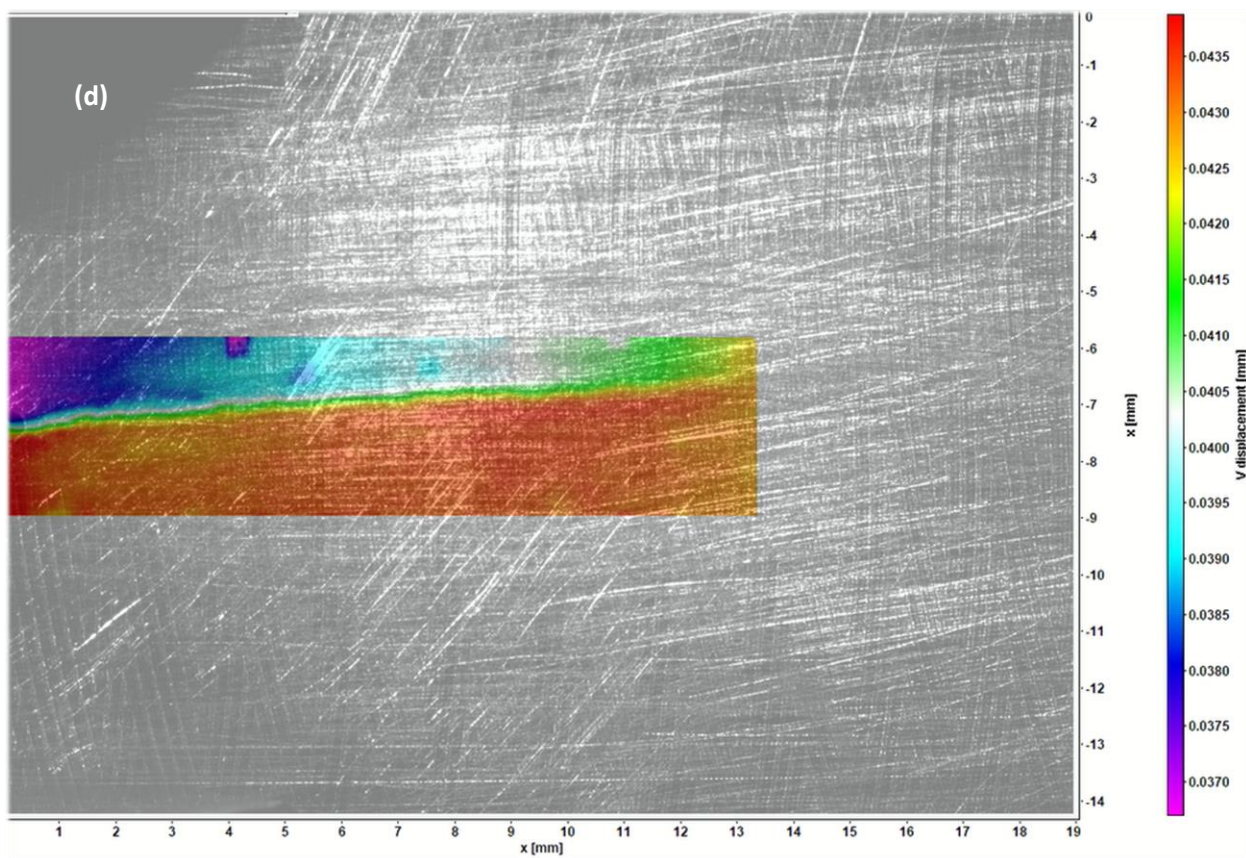
This section describes the progression of each of the nine cycles analyzed in the form of processed images, with a greater concentration of images around the opening load recorded for that cycle. Following the colored images showing progression, first a plot showing the shape progression of the fracture with increasing load will be shown, and then a magnification of the observed crack tip, to display the observed opening load range. A tail has been added to the shape progression plots, to demonstrate that there is generally a small tail leading down to the actual crack tip as it progresses with each cycle. Following these two plots for each cycle, a plot further confirming the opening load as represented by this method will be displayed.

4.1 $\Delta K=10 \text{ MPa}\cdot\sqrt{\text{m}}$

4.1.1 Cycle 1







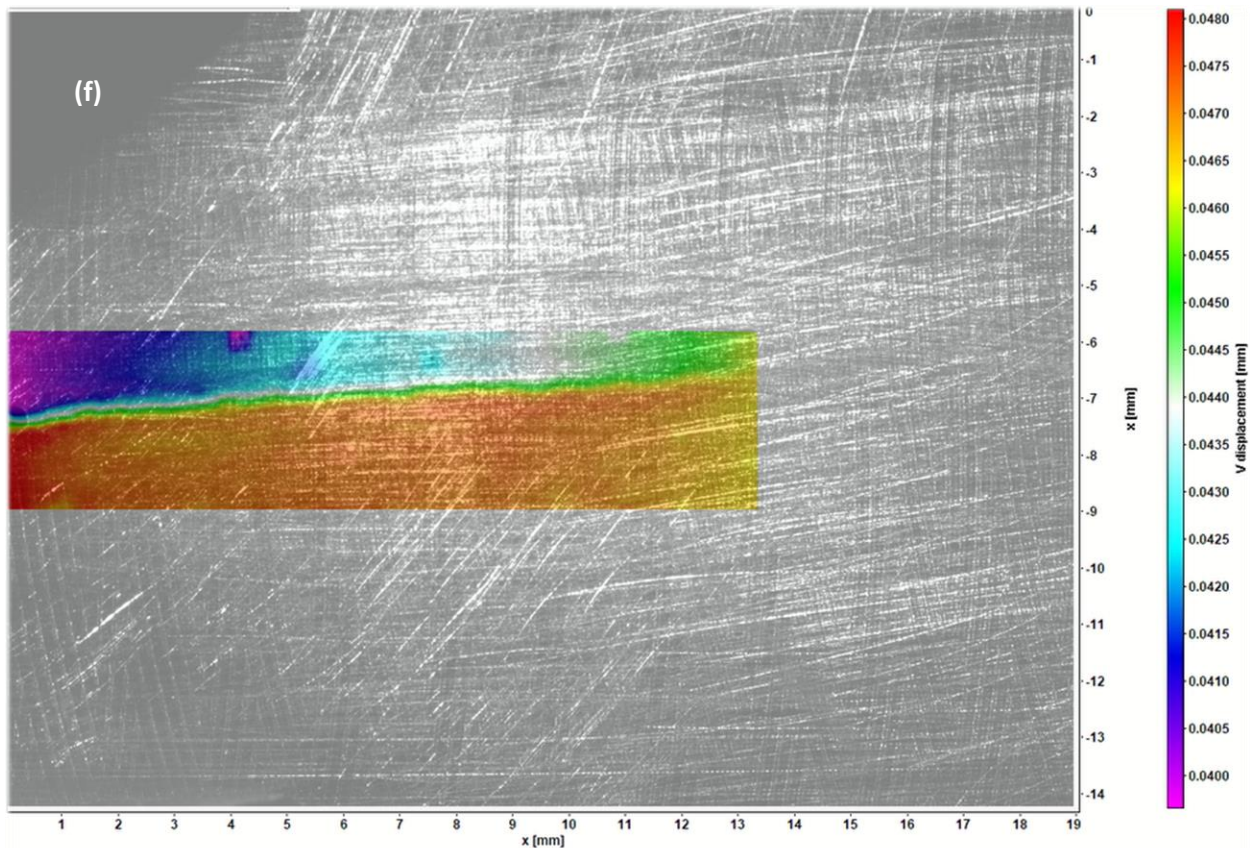


Figure 4.1: Series of colored images showing progression of $\Delta K=10$ MPa $\sqrt{\text{m}}$ Cycle 1 from minimum to maximum load (a) \sim 814 N, (b) \sim 1329 N, (c) \sim 1586 N, (d) \sim 1843 N, (e) \sim 2357 N, (f) \sim 3000 N. The color scheme indicates the magnitude of the vertical displacement of each pixel.

The plots for this cycle are the only ones not generated from data acquired from the colored images. Instead, the data for these plots was pulled from the contrast images for the cycle one data set, as the colored images had not been established as part of the method yet. A collection of colored images was eventually generated from the data set, and used to experiment with applying a scale directly in the DaVis software, an approach which was ultimately set aside in favor of applying the pixel to millimeter conversion in the code for plot generation. With all this in mind, it should be known that the colored images above may not match up perfectly with the data used for the plots below, and are instead intended to provide the clearest image of this cycle available given the change in methods.

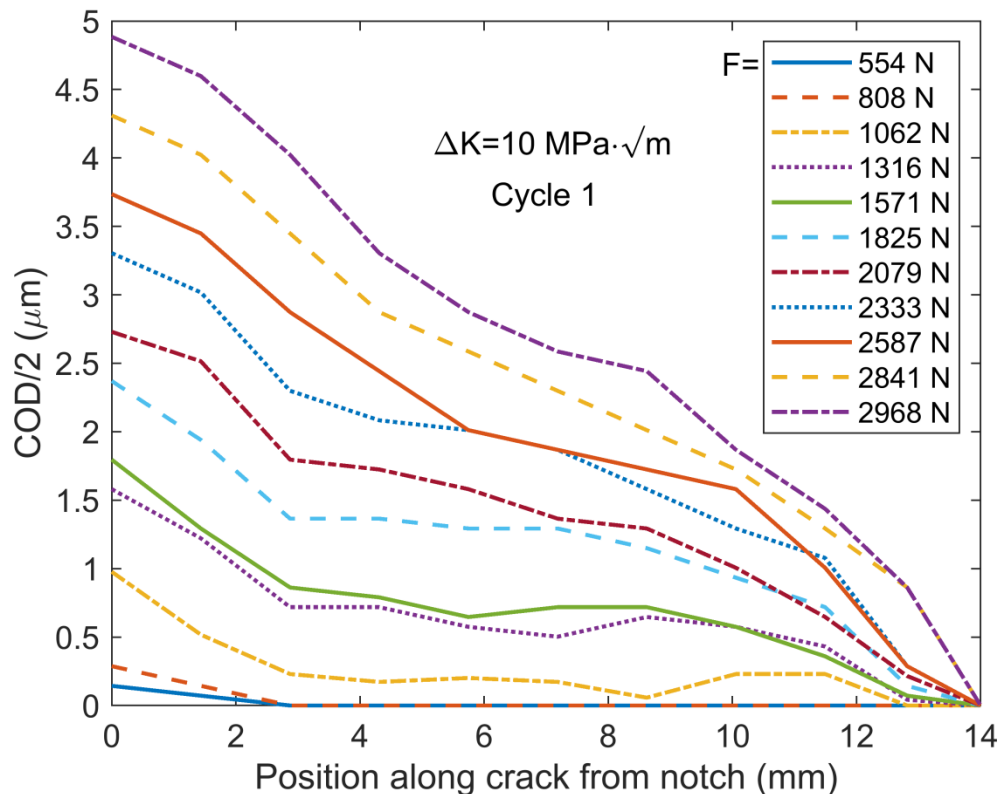


Figure 4.2: Half of the crack opening displacement (COD) evolution during the loading in cycle 1. The observed crack tip is located at horizontal position $x = 12.815 \text{ mm}$

The displacement values in the plots generated for the $\Delta K = 10 \text{ MPa}\cdot\sqrt{\text{m}}$ data set were calculated by hand, with coordinates being identified and compared on paper before COD values were entered into the code for plot generation. Therefore the resulting plots are not as smooth in appearance. However, plots such as Figure 4.2 can be taken as a good approximation of the crack opening profile with increasing load. It is, however, important to realize that the plot compares the difference between the top and bottom displacements of the crack plane at each given x -value, as opposed to just data from the top or bottom separately. Therefore, this is not an exact point for point mapping of one half of the crack plane, but rather a visualization of how the crack changes in shape with increasing load.

The observable crack tip is not what is represented by the lines going to zero in this image. It is known that the fracture should extend for a small distance beyond the observed crack tip, as it is progressing. However, at the time of analysis for these data sets, a method had not been developed to precisely determine the shape or extent of that development, and the lines in these zoomed out

images were extended to an arbitrary zero value beyond the observed crack tip simply to represent that there is crack extension beyond the observed value.

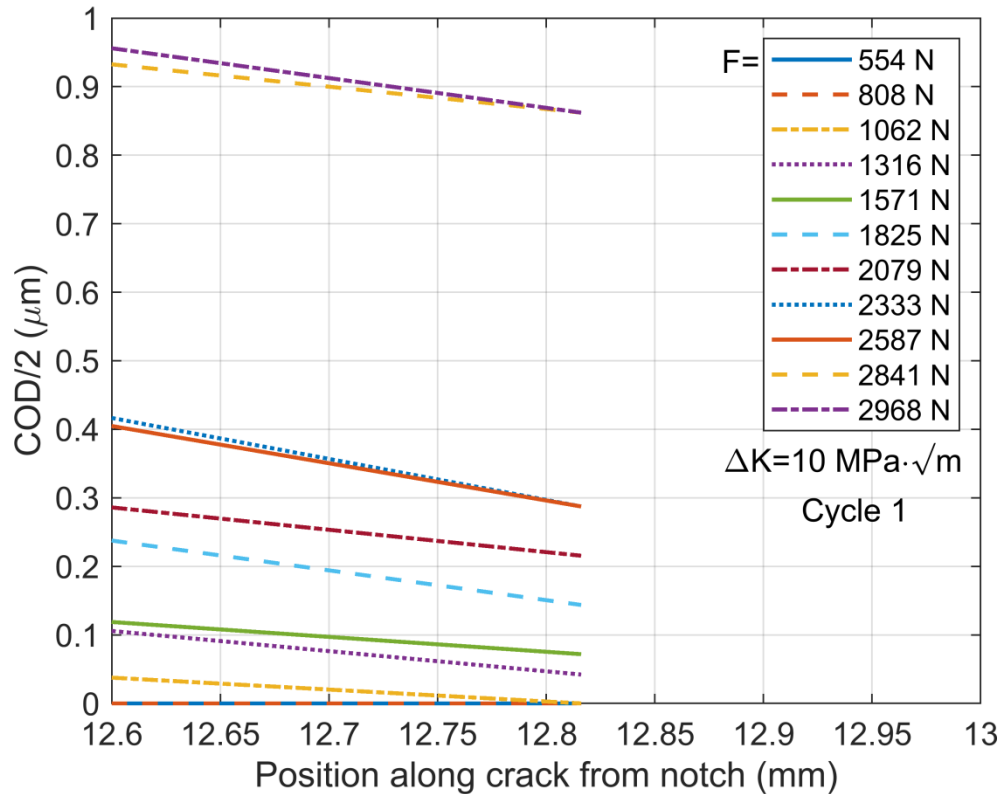


Figure 4.3: Crack tip focus for approximate opening load range identification.

Figure 4.3 shows the COD in the zoomed in region near the crack tip. The range in which the crack tip is open can be identified by observing the last line to touch the x axis at or before the crack tip, and the first line to not touch the x axis. In this case, we see a rough range of 1062 N to 1316 N for the opening load of Cycle 1 in the $\Delta K=10 \text{ MPa}\cdot\sqrt{\text{m}}$ data set. The observed crack length can be identified in these zoomed plots, which have the arbitrary tail removed for clarity.

It can be seen in this plot that the load line corresponding to 2587 N passes slightly below the 2333 N line, which does not agree with assumed behavior. This is likely due simply to the relatively unrefined nature of the method when this data was processed.

Figures such as Figure 4.3 and similar figures in this chapter are what inspired the approach of looking specifically at the end point of the crack, to identify the relationship between load and COD

at that point and identify a more precise opening load if possible. This idea was eventually developed into the third kind of plot featured in this chapter, shown below.

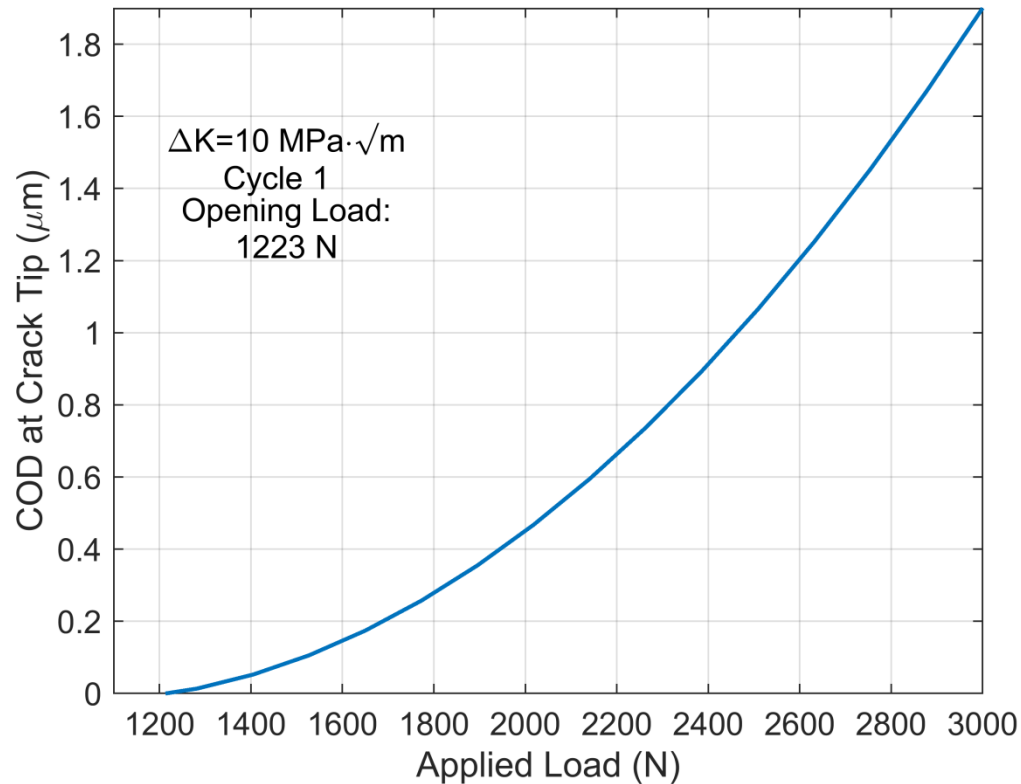
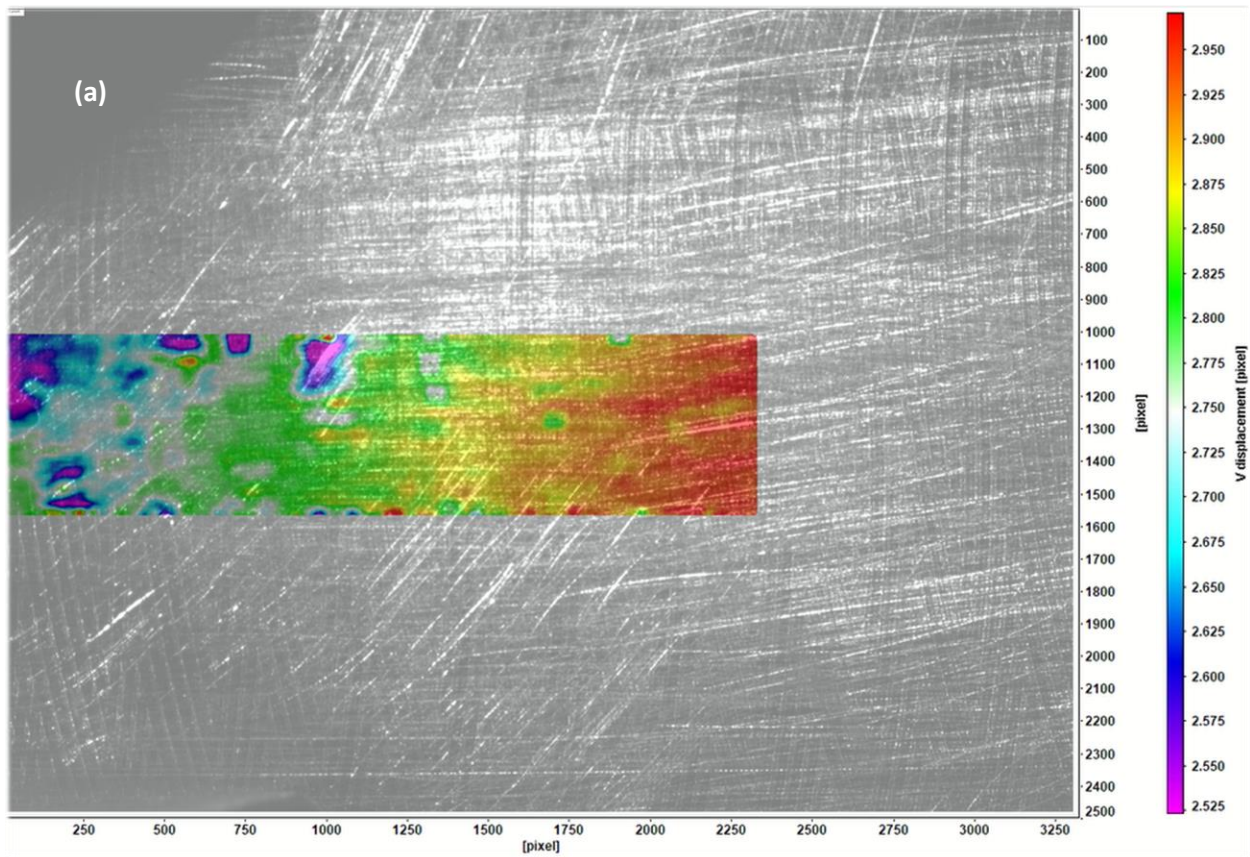
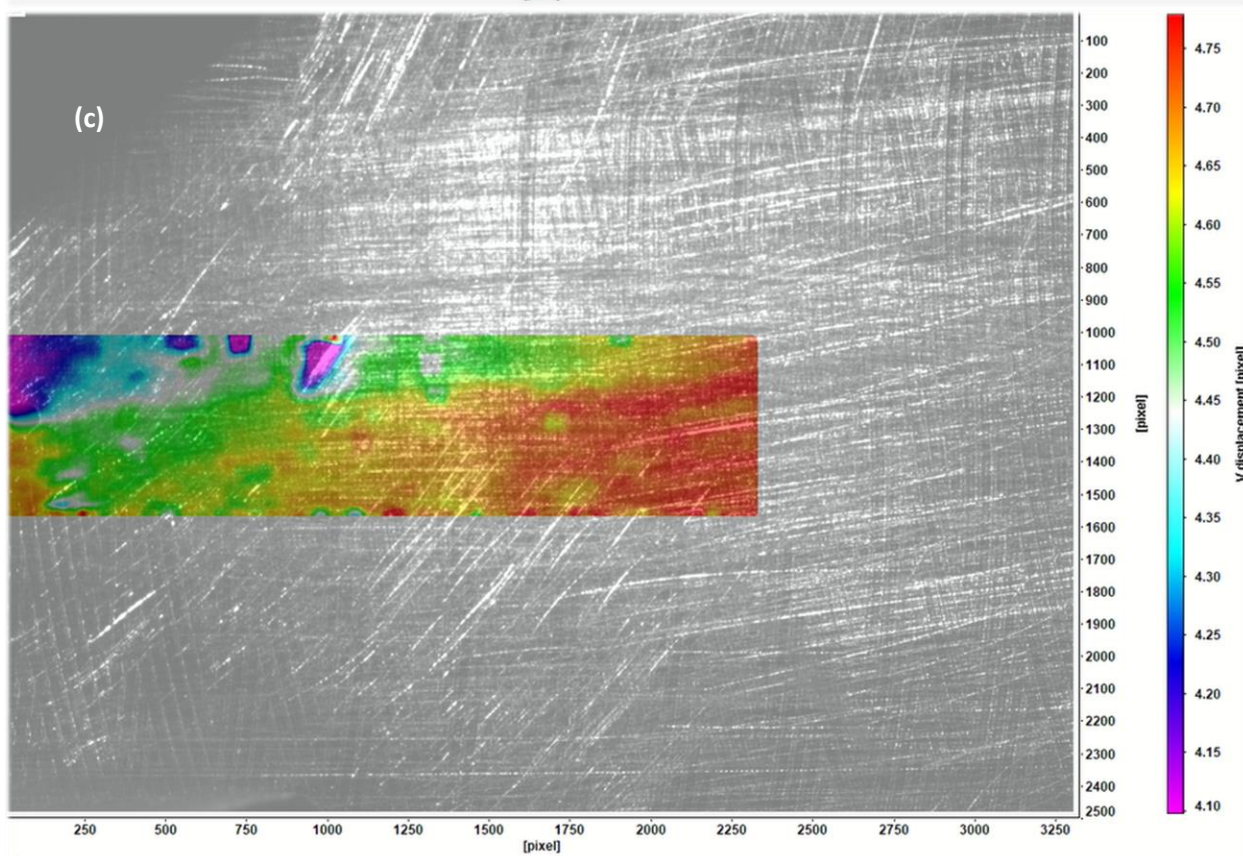
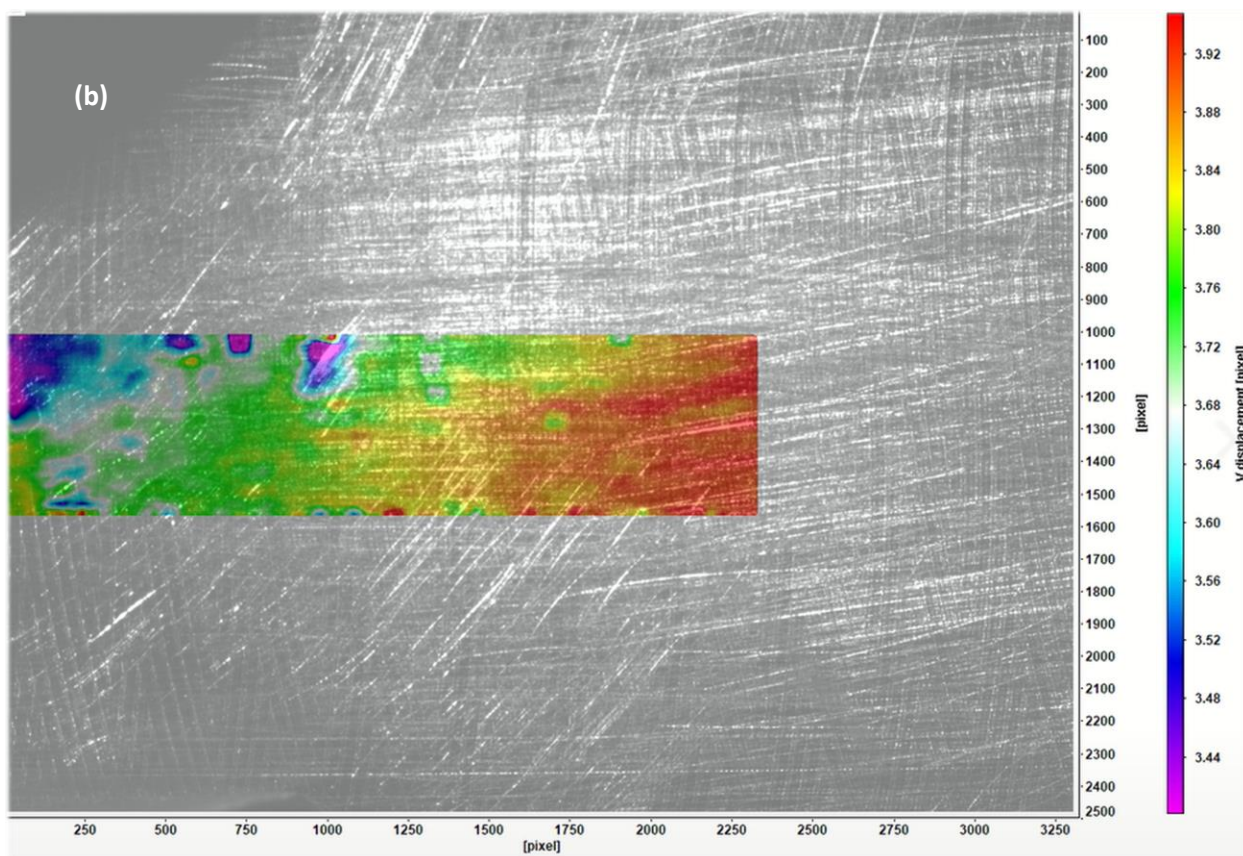


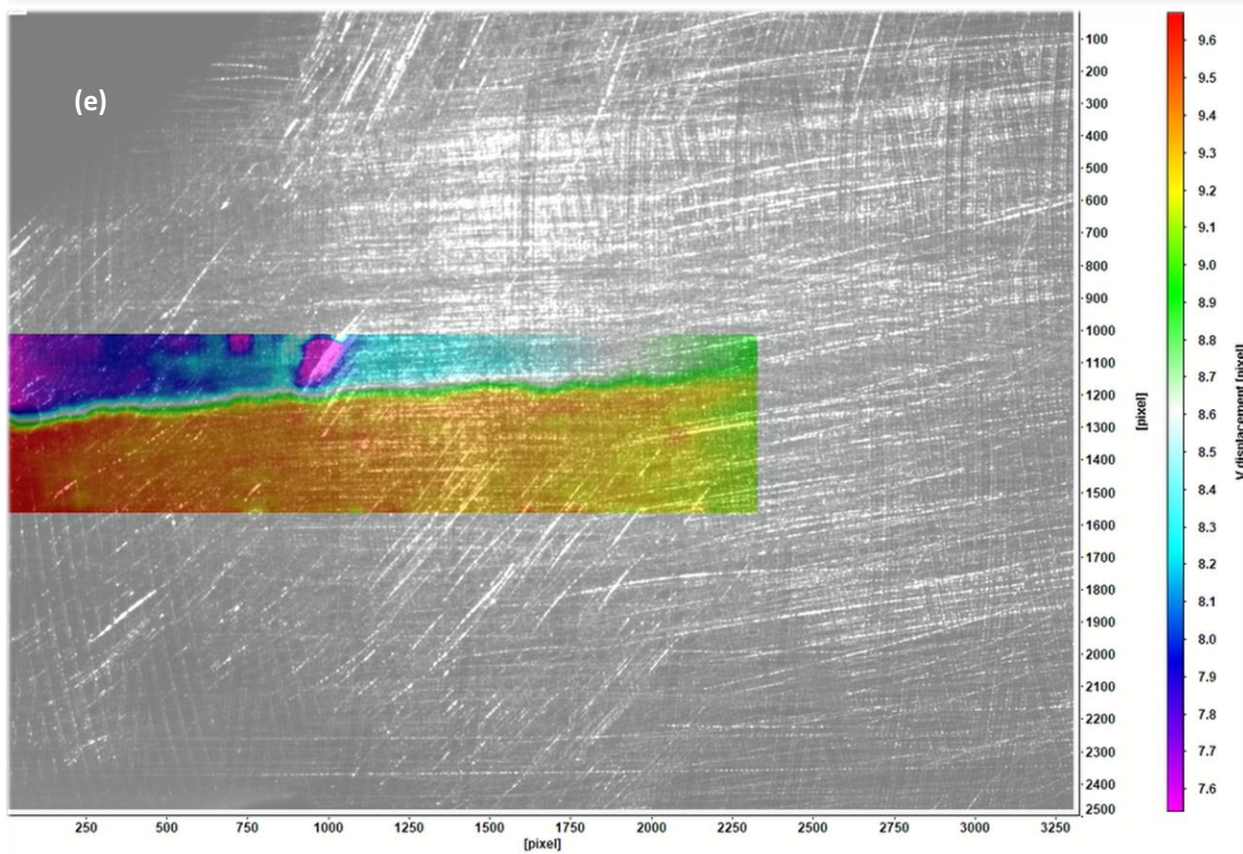
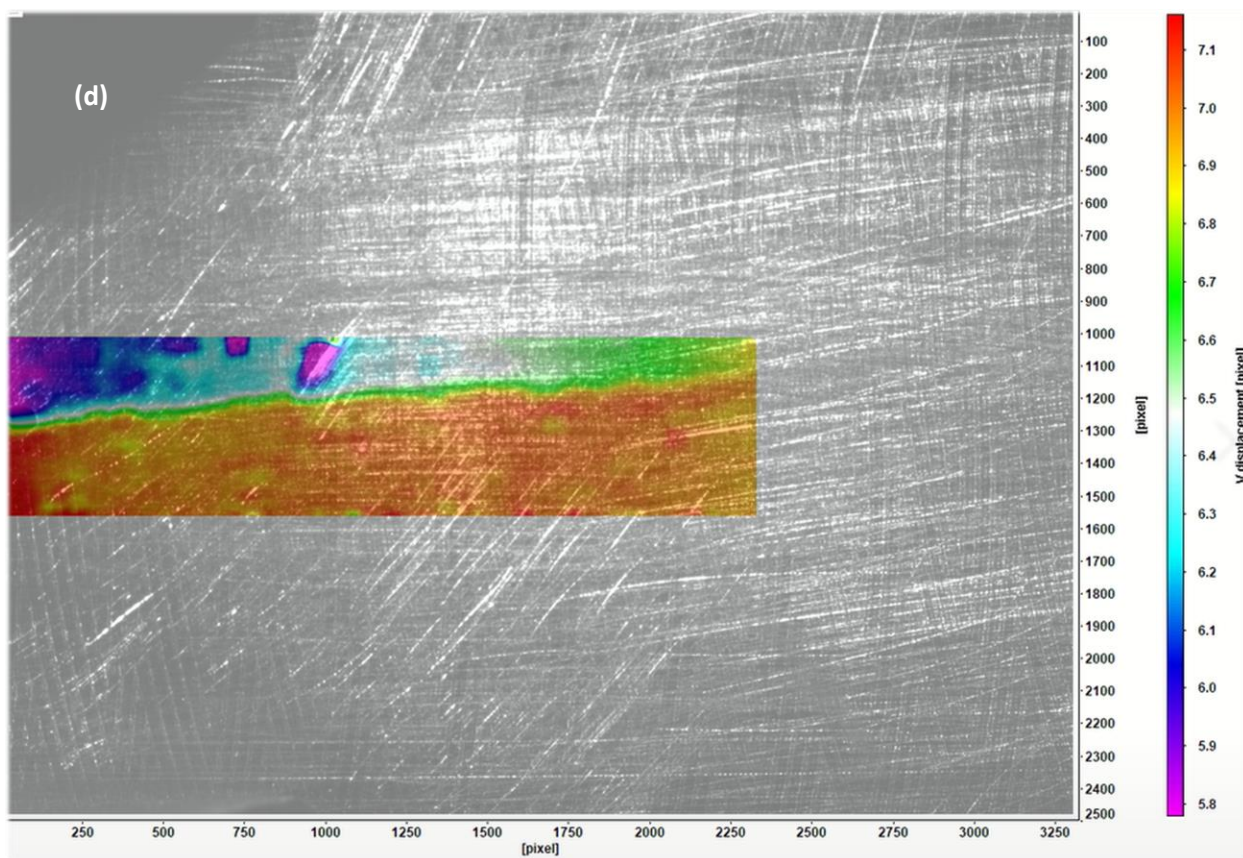
Figure 4.4: Variation of the crack tip opening displacement as a function of applied load during cycle 1.

Figure 4.4 presents the evolution of COD at the crack tip as a function of applied load. This graph was generated by plotting the displacement of the fracture plane at the crack tip alone versus the applied load. The point at which the COD curve intersects the x axis is the opening load for the cycle. In this case, an opening load of roughly 1223 N is identified for the cycle, which exists within the range displayed in Figure 4.3.

4.1.2 Cycle 2







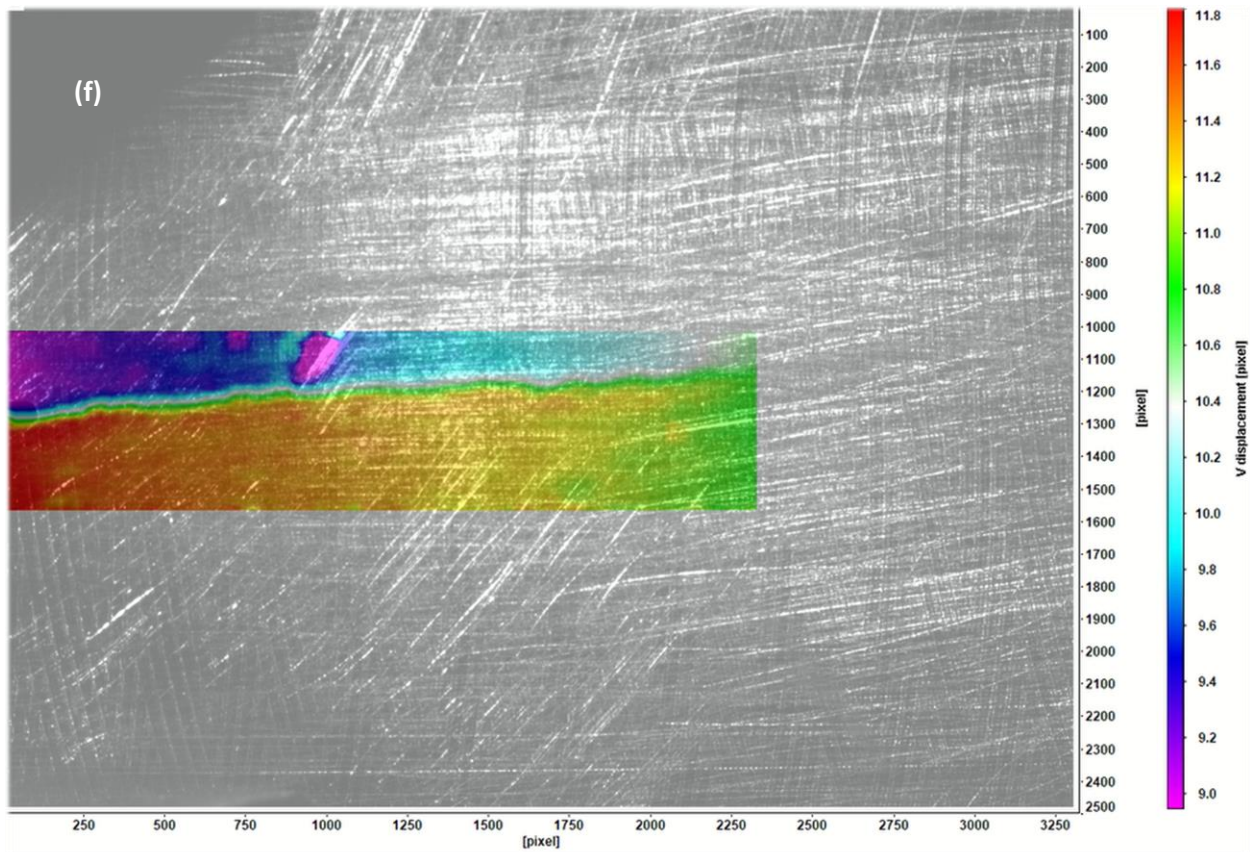


Figure 4.5: Series of colored images showing progression of $\Delta K=10$ MPa $\sqrt{\text{m}}$ Cycle 2 from minimum to maximum load (a) \sim 833 N, (b) \sim 1100 N, (c) \sim 1367 N, (d) \sim 1900 N, (e) \sim 2433 N, (f) \sim 3100 N. The color scheme indicates the magnitude of the vertical displacement of each pixel.

This cycle was the first in which the data collection was based on the colored images, and this is reflected in the smoother nature of the resulting plots. The displacement was still calculated manually, so the plots are still not as smooth at this point as they will be later, in the next section of this thesis.

It can be seen from these first two cycles covered that this data set generates less distinct data at lower load levels, which is assumed to be due to the slower crack opening process at this point in the specimen's life cycle. While some noise persists at higher load levels, with each completed cycle, the images generally became clearer and easier to read, as the method for acquiring them improved and more experience was developed.

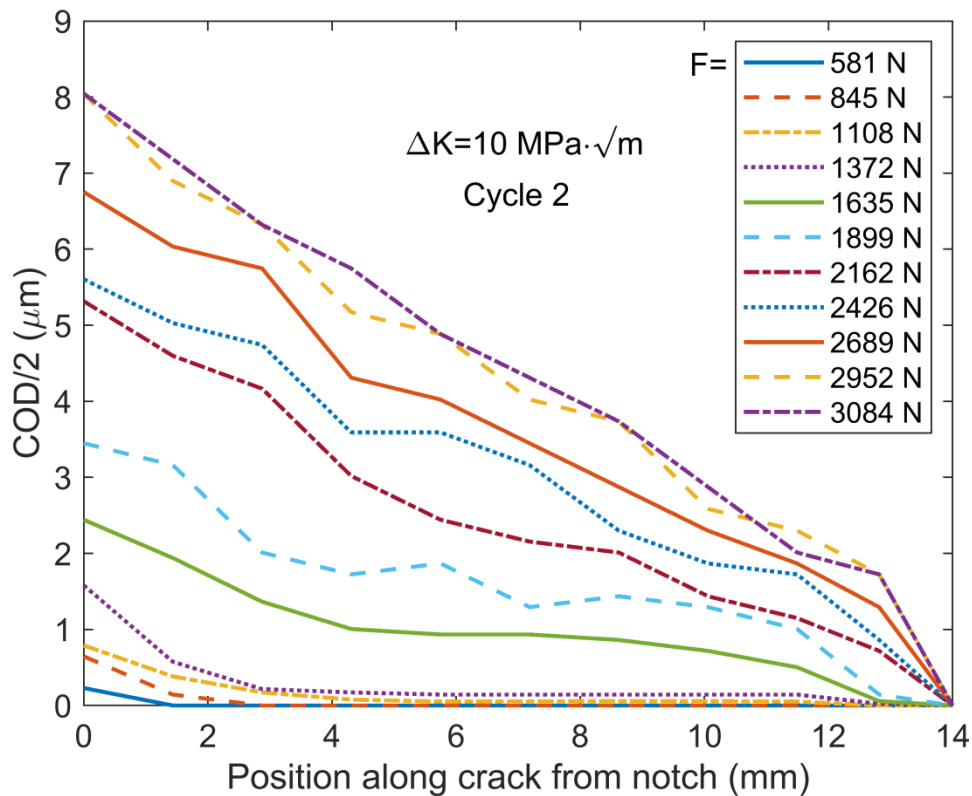


Figure 4.6: Half of the crack opening displacement (COD) evolution during the loading in cycle 2. The observed crack tip is located at horizontal position $x = 12.815$ mm.

Figure 4.6 shows the evolution of half of COD for cycle 2. One can observe that the first COD line that is distinctly above the horizontal axis, indicating the crack starts to open for the majority of its length is for a force of 1372 N. However, in this case the crack tip is still closed. The first clear opening of the crack tip is for the COD curve corresponding to a load of 2162 N. As the applied load increased further, the crack opened up even more, with the maximum COD corresponding to the maximum applied load in the cycle of 3084 N.

In the first plotting attempt of this data (not shown in this document), displacement values that were very close to zero were approximated as zero. While this approximation was found to produce reasonable plots, the data was later reevaluated and fit to 4th degree polynomials, to account for the range of near zero values that actually existed on these curves at lower loads. The data near zero fitted to a 4th degree polynomial is shown in Figure 4.6.

This plot also serves as further evidence of the impact of experience and development of the method on the quality of data collection and analysis, as there is far less intersection and random variation in the COD lines in this figure compared to that for the previous cycle.

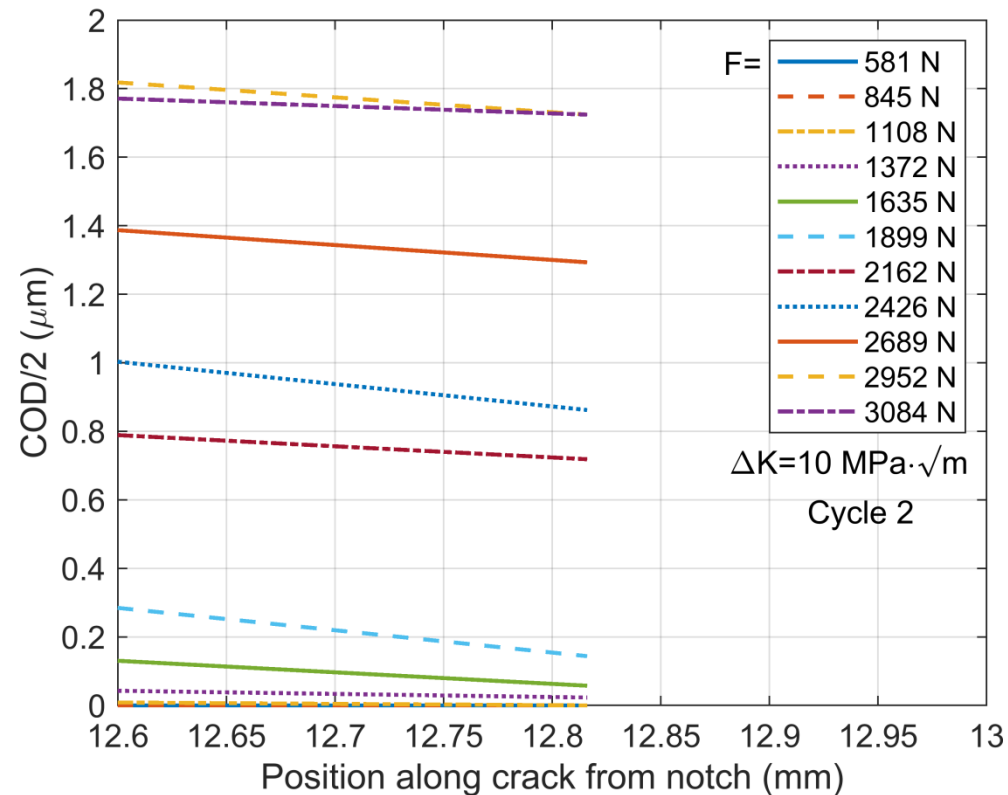


Figure 4.7: Crack tip focus for approximate opening load range identification

As it can be more clearly observed from Figure 4.7, which is a magnification of Figure 4.6 in the crack tip region, a load range between 1108 N & 1372 N can be identified in this plot when the crack is closed, with the 1372 N line running very close to the x axis, but not quite impacting it by the identified crack tip.

The implementation of 4th degree polynomials to map the less well defined lower load levels in this set of cycles also helped to clarify the opening load range, although the zoomed in images were generally less impacted by any erratic behavior in the load lines than the full image. Approaching the identified crack tip, data for each load level generally converged in a much more tidy fashion.

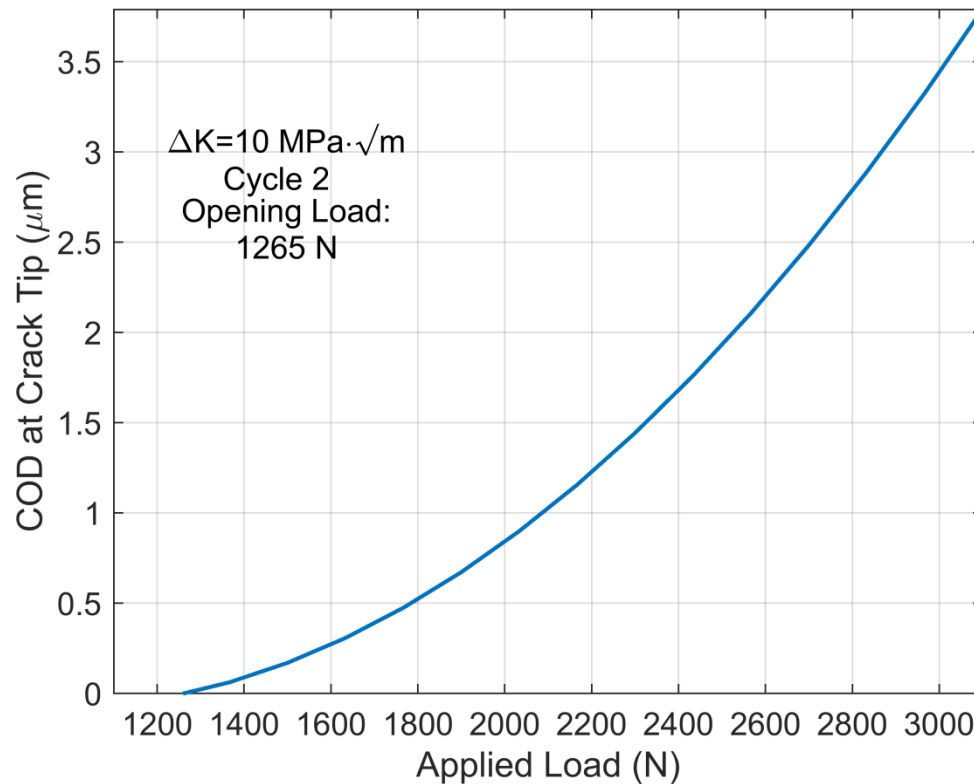
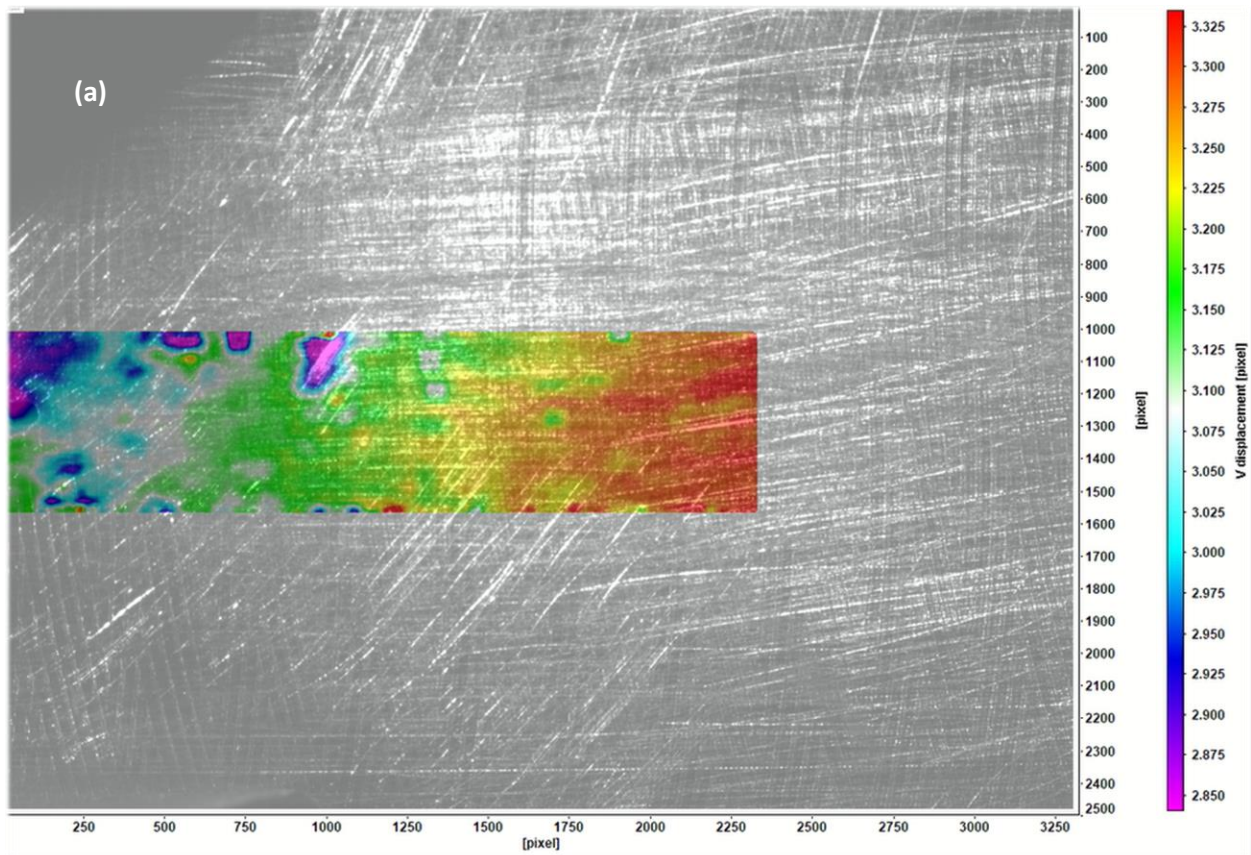
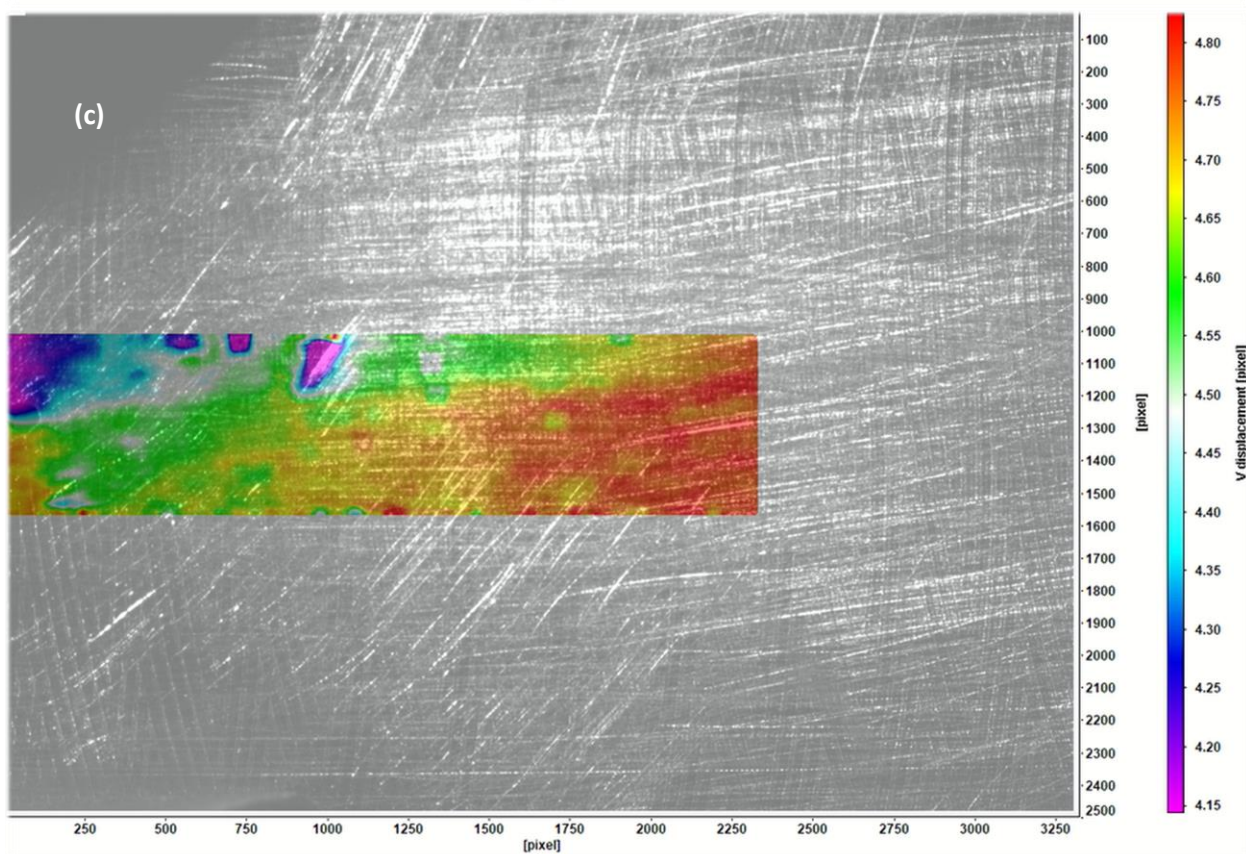
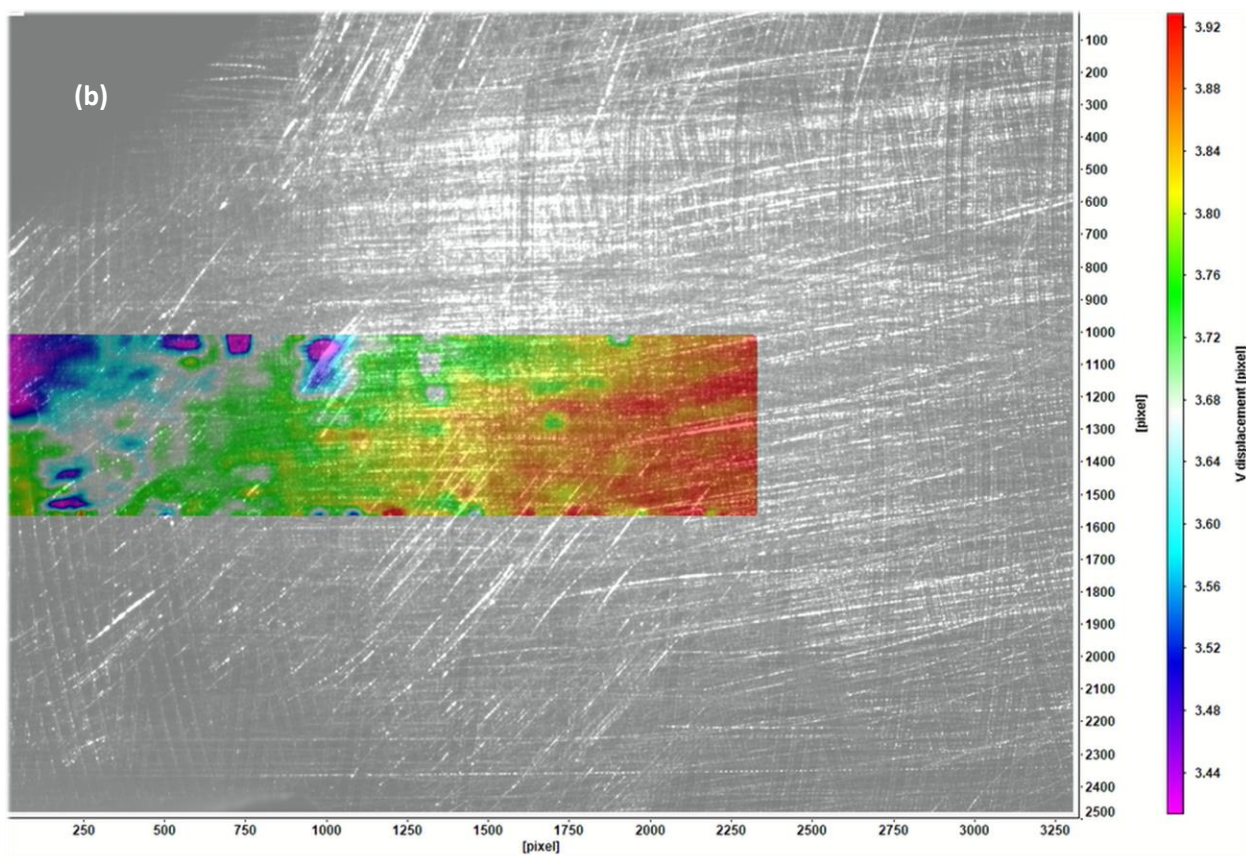


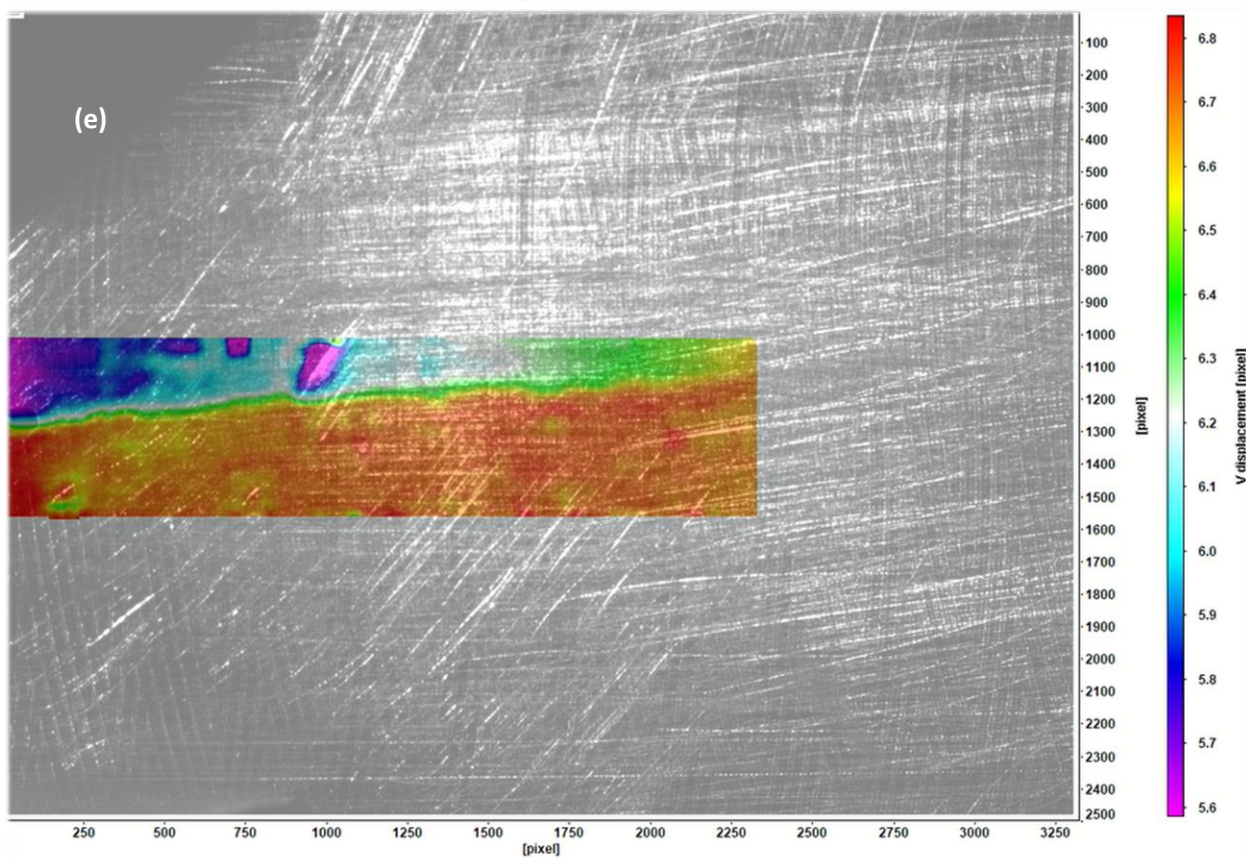
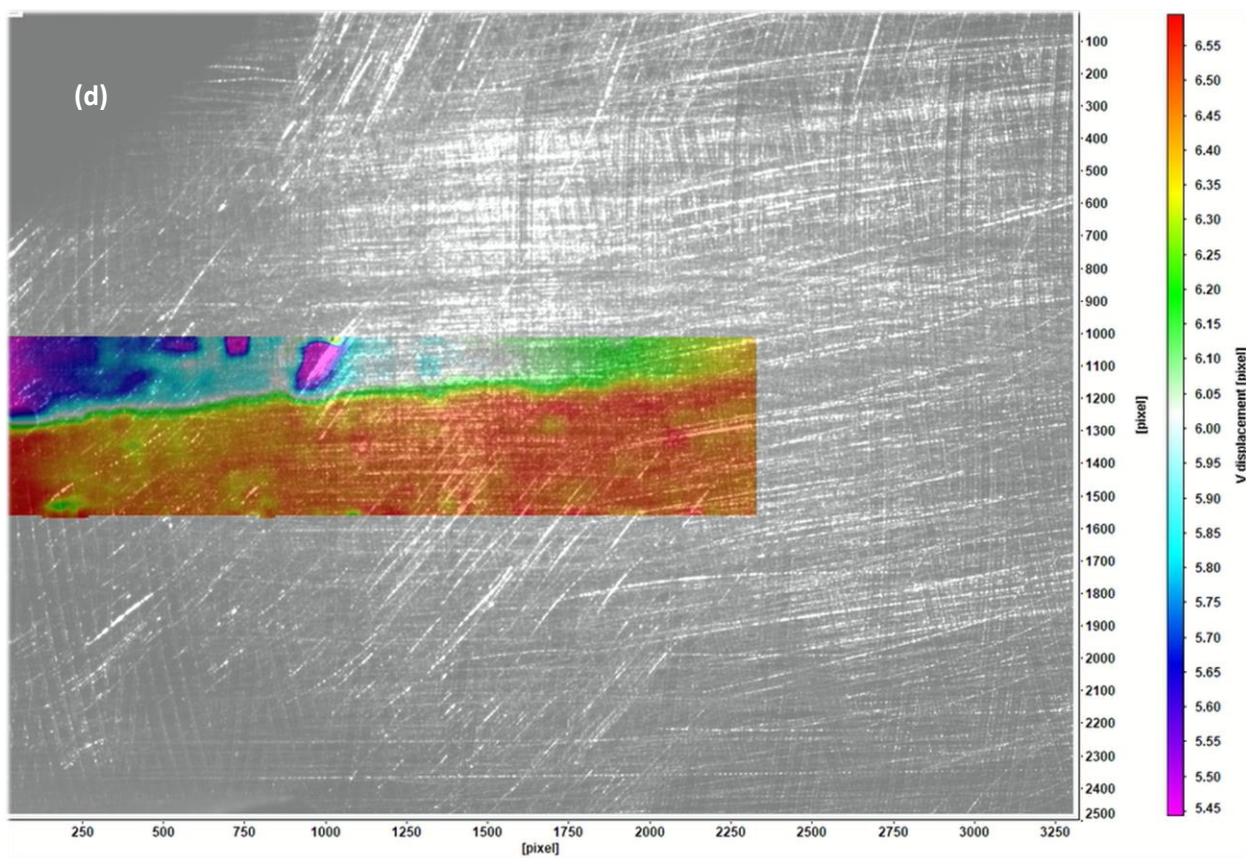
Figure 4.8: Variation of the crack tip opening displacement as a function of applied load during cycle 2.

Figure 4.8 shows the evolution of the COD at the crack tip with applied load. The curve plots the increase in crack tip COD for this cycle against applied load, and it shows an x-intercept of roughly 1265 N, which once again falls into the range displayed in the previous plot. The success of this plot in predicting an opening load within the range identified in the zoomed plot for this cycle establishes the potential viability of these plots as a method for identifying opening loads more precisely. Additionally, a trend can now be seen in this data set indicating that the COD value at the crack tip displays a concave up quadratic behavior with increasing load, which is consistent with the assumed behavior, as it makes sense that the value would grow exponentially until fracture as the specimen is pushed toward its limits.

4.1.3 Cycle 3







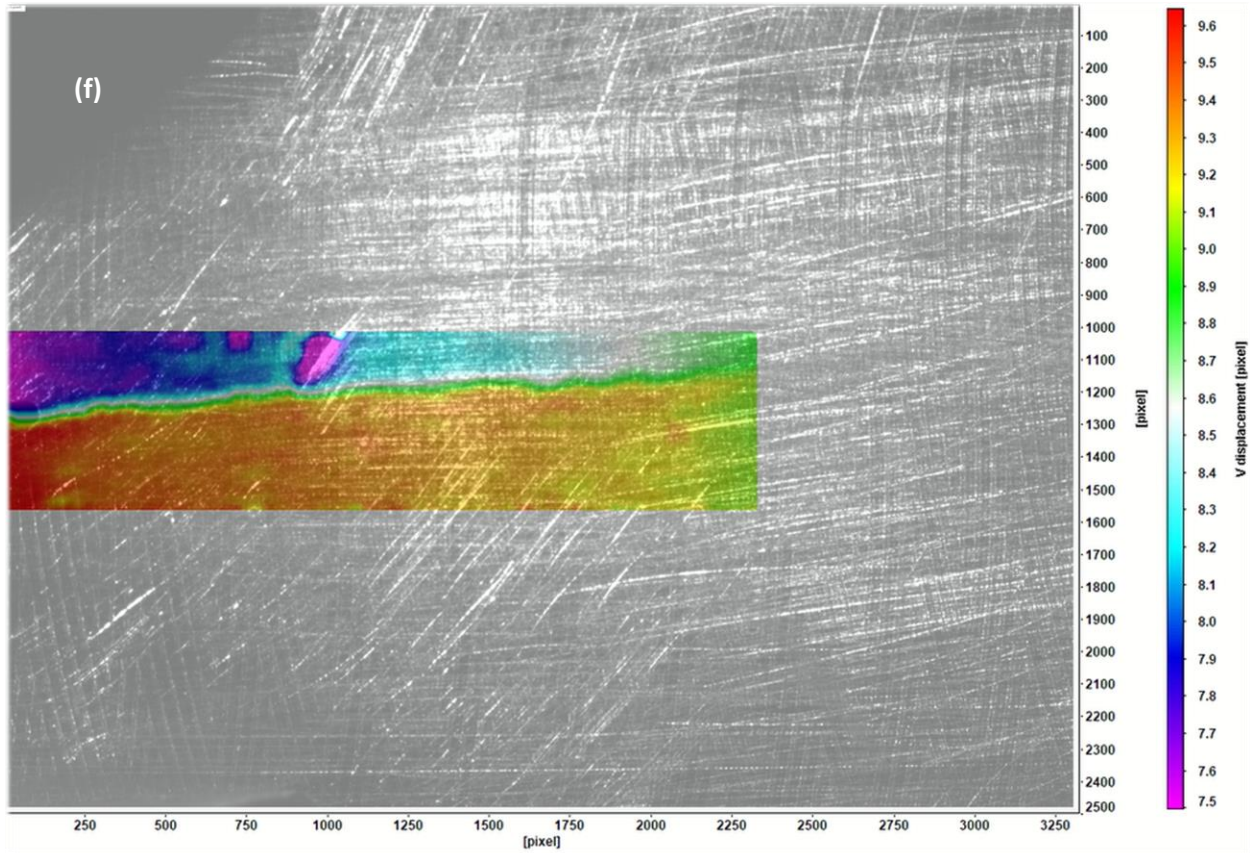


**Figure 4.9: Series of colored images showing the progression of the vertical displacements in the crack tip region at $\Delta K=10 \text{ MPa}\cdot\sqrt{\text{m}}$ Cycle 3 from minimum to maximum load
(a) $\sim 860 \text{ N}$, (b) $\sim 1140 \text{ N}$, (c) $\sim 1420 \text{ N}$, (d) $\sim 1980 \text{ N}$, (e) $\sim 2540 \text{ N}$, (f) $\sim 3100 \text{ N}$.**

Figure 4.9 shows the evolution of the displacements of each pixel in the near crack tip region during cycle 3 of measurements. Evident again in this set of images is the trademark early cycle noise of this data set. However, the crack plane remains clearly visible within the masked area, and it can be seen that the pixel scale on these images is consistent with the previous cycle's set of images, which is important for establishing that the scale is consistent within a given data set, and each data set can have a pixel to millimeter conversion value identified that applies to all of its pictures.

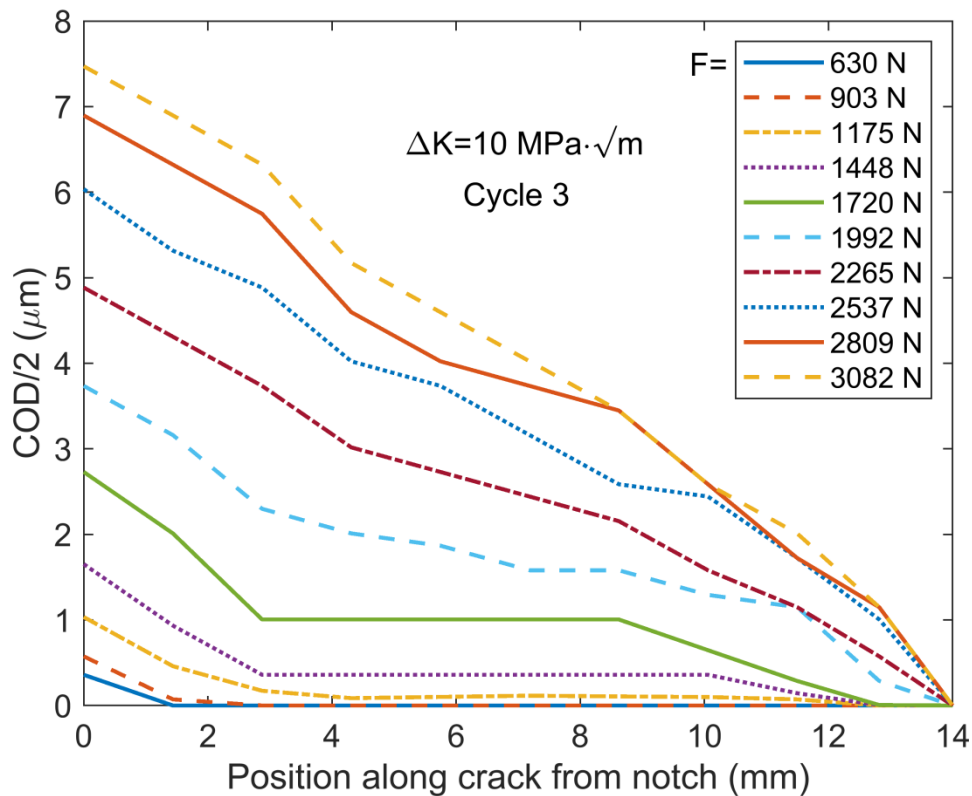


Figure 4.10: Half of the crack opening displacement (COD) evolution during the loading in cycle 3. The observed crack tip is located at horizontal position $x = 12.815 \text{ mm}$.

Figure 4.10 shows half of the COD progression with applied load. It should be noted that in this data set, curves associated with lower load levels demonstrate behavior in which COD is constant or relatively constant over a significant region of the crack length, i.e., roughly between positions $x = 3 \text{ mm}$ and $x = 10 \text{ mm}$. In reality, it is likely that these regions which demonstrate constant displacement values simply have a more gradual downward trend. If the location of interest existed within the constant regions, it would be important to reevaluate and refine the data to ensure a reading that is as accurate as possible. However, to define the rough shape and COD progression of the fracture, and considering the manual approach to identifying the COD values used in these cycles, the constant regions are acceptable.

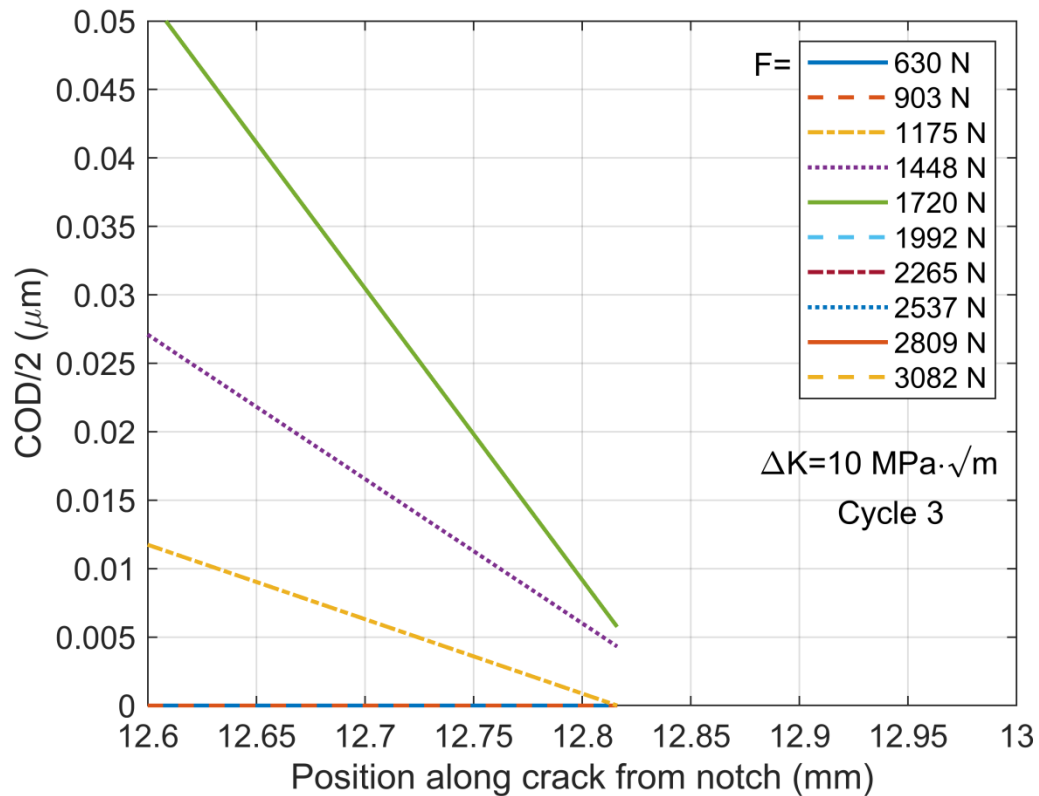


Figure 4.11: Crack tip focus for approximate opening load range identification.

Figure 4.11 shows a magnification of the previous plot in the crack tip region. The spacing between the various curves in these plots is somewhat more dramatic than in the previous two cycles, with a number of curves coming extremely close to the x-axis, and necessitating a high level of magnification to identify the opening load range. In this figure, it can be seen that the range exists between 1175 N and 1448 N.

It should also be noted that the load lines appear to increase the steepness of their approach to the x-axis as the associated load increases, helping to define a general fracture shape progression that appears somewhat akin to a zipper opening.

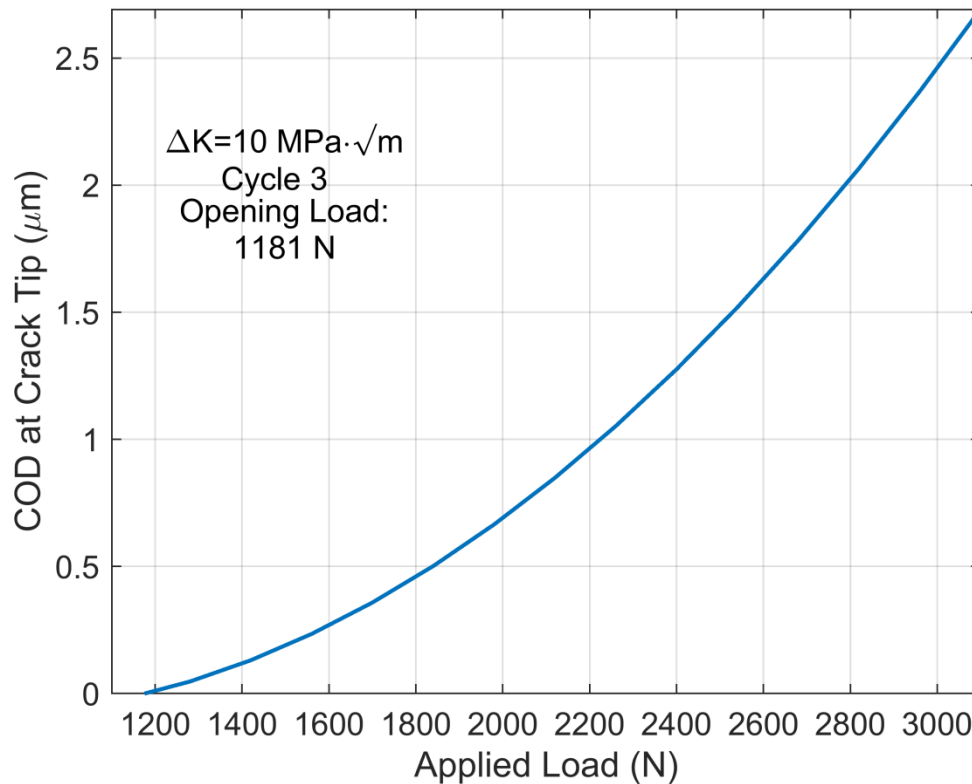


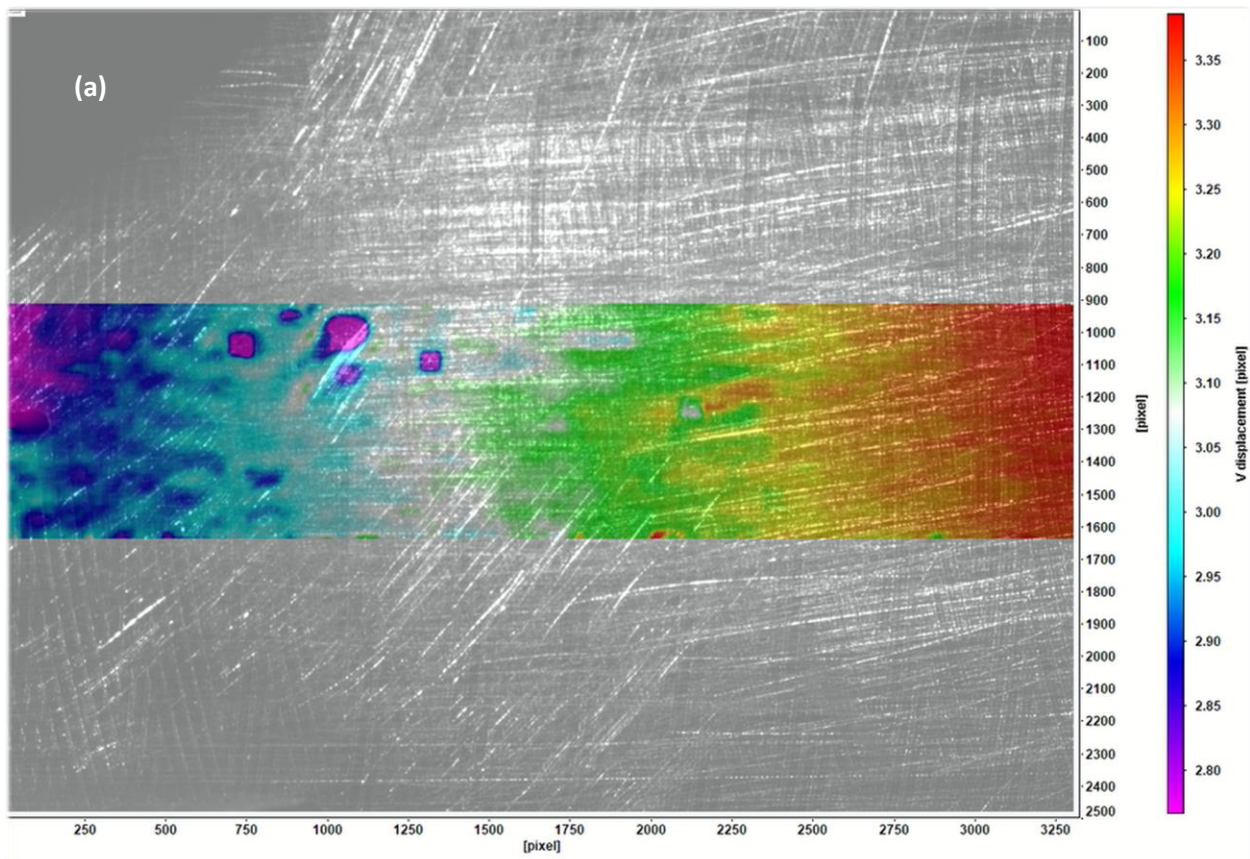
Figure 4.12: Variation of the crack tip opening displacement as a function of applied load during cycle 3.

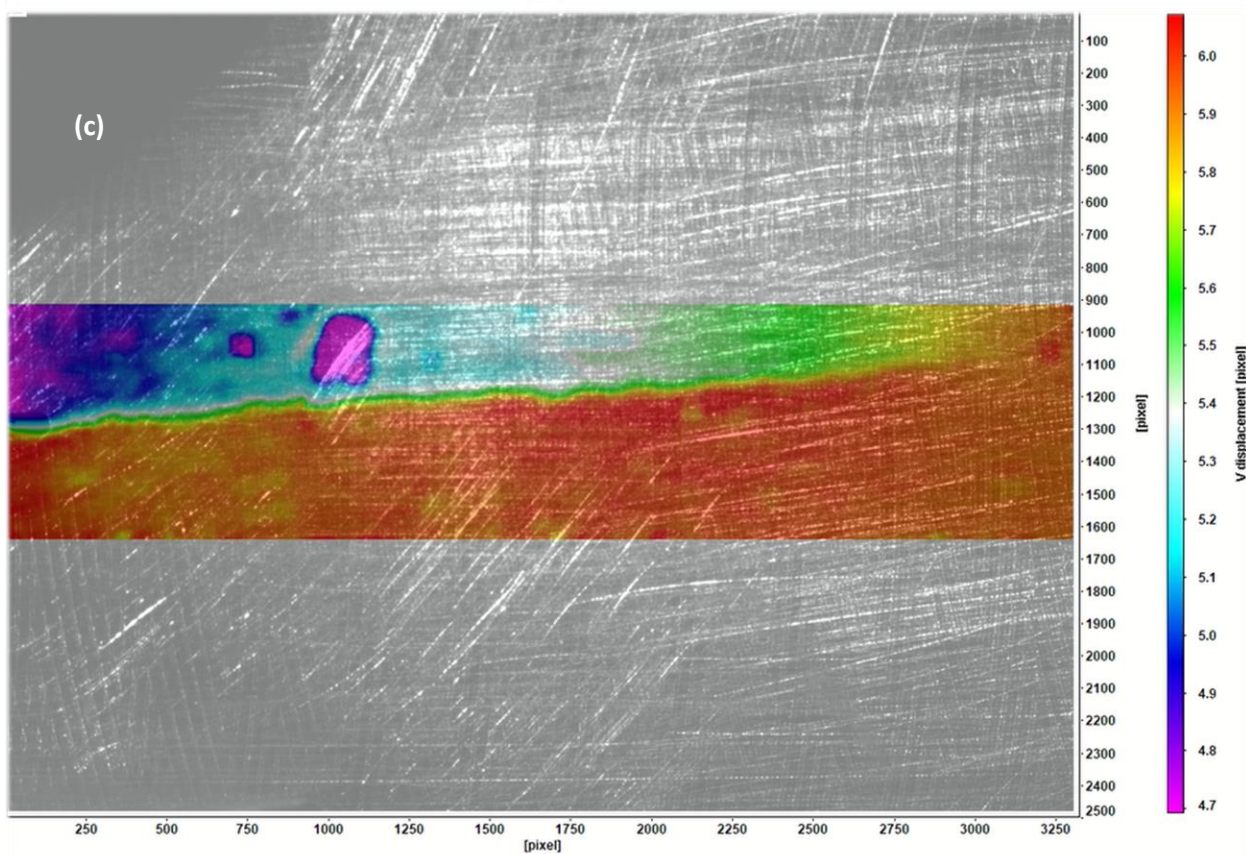
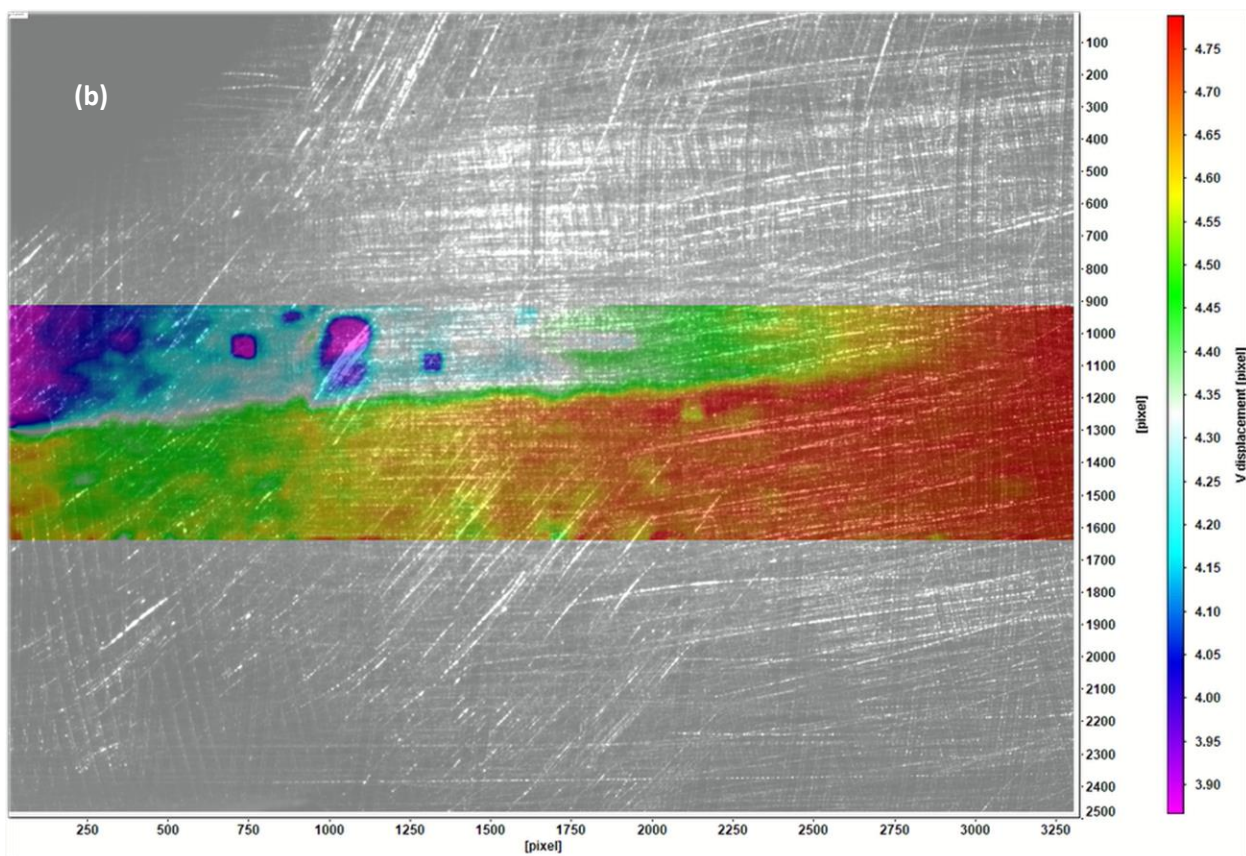
Figure 4.12 shows the variation of the crack opening displacement at the crack tip with applied load for cycle 3. Fitting the CTOD data against applied load displays an opening load of roughly 1181 N for this cycle, barely within the range displayed on the previous figure. It is possible that the closeness of this value to the lower end of the range (1175 N) is linked to the closeness of the curves to the x axis, or perhaps to the steepness of their approach to the crack tip.

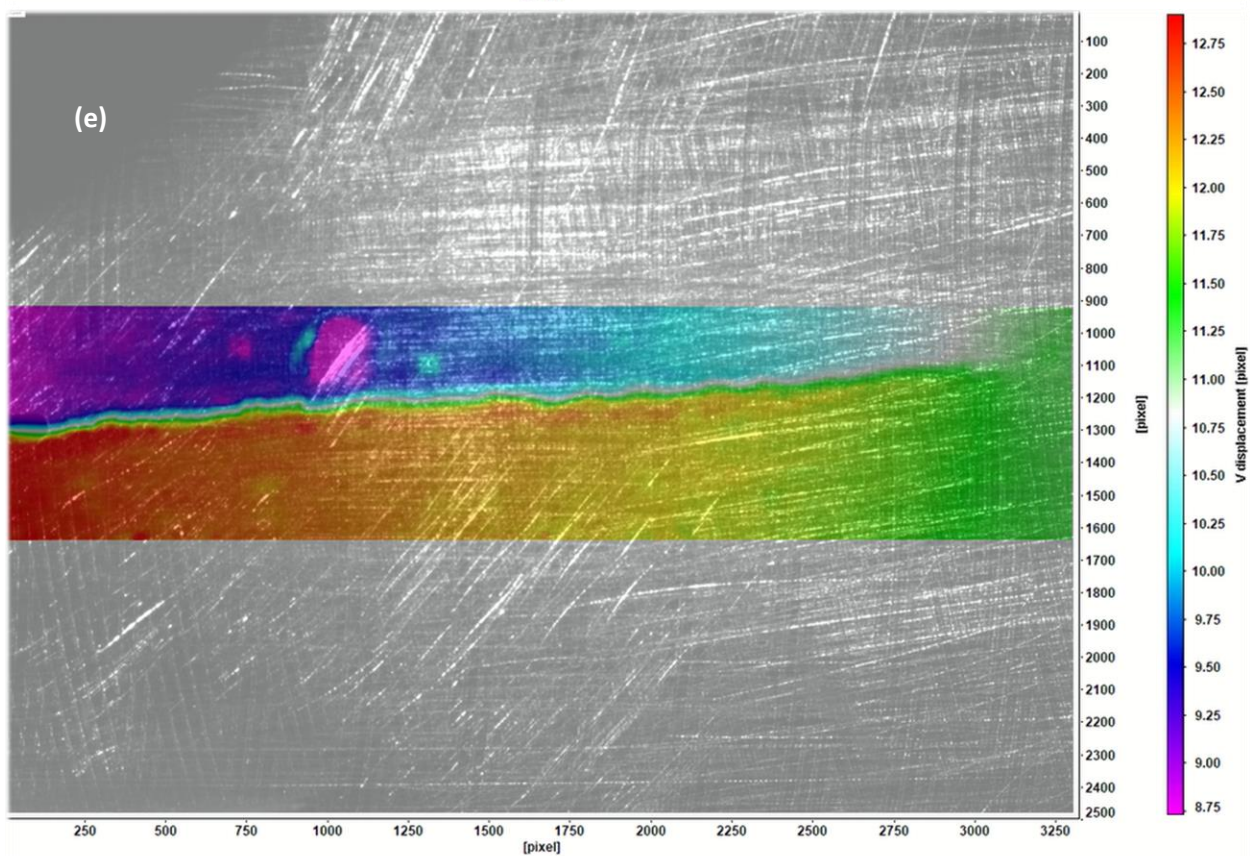
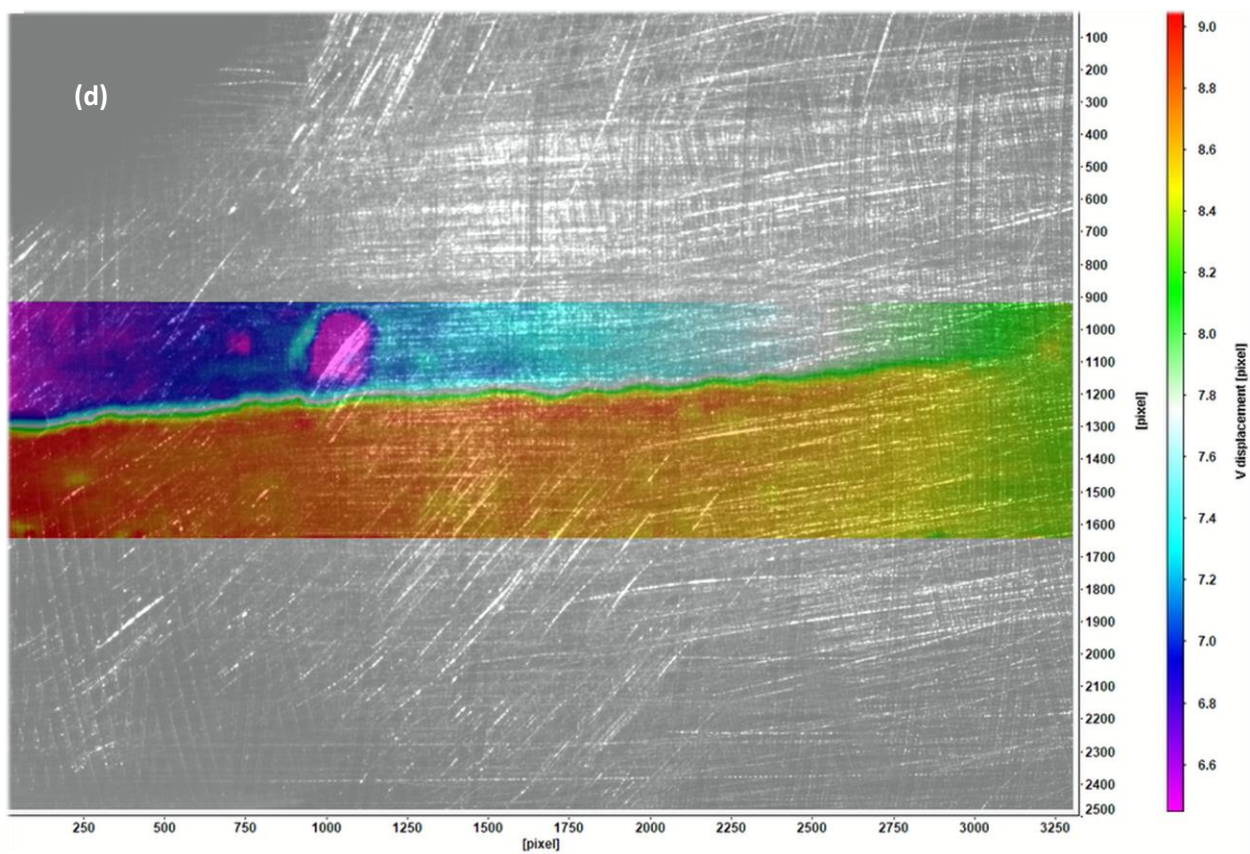
This plot continues the trend for this data set of concave up quadratic fits for the CTOD value. This is a very positive outcome, as all cycles in this data set had zoomed images and opening load plots in agreement, and additionally all opening load plots conformed to the assumed behavior of a fracture. With this knowledge in hand, it was determined that the specimen could be advanced to the next level, $\Delta K=15 \text{ MPa}\cdot\sqrt{\text{m}}$.

4.2 $\Delta K=15 \text{ MPa}\cdot\sqrt{\text{m}}$

4.2.1 Cycle 1







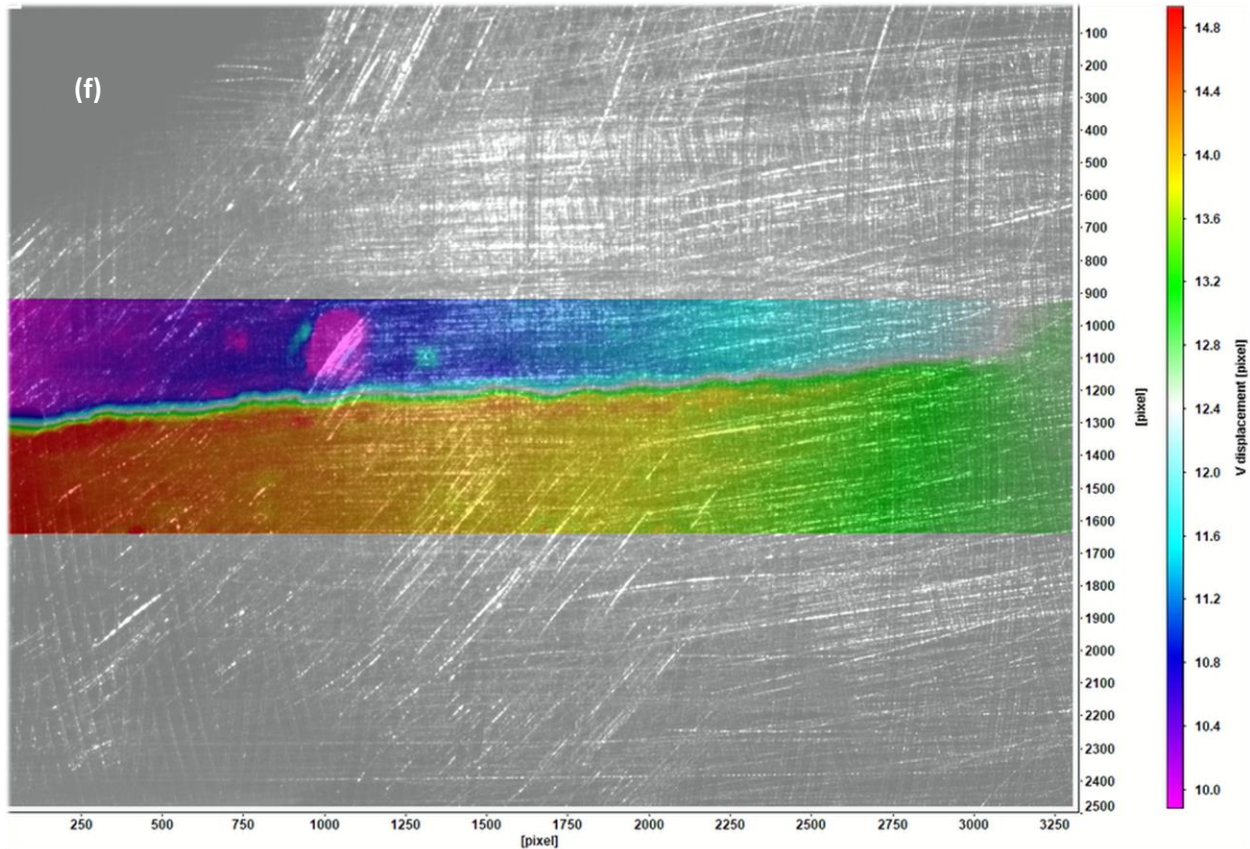


**Figure 4.13: Series of colored images showing the progression of the vertical displacement of each pixel at $\Delta K=15$ MPa· \sqrt{m} Cycle 1 from minimum to maximum load
(a)=~833 N, (b)=~1100 N, (c)=~1367 N, (d)=~1900 N, (e)=~2433 N, (f)=~3100 N**

Figure 4.13 shows the evolution of the crack opening displacements for $\Delta K=15$ MPa· \sqrt{m} and cycle 1. At this point in the project, the use of the colored images to gather data was coming into its own. However, it was determined that the old method of manually calculating displacement values at several x values along the crack length, each for several load values, would be far too time consuming as the crack grew. Fortunately, it became apparent that for a given point on the x-axis, displacement with increasing load would follow a trend that could be fit to a curve. Therefore, going forward, the fracture growth mapping plots were developed by producing separate displacement vs. time vectors for points above (top) and below (bottom) the crack plane, with a similar number of x values to previous data sets, but fewer load values. These vectors were then fit depending on their shape, and the fit curves of given top and bottom x values were compared to develop displacement approximations for a larger data set with less overall work. This resulted in much smoother plots.

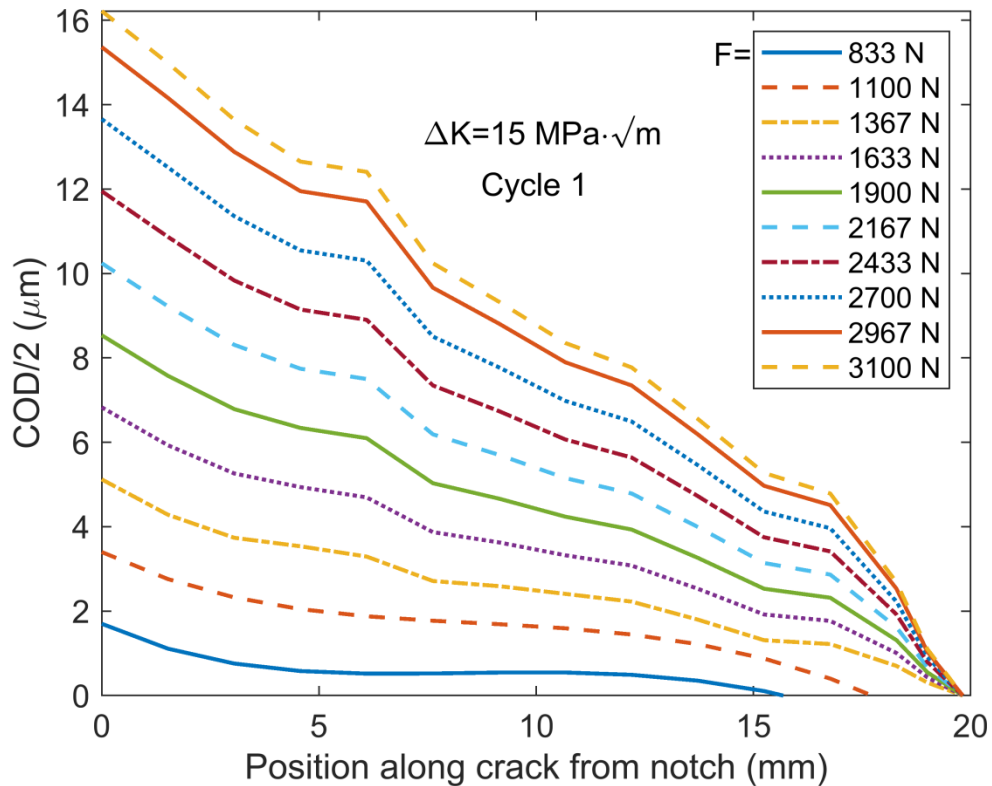


Figure 4.14: Half of the crack opening displacement (COD) evolution during the loading in cycle 1. The observed crack tip is located at horizontal position $x = 19 \text{ mm}$.

From Figure 4.14, it can be seen that the crack is much more open at $\Delta K = 15 \text{ MPa}\cdot\sqrt{\text{m}}$, and therefore it can be predicted that the opening load will be lower. In order to make sure these representations of crack opening shape matched with what was observed in the colored images, as well as with the opening load from the CTOD vs. load figure developed for the cycle, more effort had to go into ensuring a good fit curve was developed for the data at critical load levels.

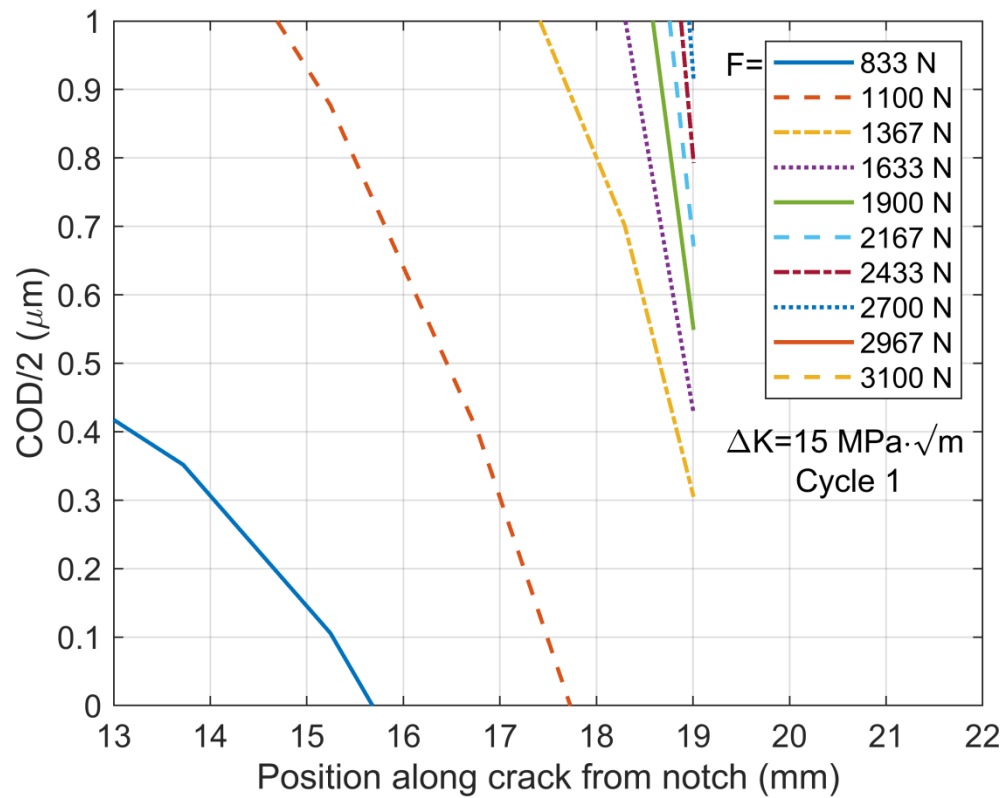


Figure 4.15: Crack tip focus for approximate opening load range identification.

From the zoomed image in Figure 4.15, it can be observed that the curves approach the x axis at a much steeper angle near the crack tip than in previous similar figures, almost overlapping with each other as they approach the end of the crack. A range for opening load between 1100 N and 1367 N can be identified in this plot.

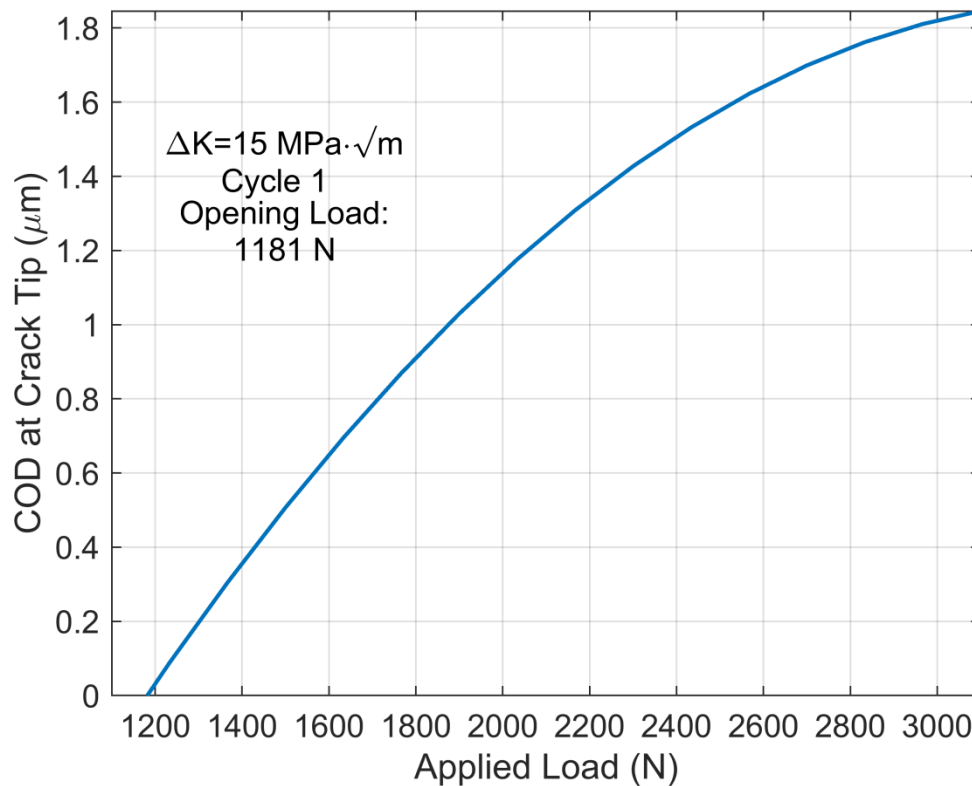
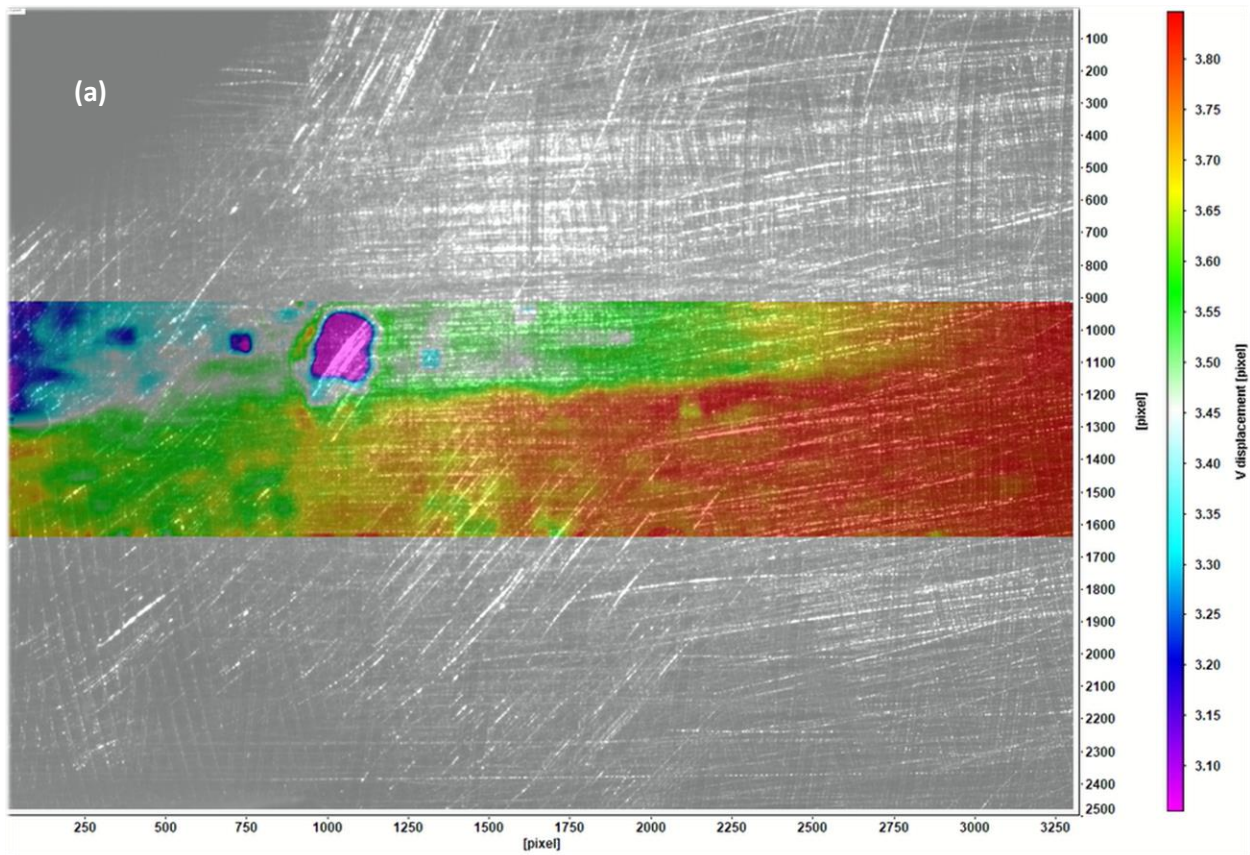
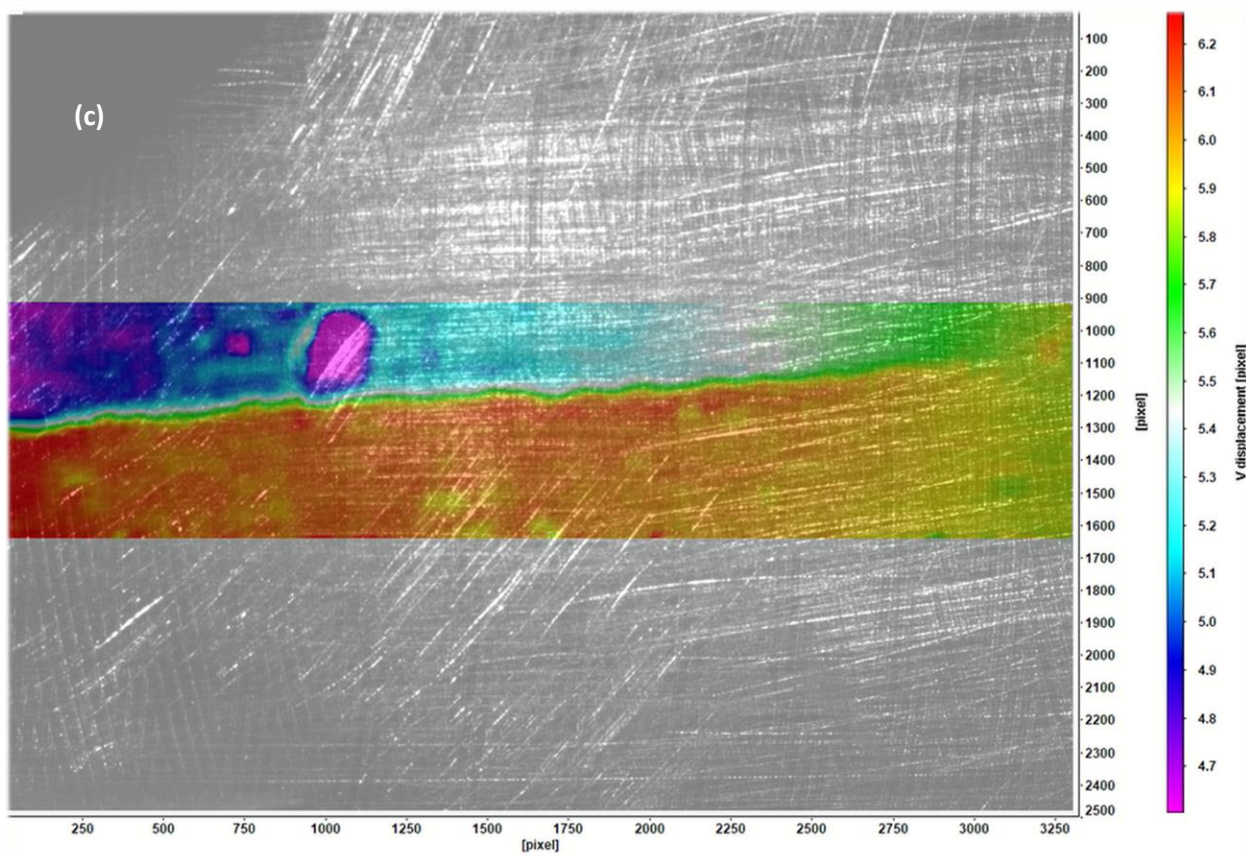
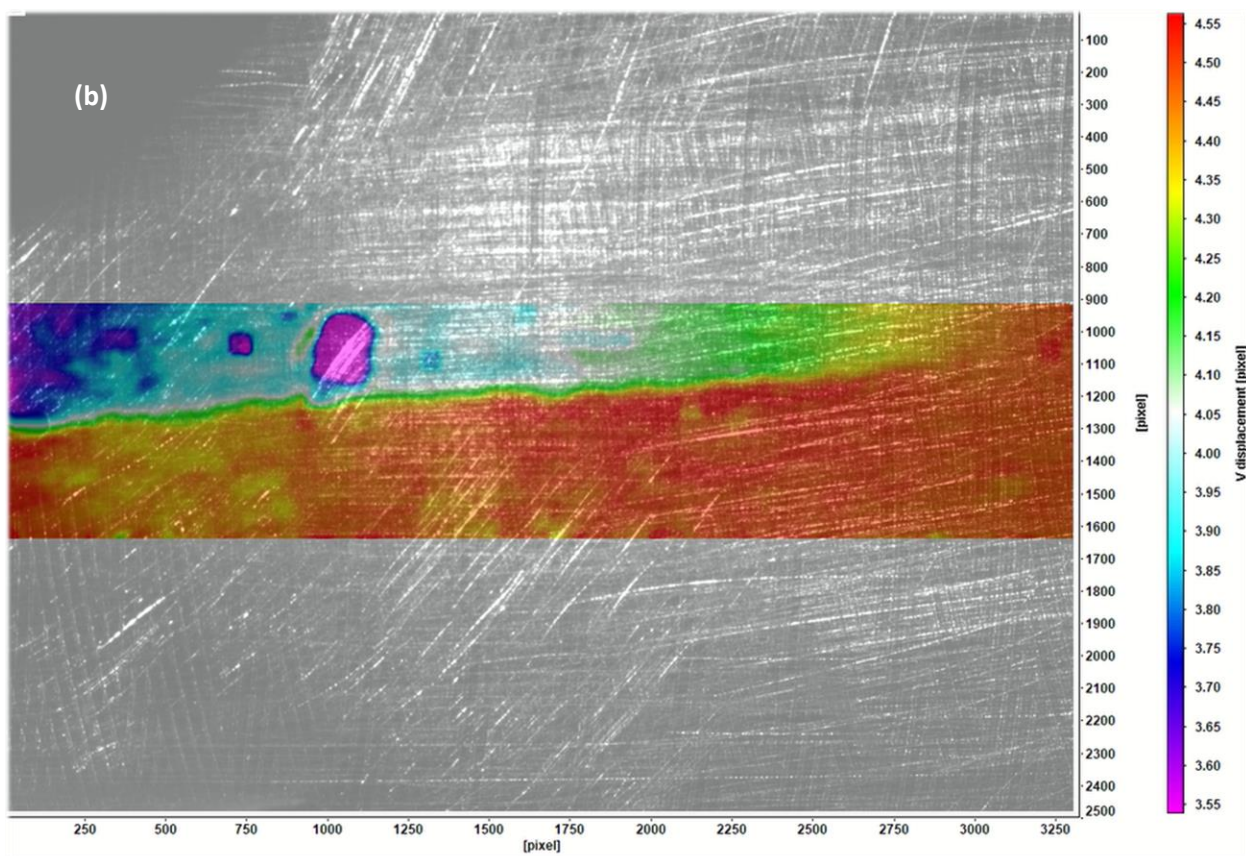


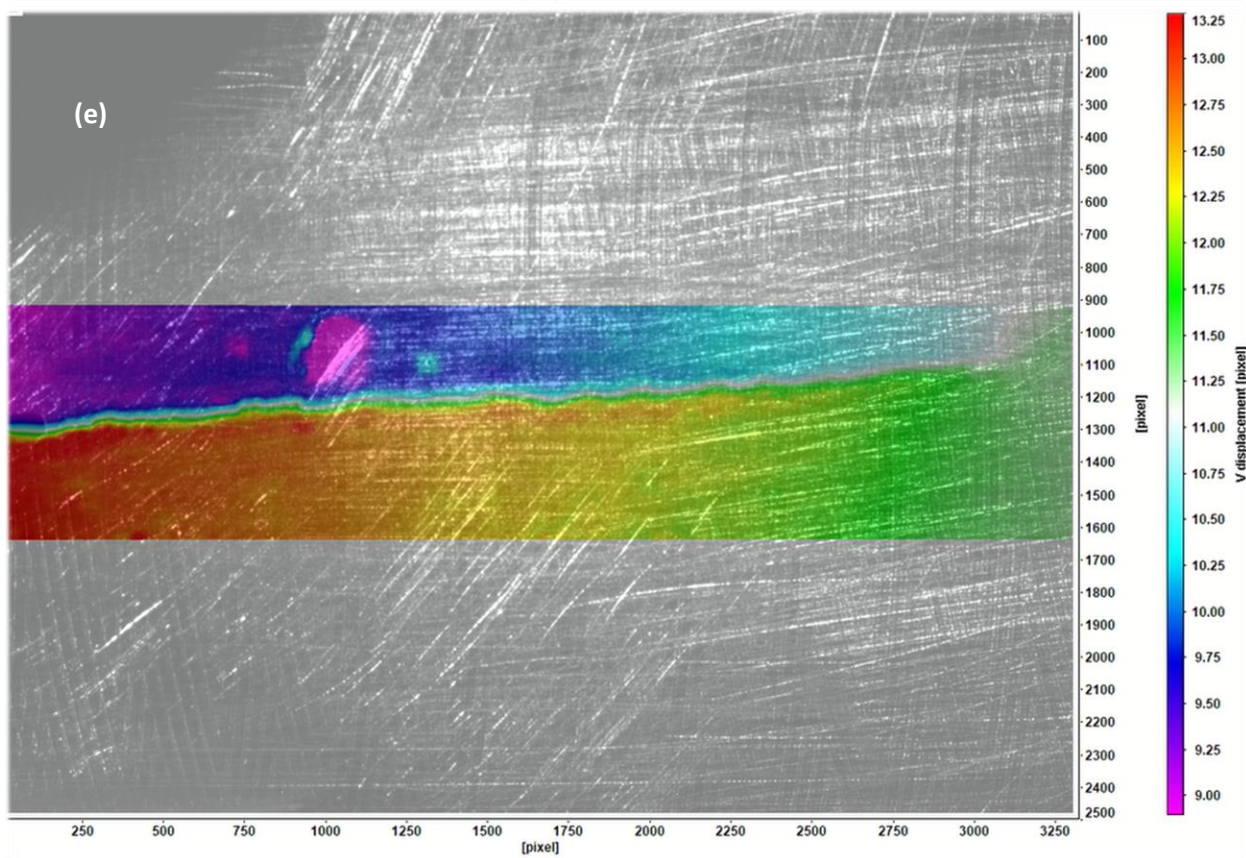
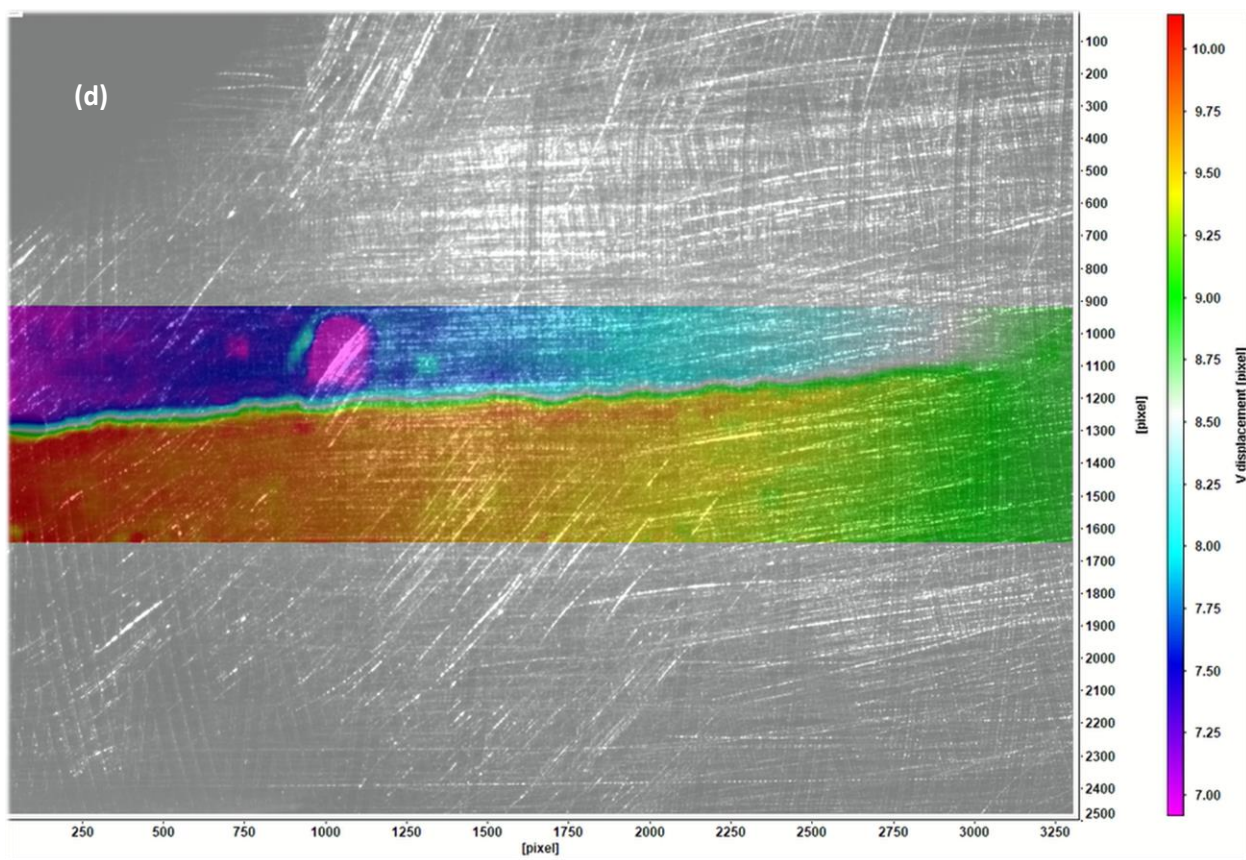
Figure 4.16: Variation of the crack tip opening displacement as a function of applied load during cycle 1.

The CTOD vs. load plot in Figure 4.16 shows an opening load of 1181 N for this cycle, which is lower than the average value for the $\Delta K=10 \text{ MPa}\cdot\sqrt{\text{m}}$ data set, as predicted. However, it is important to note that while the previous figures of this type showed concave up behavior, which fits with the natural assumption that displacement will grow with increasing load until the point of fracture, this figure shows concave down behavior. While this is how the relative data points behaved in this cycle up to 3100 N, it is possible that the behavior does not continue to perfectly match this curve after that point. It is not feasible that displacement would go below the peak in this figure as load increases beyond 3100 N.

4.2.2 Cycle 2







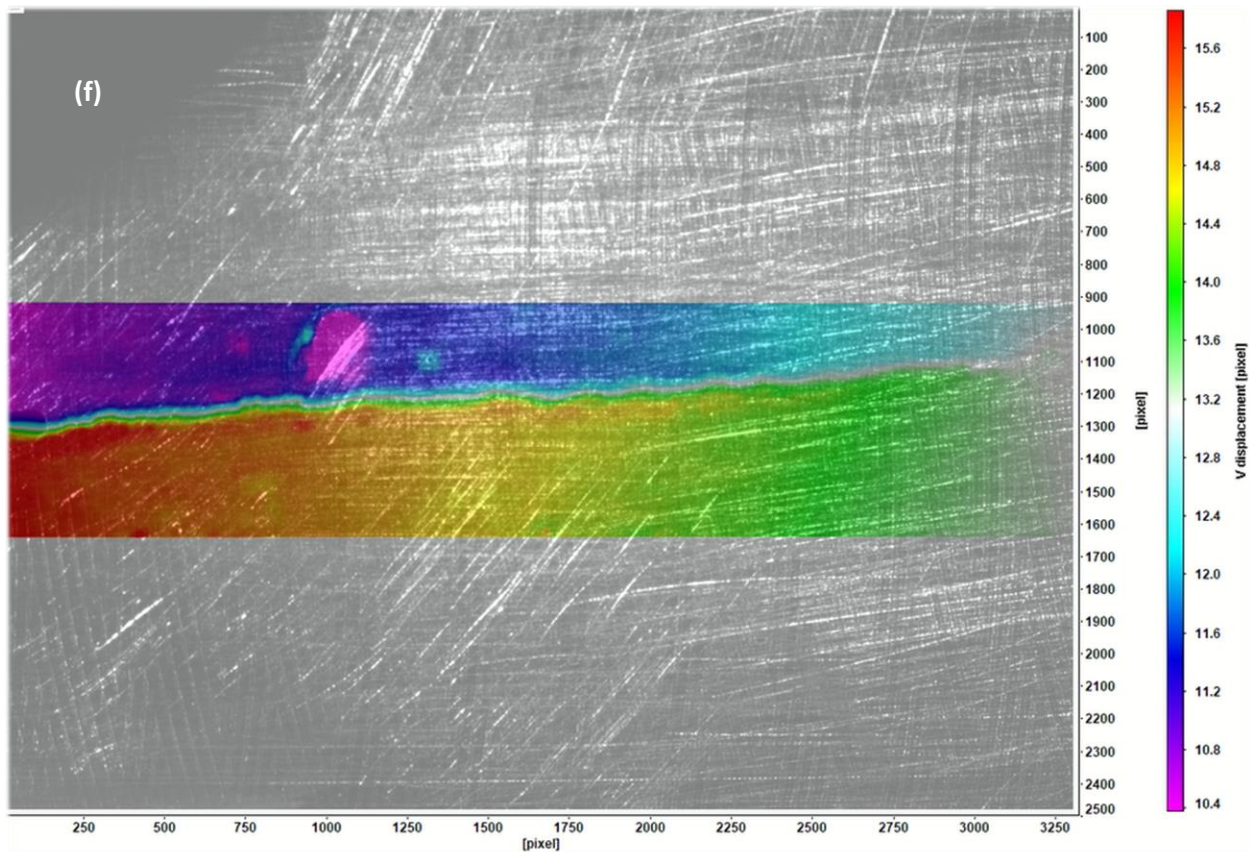


**Figure 4.17: Series of colored images showing the progression of vertical displacement for each pixel at $\Delta K=15$ MPa·√m
Cycle 2 from minimum to maximum load**

(a)=~833 N, (b)=~1100 N, (c)=~1367 N, (d)=~1900 N, (e)=~2433 N, (f)=~3100 N

This cycle stands as a good example of the challenges that can come up in this analysis method. While color differentials are easy to identify along the crack, they become less distinct around the crack tip, as the crack shape suddenly closes toward a very low COD value. At the identified crack tip in this image, both the top and bottom of the fracture exist right on the edge of the colorless region, so it is important to consider them in context of the colors that lead up to that point, identifying the top of the crack as existing toward the blue edge of the colorless region on the scale to the right of the pictures, and the bottom being on the green edge of the colorless region on that scale. In so doing, a very small displacement difference can be identified. Recommendations for improving identification of such minute differences will be discussed later on in this document.

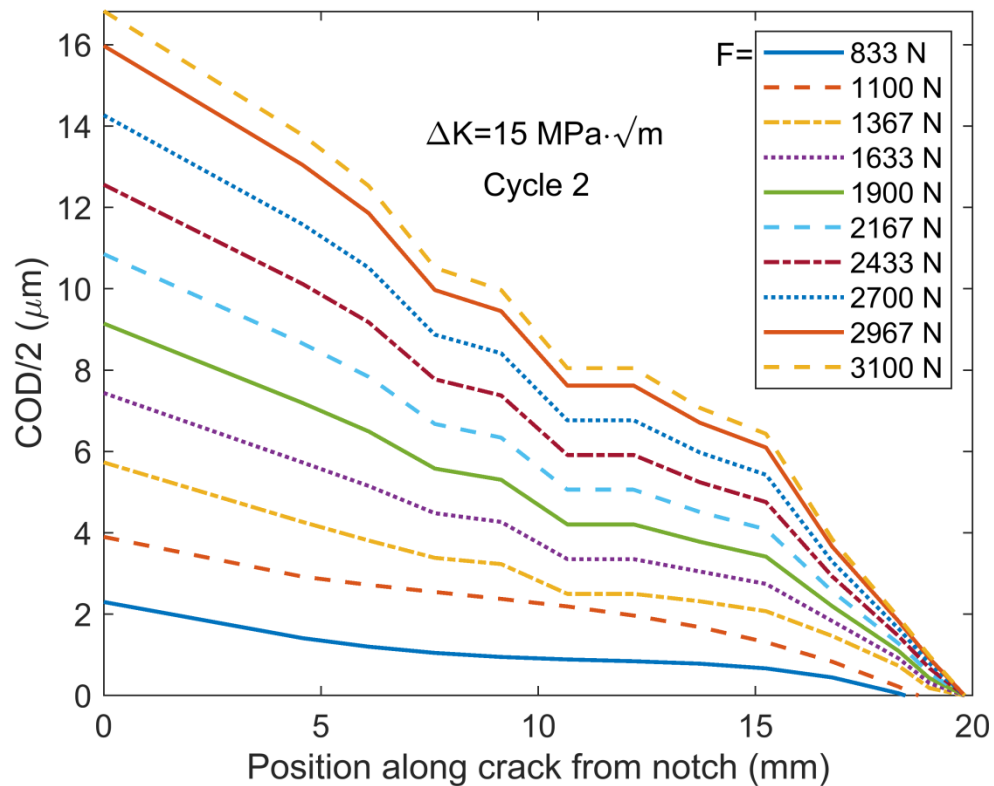


Figure 4.18: Half of the crack opening displacement (COD) evolution during the loading in cycle 2. The observed crack tip is located at horizontal position $x = 19$ mm.

Figure 4.18 shows half of the COD versus applied load. This figure also displays the crack being more open at lower load levels than in the previous data set, with a very small portion of the crack tip being closed at low load values. Progression of the crack opening displacement of the fracture is still slow enough such that the opening load is still significant. Again, the shape of the crack tends toward more of an unzipping motion, as opposed to a V shape, establishing consistency between the crack shape in this data set, and that in the last.

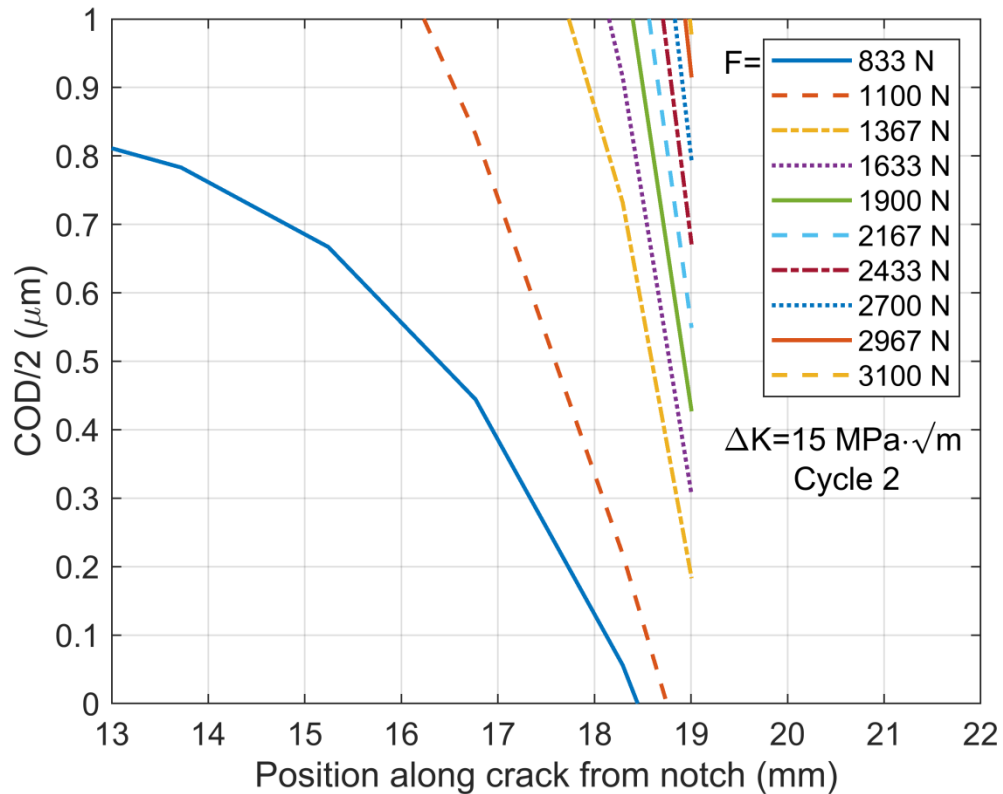


Figure 4.19: Crack tip focus for approximate opening load range identification.

Figure 4.19 displays an opening load range of 1100 N to 1367 N, indicating that the opening load for this cycle is similar to the value determined for Cycle 1. This demonstrates a valuable consistency for this data set. The lower load lines exist much closer to the higher load lines in this cycle than in the last. This serves as an indication of how open the crack is from the beginning of the cycle, and consequently, indicates that the opening load will be lower than it was in the previous cycle.

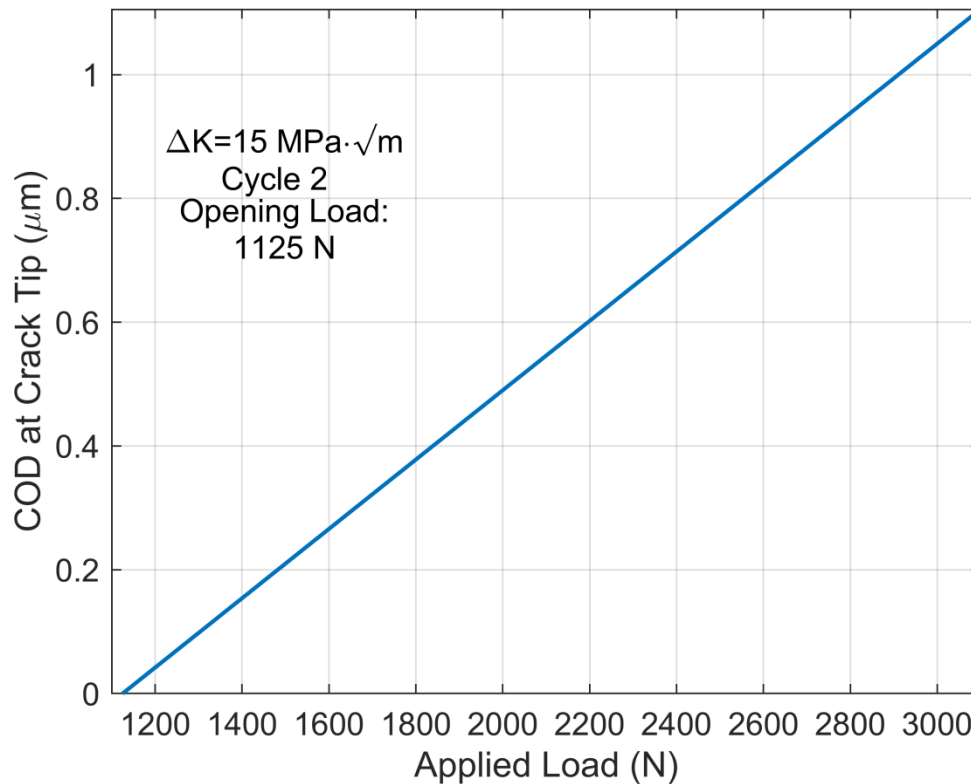
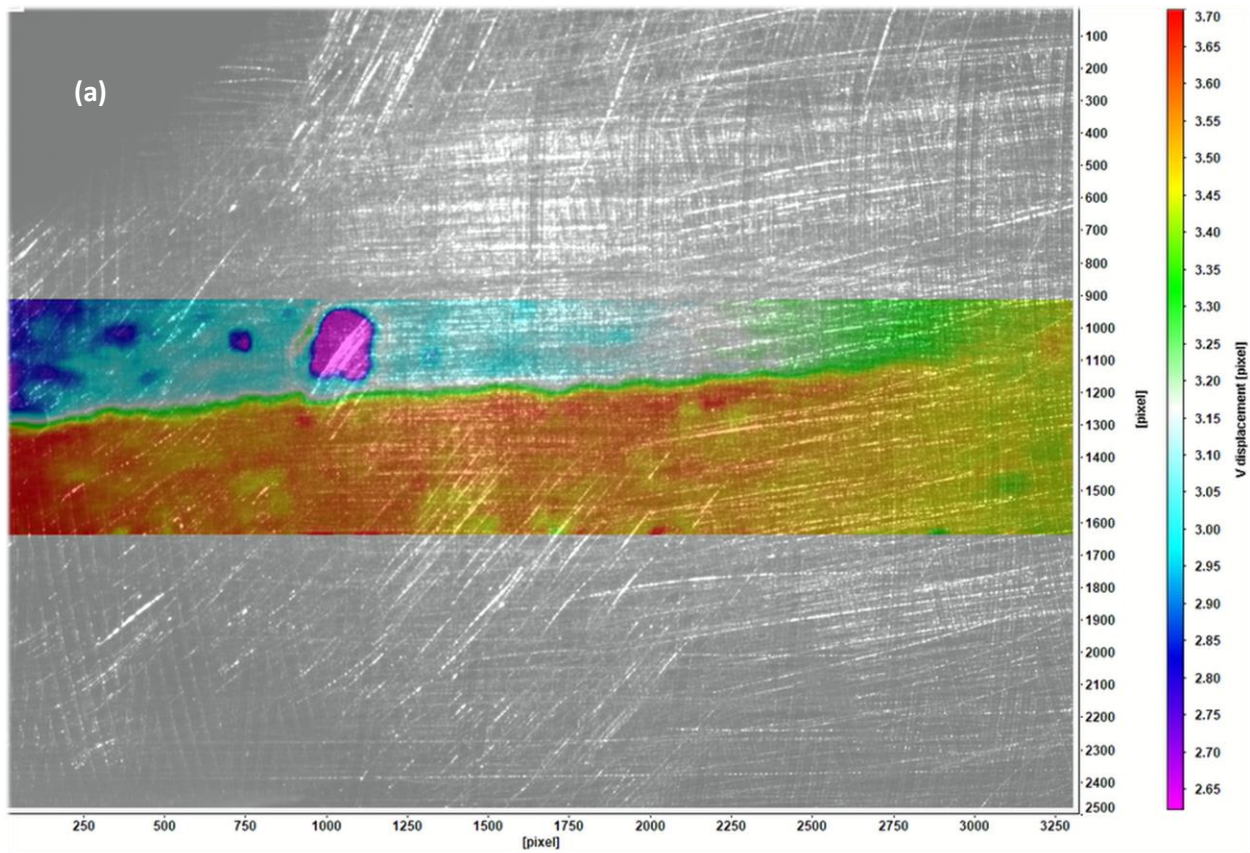


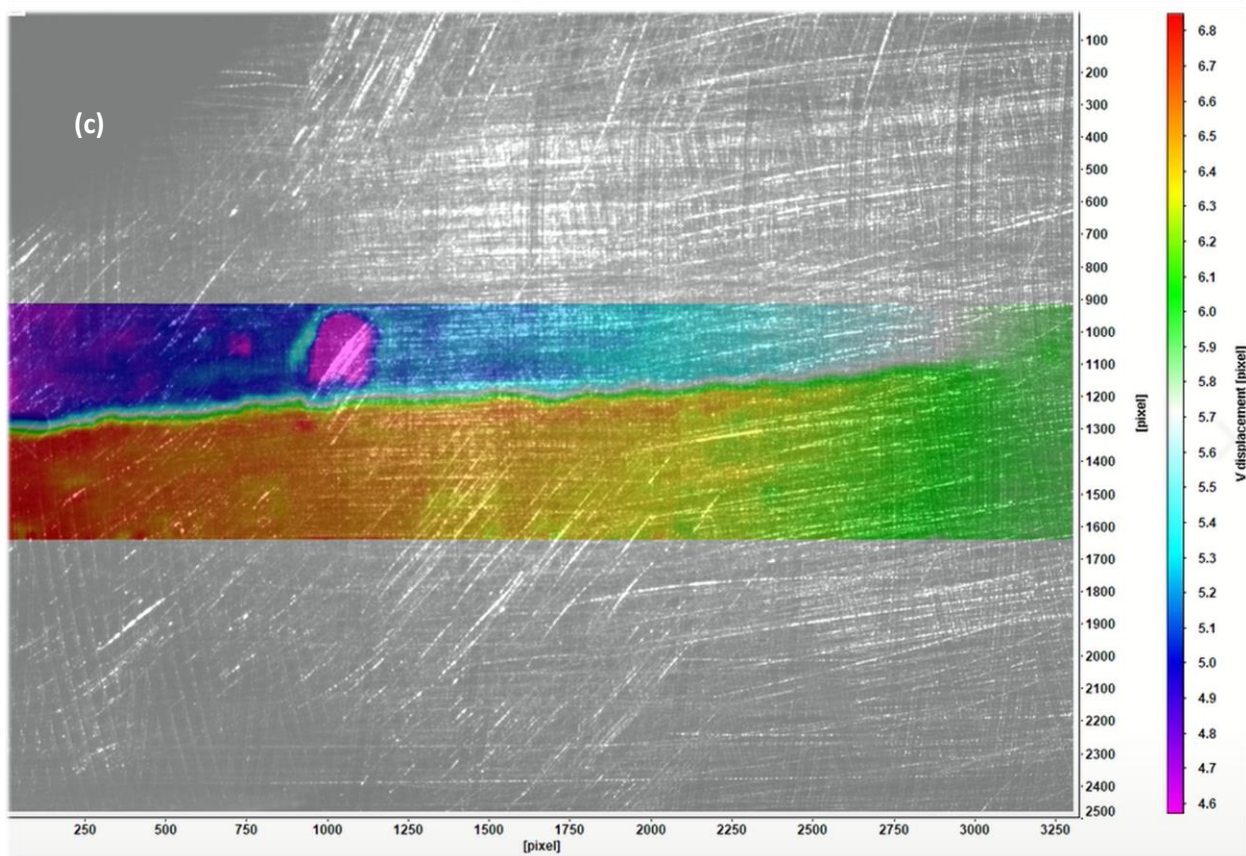
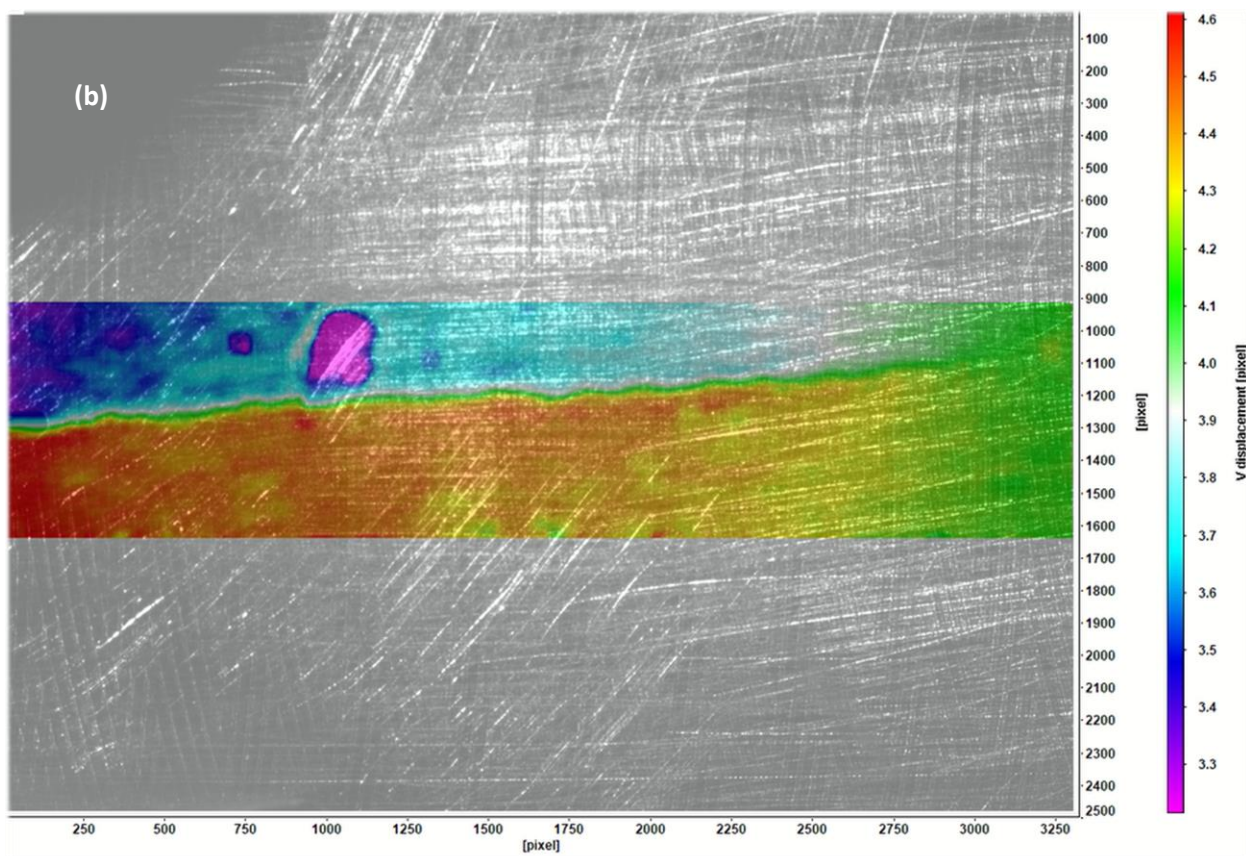
Figure 4.20: Variation of the crack tip opening displacement as a function of applied load during cycle 2.

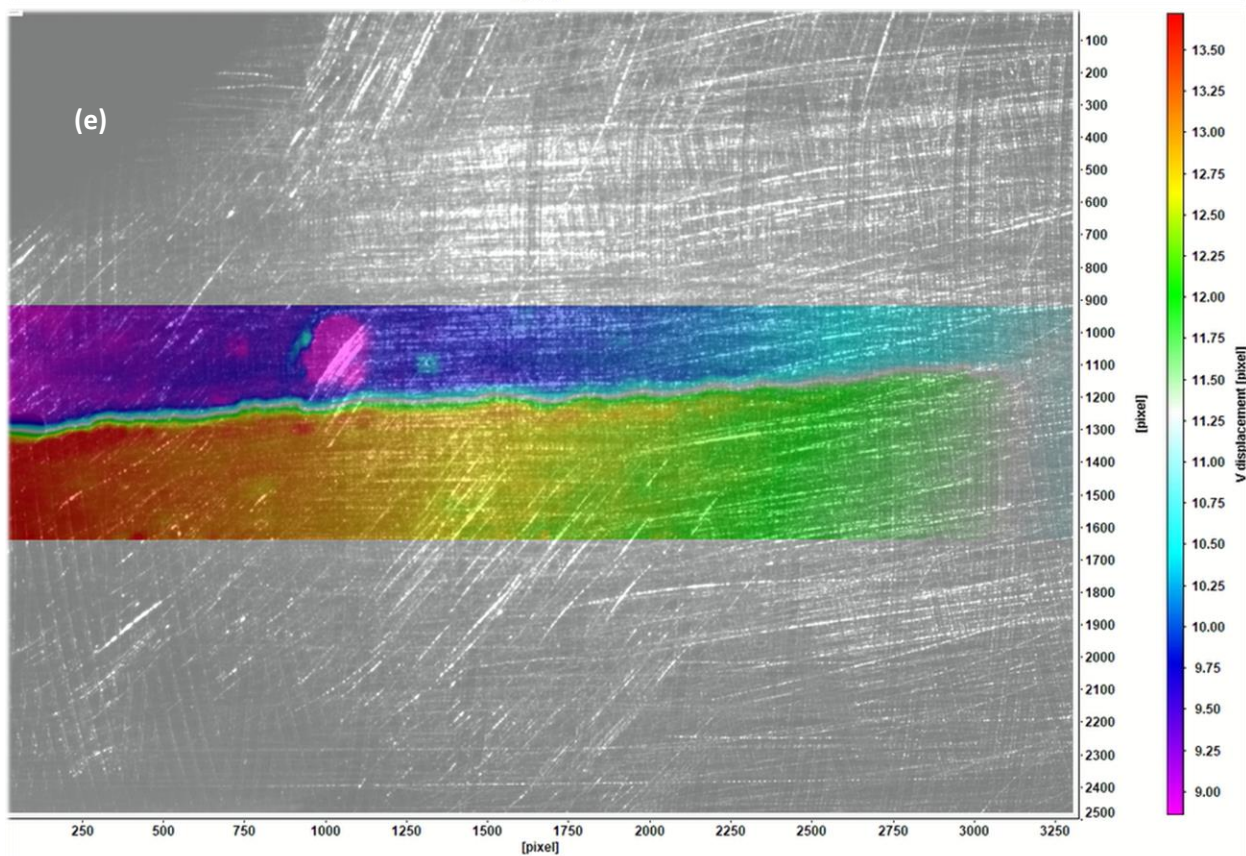
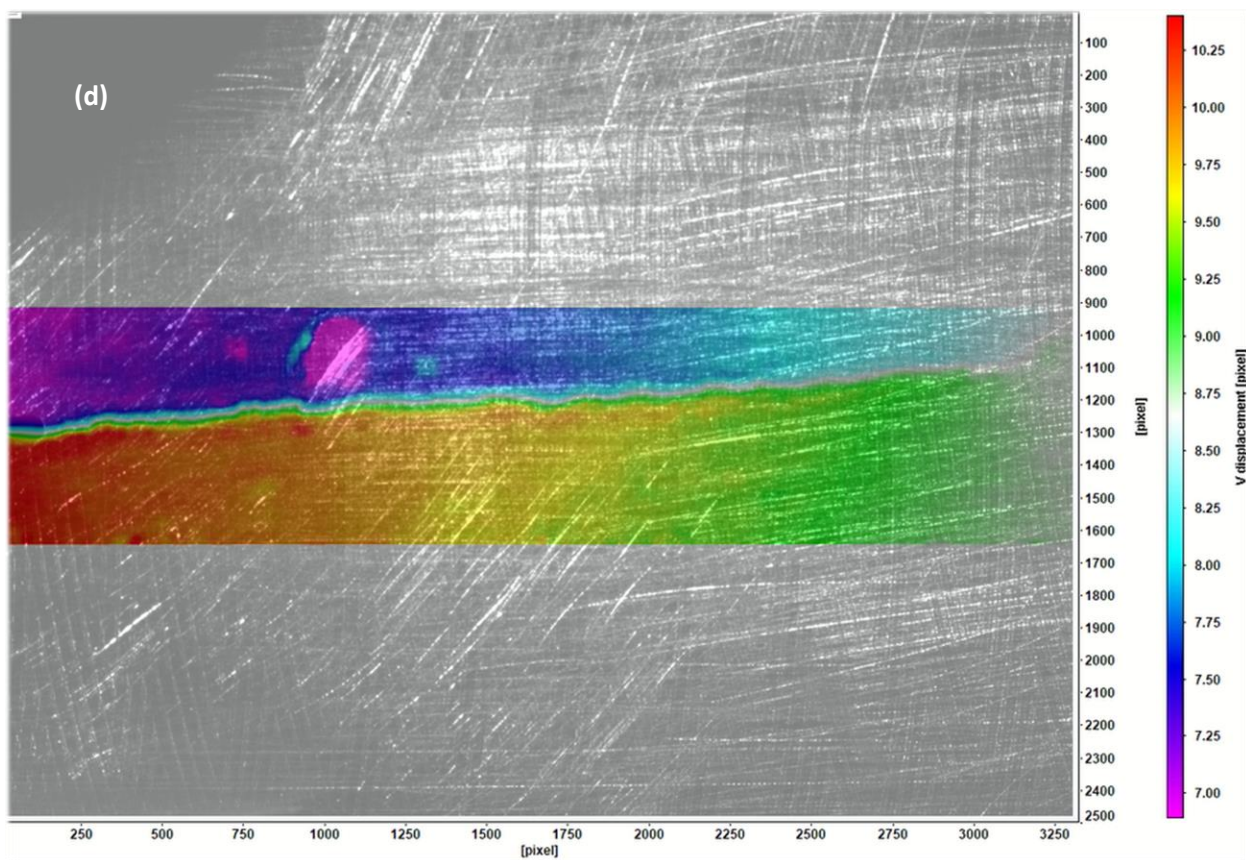
Interestingly, the COD at the crack tip evolution with applied load plotted in Figure 4.20 exhibits a nearly linear behavior with increasing load. It intersected the x axis at 1125 N for the opening load, a value fairly close to that for Cycle 1, and within the predicted range for this cycle.

The near linearity of this curve demonstrates a sharp contrast to the shape of the opening load plot in the previous cycle, establishing an inconsistency which would benefit from further investigation with more cycles, to try and determine the factors that could influence a change in their shape during testing, and to help produce more consistent results. Regardless of the shape of the plot, the important information in this project is the intersection point for identification of the opening load.

4.2.3 Cycle 3







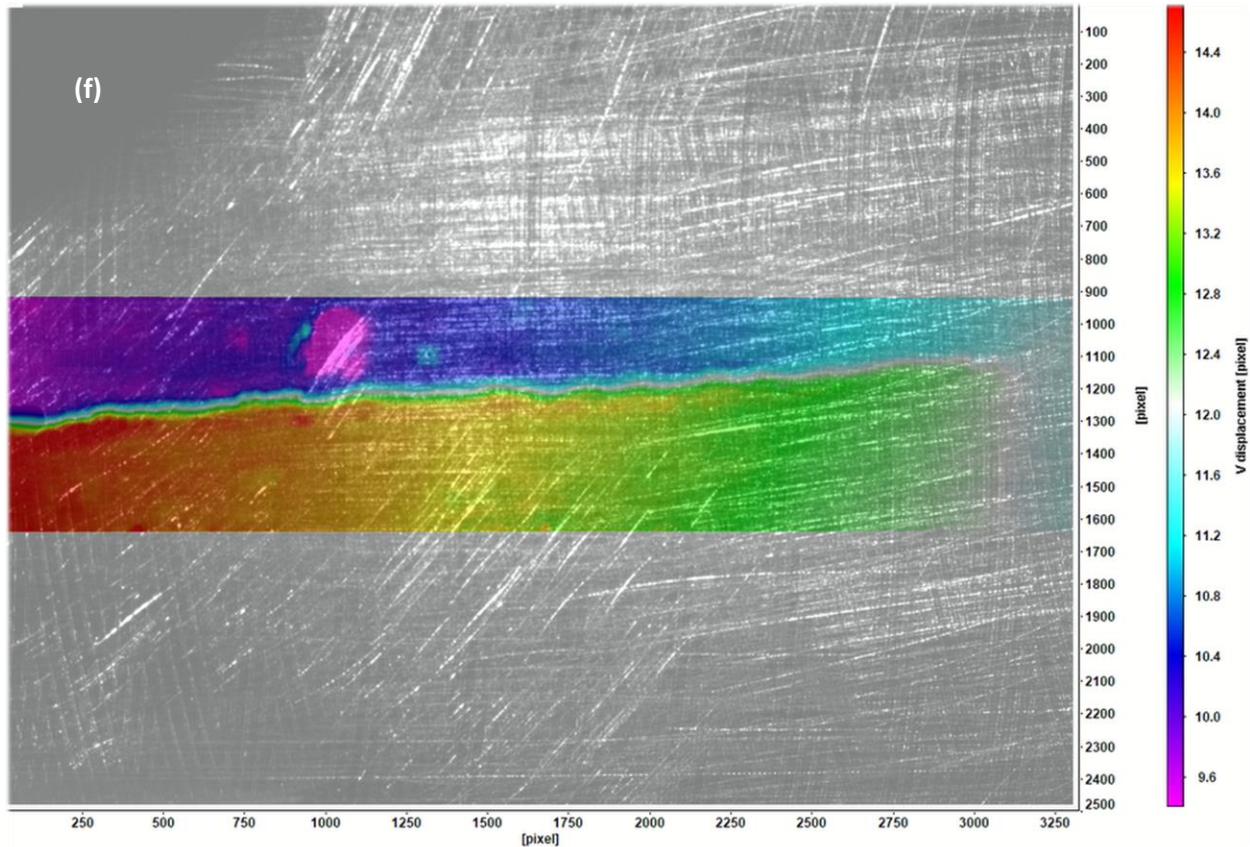


Figure 4.21: Series of colored images showing the progression of vertical displacements in the crack tip region at $\Delta K=15$ MPa·√m Cycle 3 from minimum to maximum load
(a)=~833 N, (b)=~1100 N, (c)=~1367 N, (d)=~1900 N, (e)=~2433 N, (f)=~3100 N

Figure 4.21 shows the progression of vertical displacements for pixels around the crack tip at $\Delta K=15$ MPa·√m during cycle 3 loading. This series of images offers more clarity at the crack tip at higher loads than the previous cycle, though it still demonstrates the benefits of developing a more precise way to pull data from these images. Additionally, it is important to focus not on the maximum or minimum pixel displacement values of these images on their own, but rather to take them as a combined picture. In this case, for image (f), with a maximum listed value of 14.4 and a minimum listed value of 9.6, a difference of 4.8 is identified. Compared to image (f) from the previous cycle, the maximum listed value is 1.2 pixels lower. However, thanks to the lower minimum listed value in this cycle's final image, the change in pixel differential at this load level between the two cycles is only 0.4 pixels.

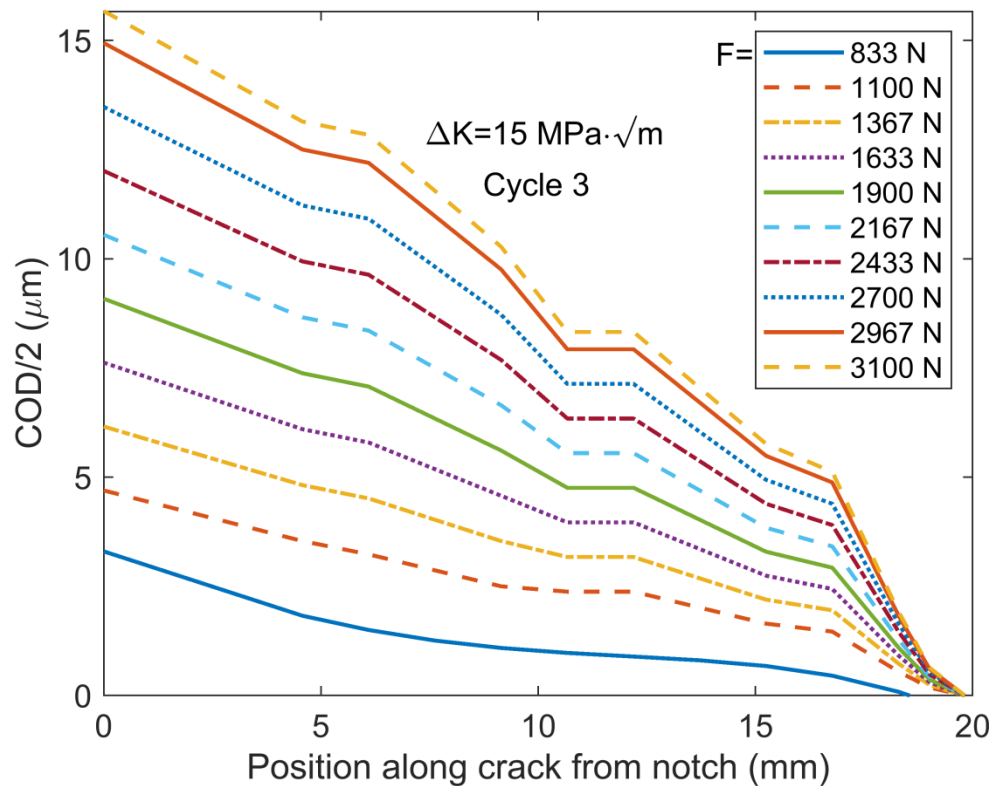


Figure 4.22: Half of the crack opening displacement (COD) evolution during the loading in cycle 3. The observed crack tip is located at horizontal position $x = 19$ mm.

From Figure 4.22, it is interesting to note that in both this cycle and the previous one, the crack is shown as being open for a greater amount of its total length at lower loads than in Cycle 1. This can be attributed to the fact that even as data is being collected in this process, the specimen is being cycled, and therefore the fracture will be developing slightly in the midst of data collection for each data set. It can already be seen, even without zooming in, that there is a larger gap between the 833 N line and the 1100 N line than in previous cycles, which is an indication of a lower opening load range than in the previous cycles.

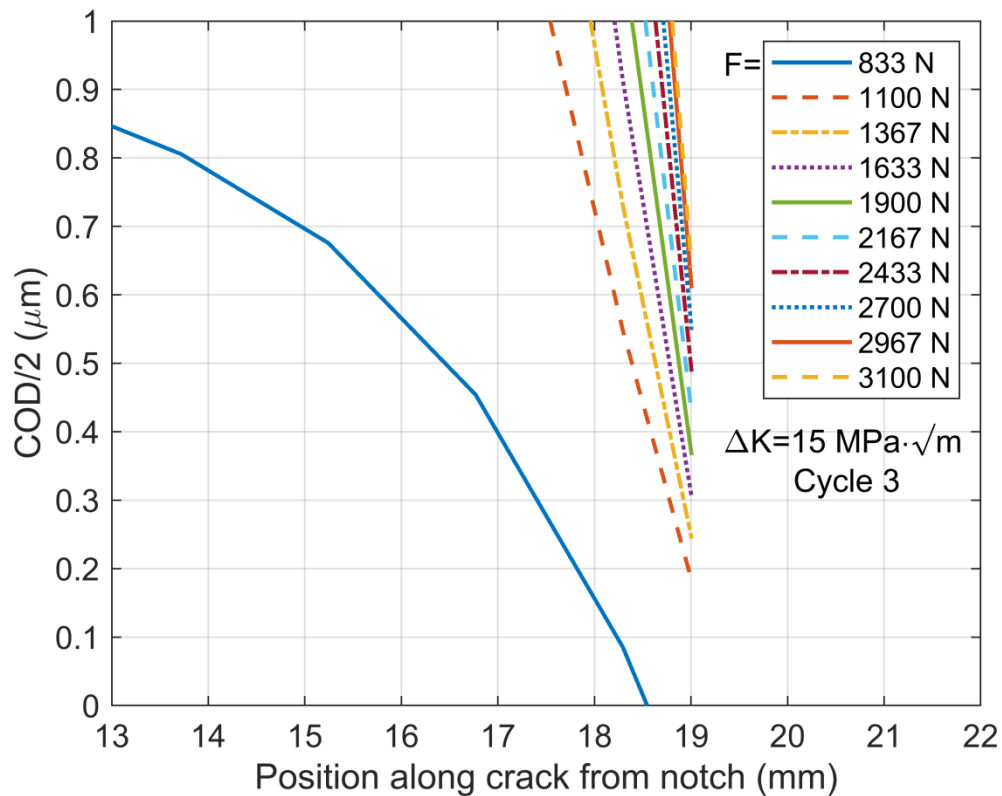


Figure 4.23: Crack tip focus for approximate opening load range identification.

When Figure 4.23 is analyzed, it can be concluded that this cycle breaks the trend set by the other two in this data set, showing a range for opening load of 833 N to 1100 N. Again, this fits with the realization of the continued development of the fracture during data collection, as opening load is shown to decrease as the fracture progresses. It should also be noted that this range is only one band lower than the previous two cycles, leaving open the possibility that the opening load for this cycle is still fairly close to the lower of the two opening loads from the previous cycles in this data set. A trend should be recognized in this data set that higher load levels approach the crack tip at increasingly steep angles as the fracture progresses and the opening load decreases.

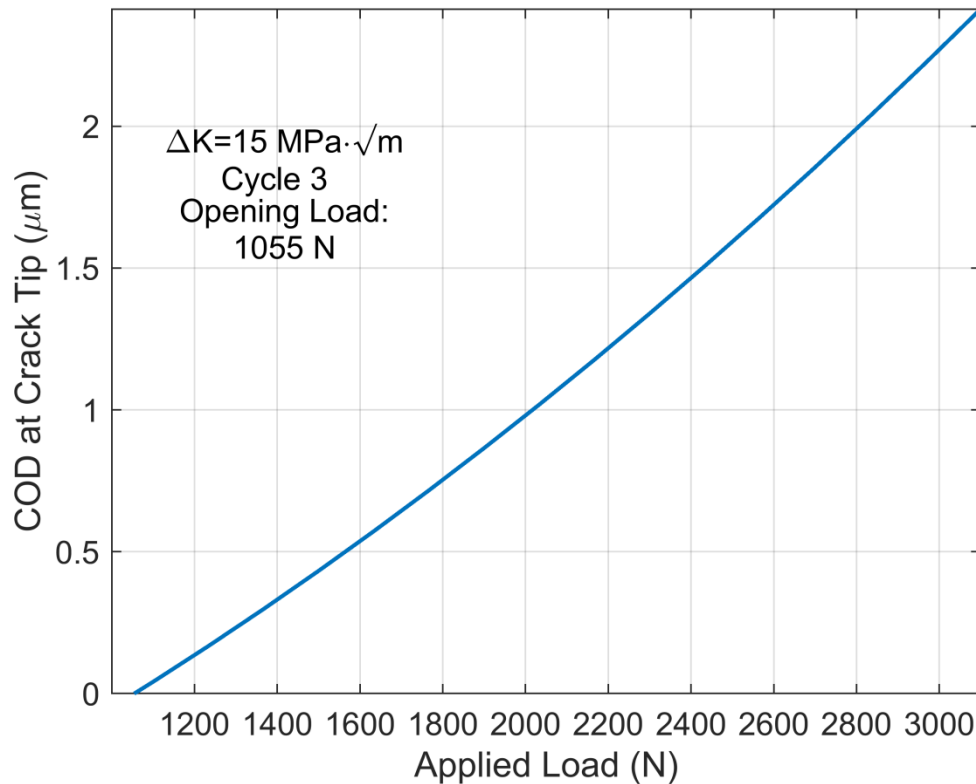
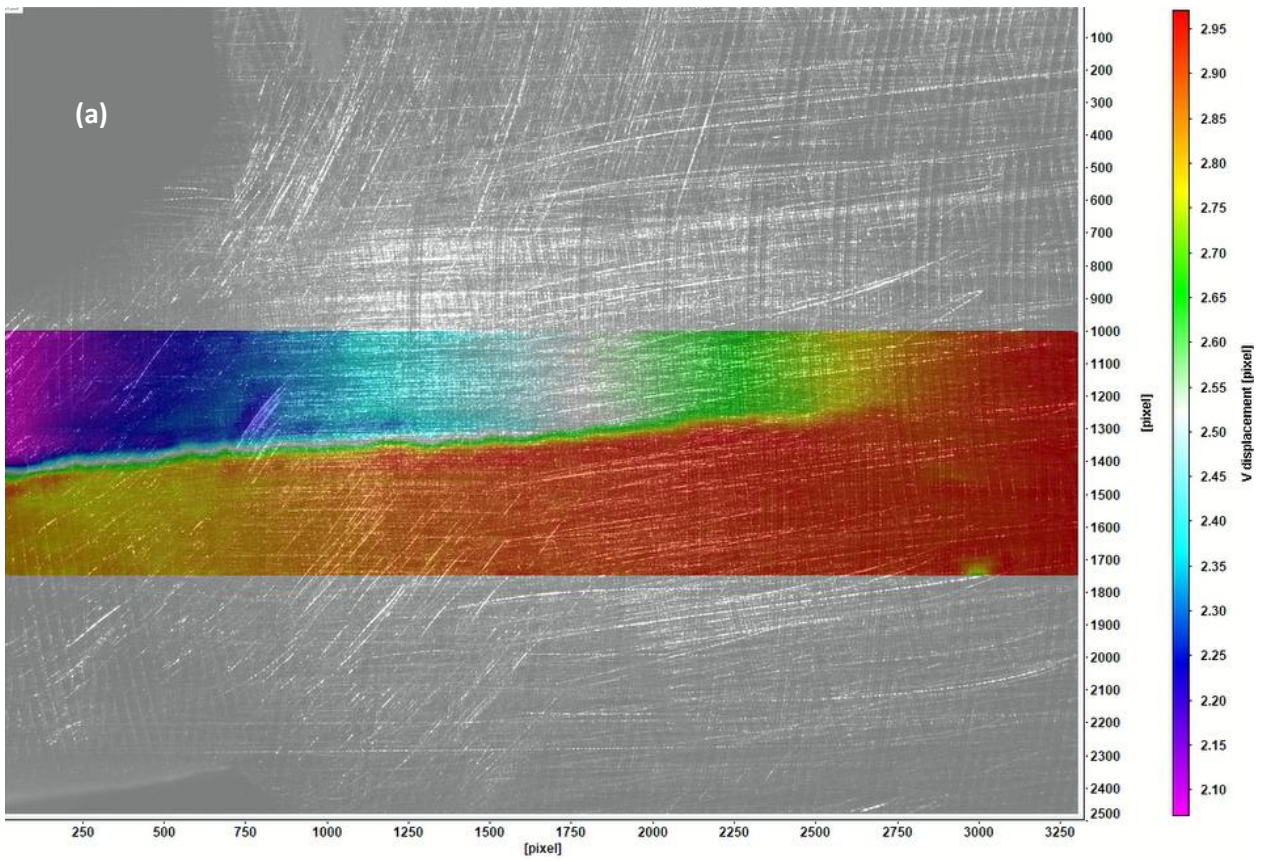


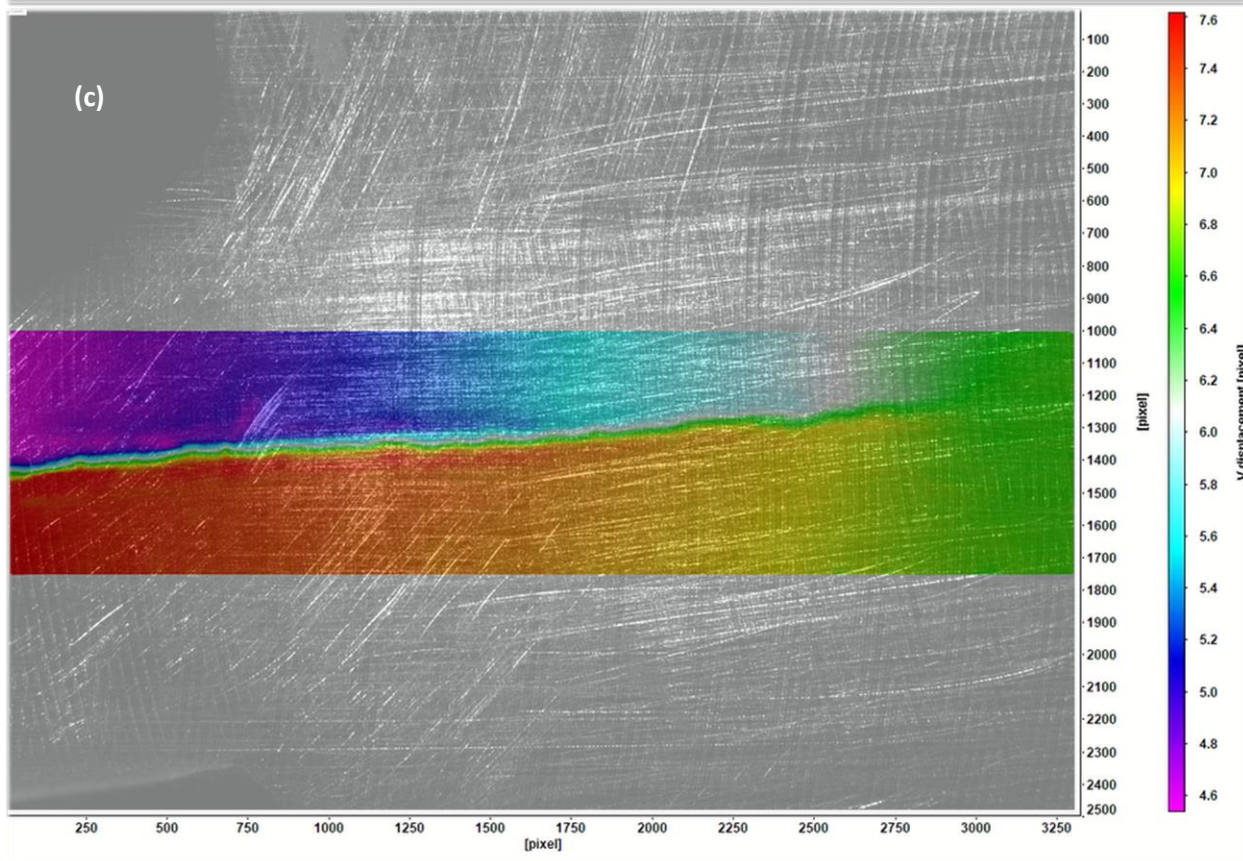
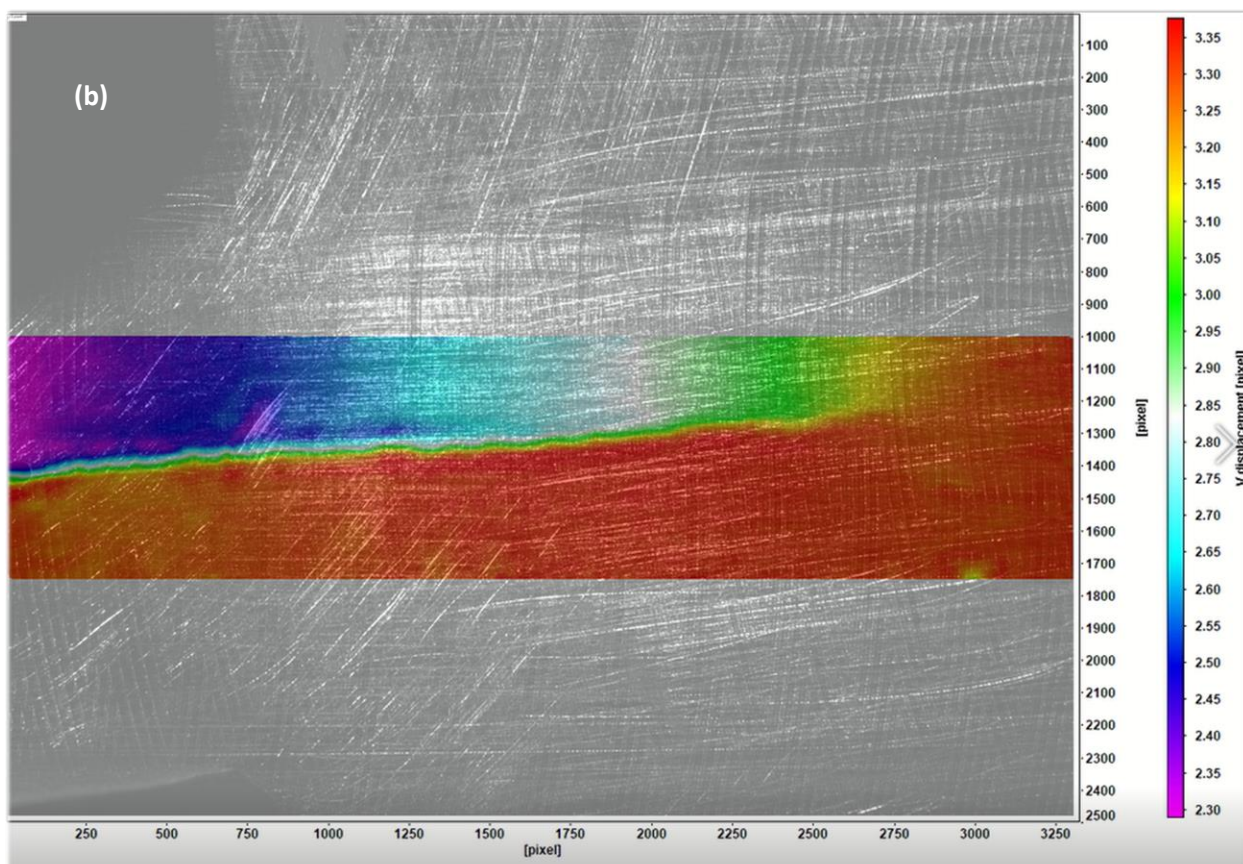
Figure 4.24: Variation of the crack tip opening displacement as a function of applied load during cycle 3.

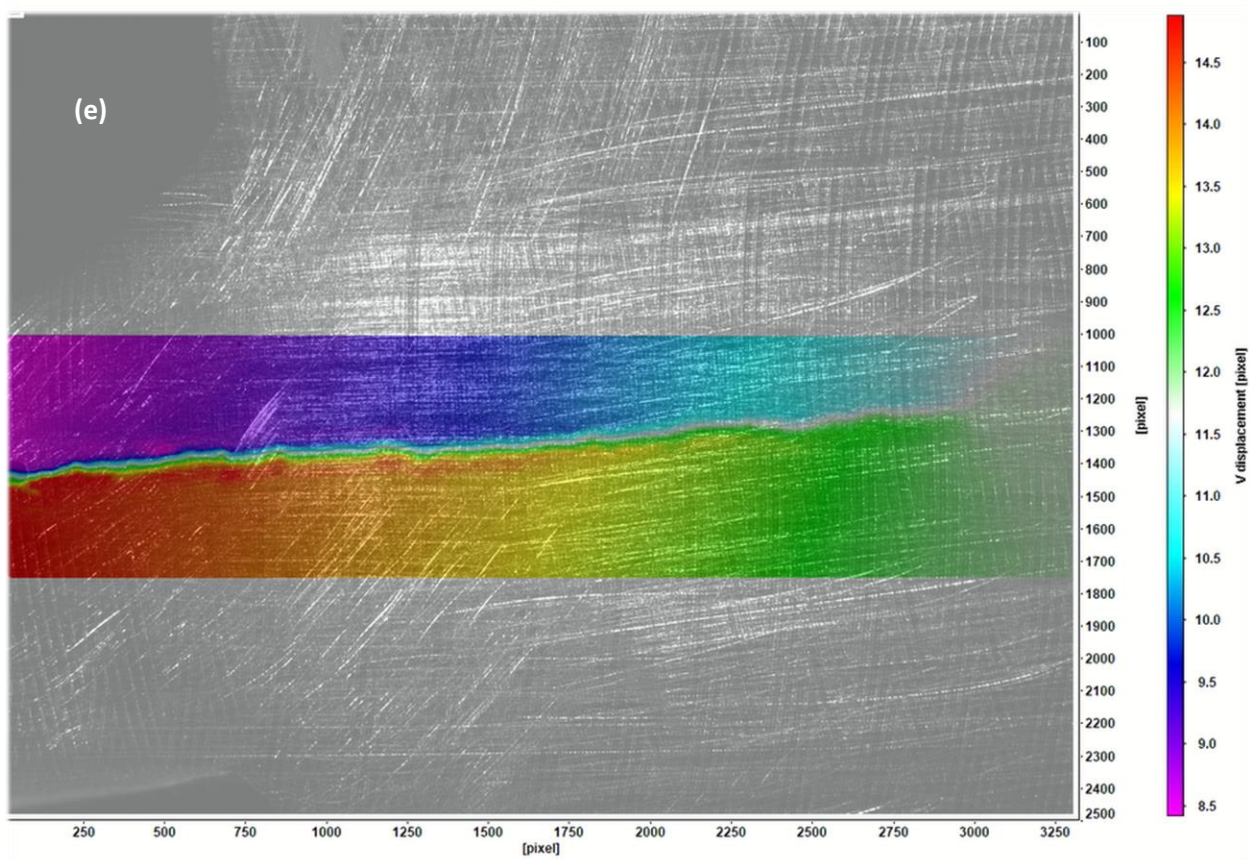
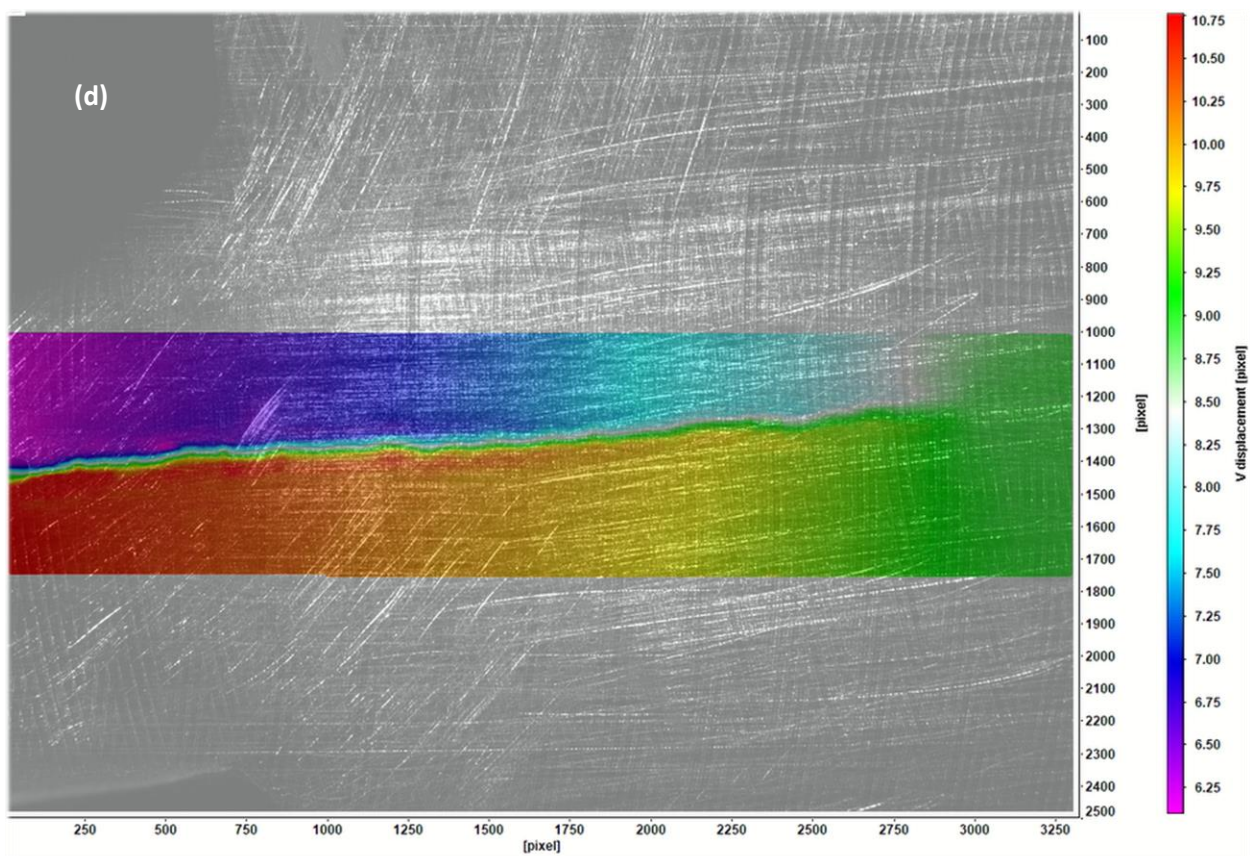
The variation of COD at the crack tip with applied load demonstrates a clear return to concave up behavior, and indicates an opening load of 1055 N for this cycle. This value is still fairly close to the other two opening load values in this data set, and serves to maintain the relative consistency of the $\Delta K=15 \text{ MPa}\cdot\sqrt{\text{m}}$ opening load results. The fact that this data set has concave up, concave down, and near linear opening load curves indicates that more investigation into the shape of these curves should be performed in future work. However, again, the opening load identified is consistent with predictions and expectations.

4.3 $\Delta K=20 \text{ MPa}\cdot\sqrt{\text{m}}$

4.3.1 Cycle 1







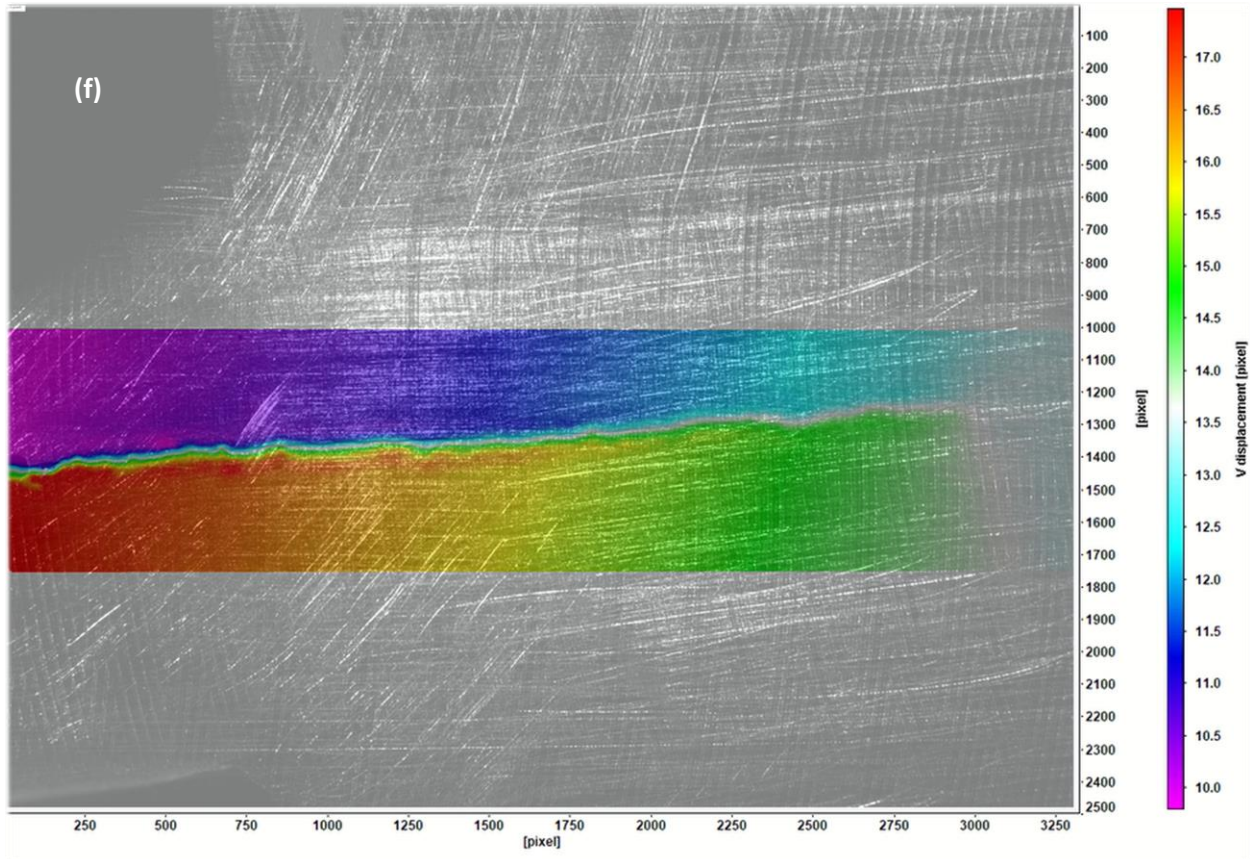


**Figure 4.25: Series of colored images showing progression of the vertical displacements of pixels near the crack tip region at $\Delta K=20$ MPa $\sqrt{\text{m}}$ Cycle 1 from minimum to maximum load
(a) \sim 557 N, (b) \sim 814 N, (c) \sim 1329 N, (d) \sim 1843 N, (e) \sim 2357 N, (f) \sim 3000 N**

While the $\Delta K=20$ MPa $\sqrt{\text{m}}$ data set benefited from very clear color images, as well as experience from previous data sets, it unfortunately was unstable to a very challenging degree, which led to difficulties which will be seen and discussed later. While the previous data set only occasionally had crack tip displacement values in the colorless region on these plots, the progression of the crack to this stage made crack tip values in or near that range more likely.

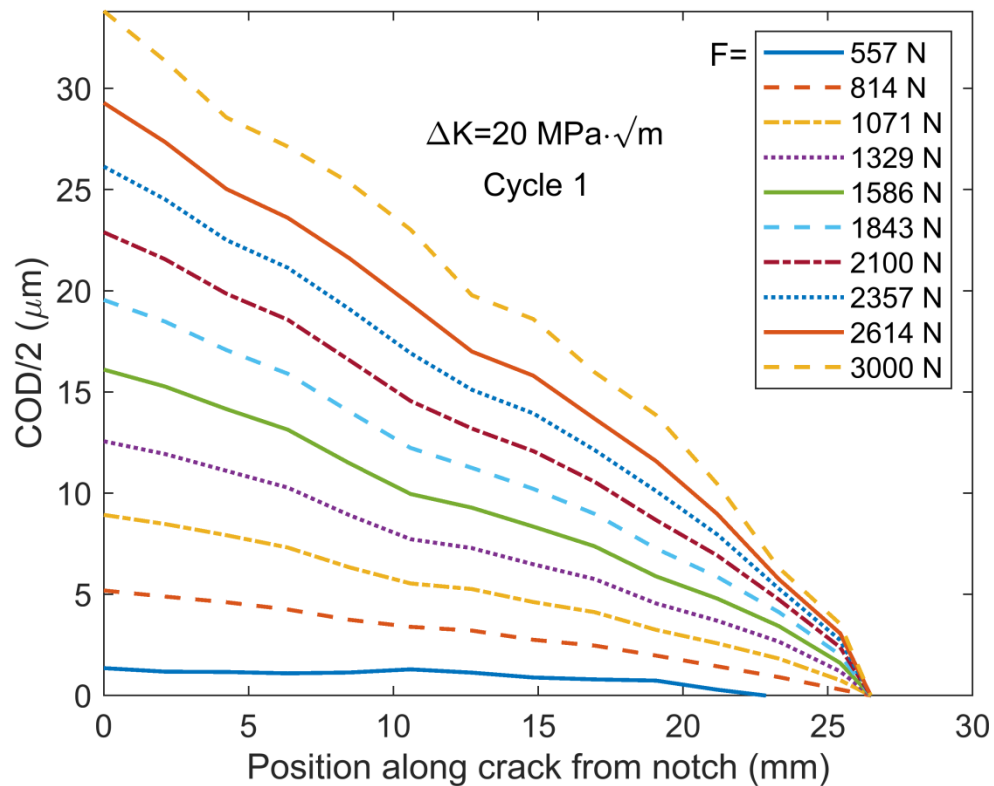


Figure 4.26: Half of the crack opening displacement (COD) evolution during the loading in cycle 1. The observed crack tip is located at horizontal position $x = 25.45 \text{ mm}$.

It can be seen from Figure 4.26 that the crack is much more open at this stage in its life, and opens much farther under similar loads. The crack is now open for a length longer than the fracture was in its entirety at the $\Delta K = 15 \text{ MPa}\cdot\sqrt{\text{m}}$ level, at only 557 N. It can be predicted that the crack tip opening load will be much lower in this data set than in the previous two. Additionally, a large gap can again be identified between the lowest displayed load line, in this case 557 N, and the next one above it, 814 N. While the zoomed plots are still used for clarity in cycles such as this, the opening load range in this cycle can almost be determined without their use.

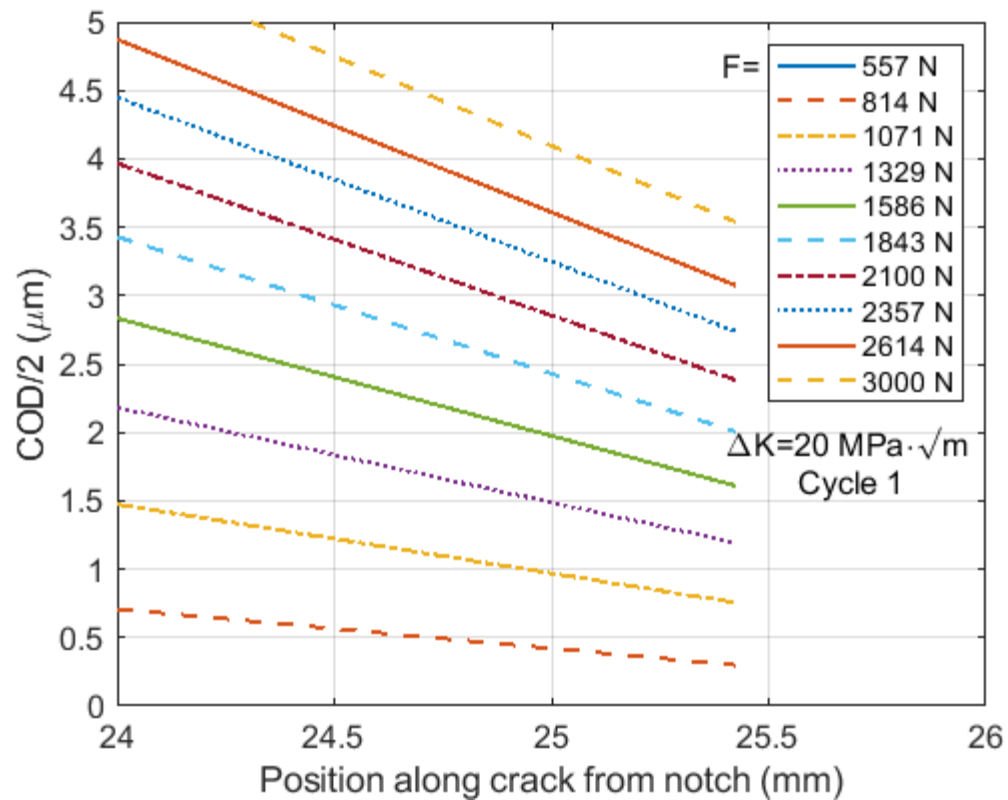


Figure 4.27: Crack tip focus for approximate opening load range identification.

Figure 4.27 shows a zoomed image of the previous plot. While the 557 N curve intersects the x axis before this plot begins, it can be seen that the opening load range given for this cycle is 557 N to 814 N. This opening load range is dramatically lower than the ranges found for previous ΔK values, and demonstrates an exponential development of the opening load value with increasing ΔK . It is also interesting to note that the lowest load curve on this cycle impacts the x axis so far back from the next line above it that it does not even appear on the zoomed plot.

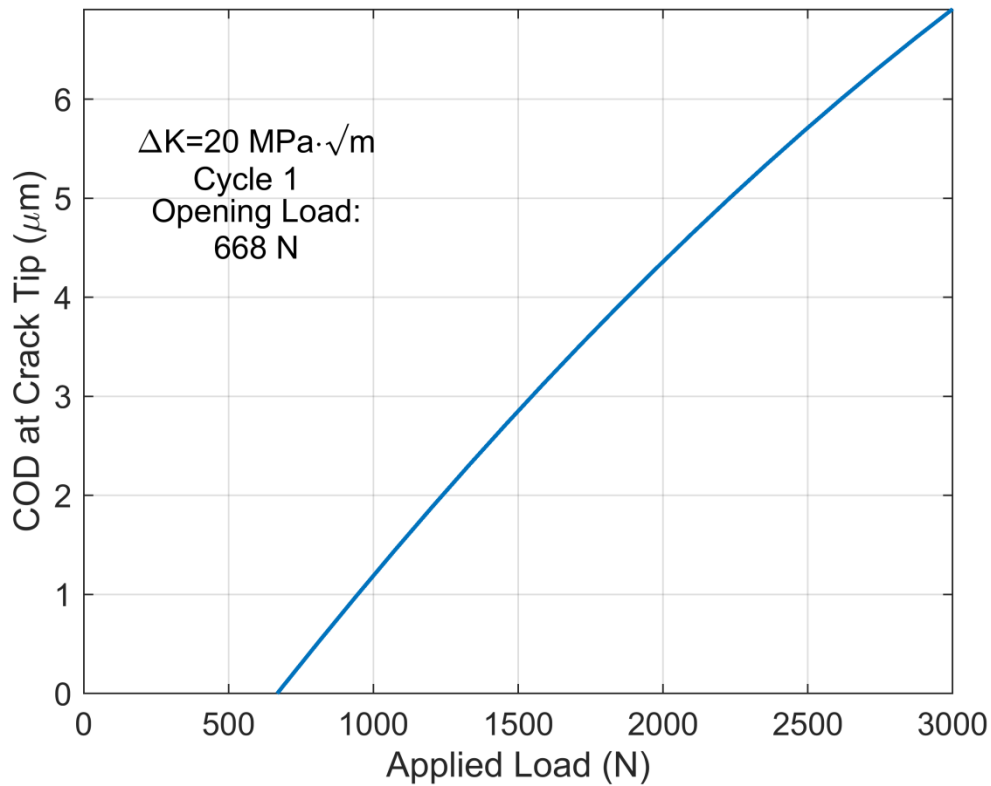
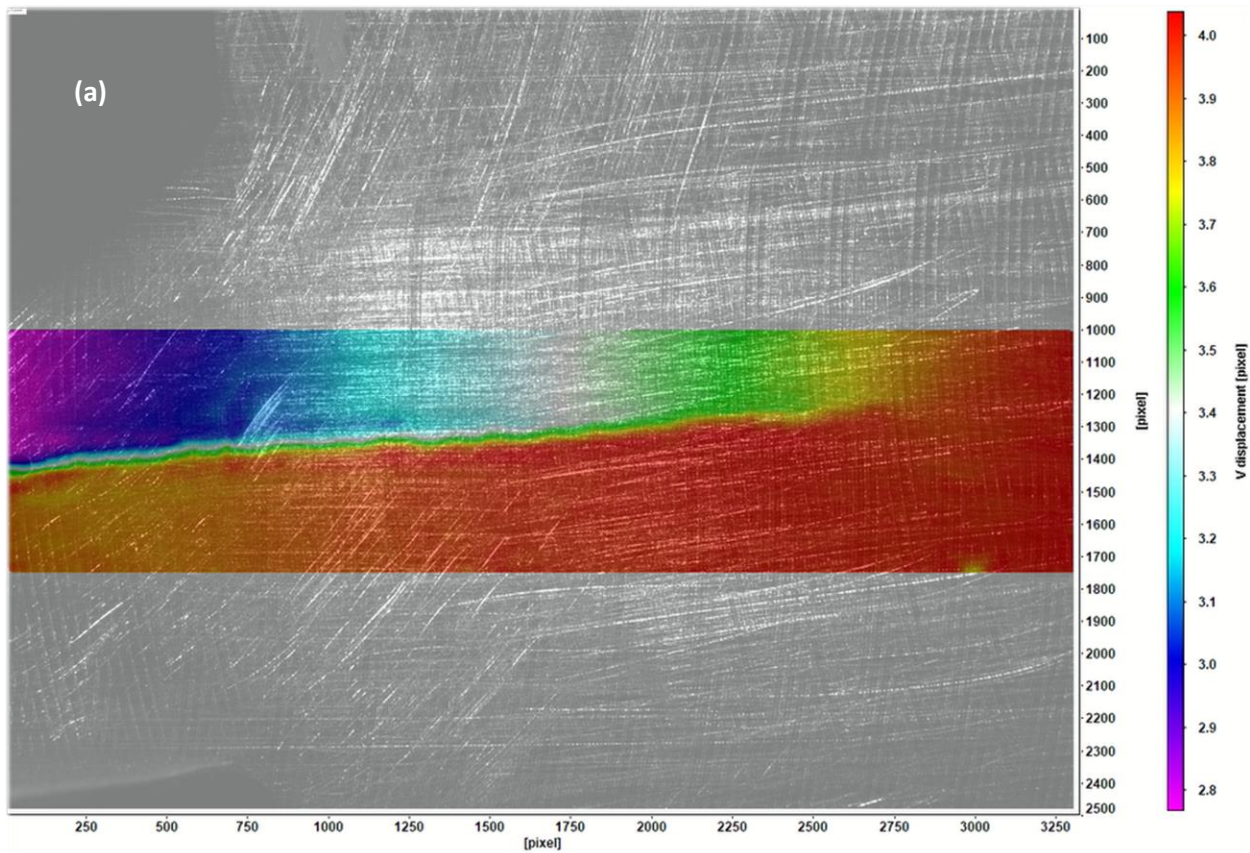
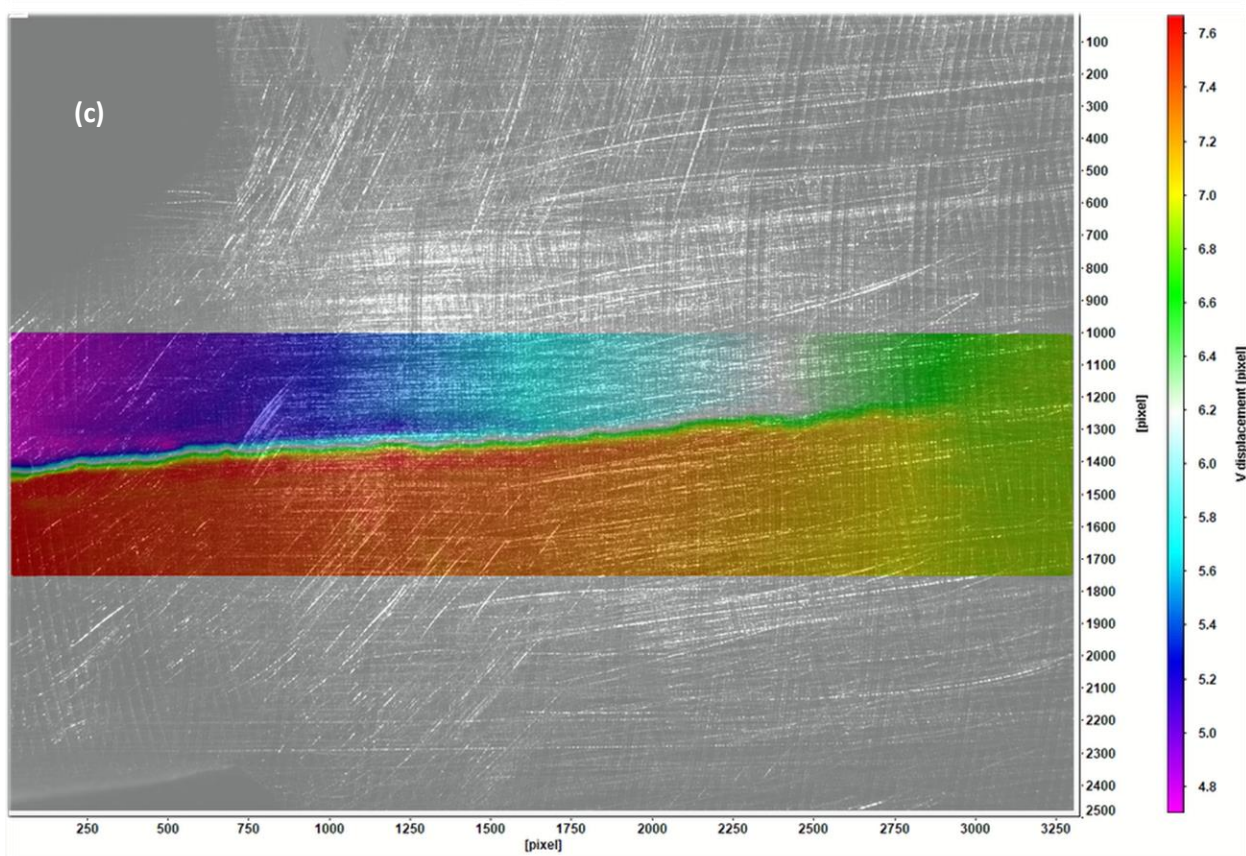
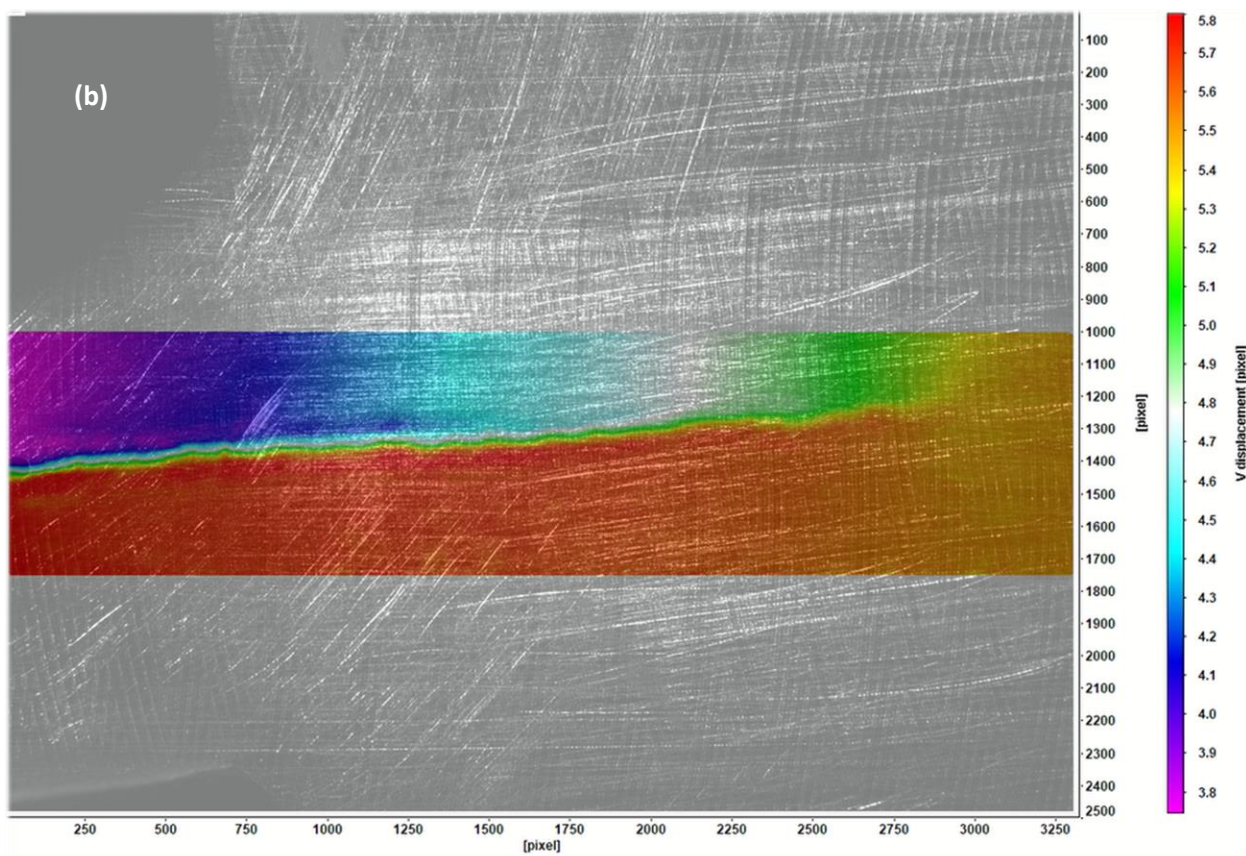


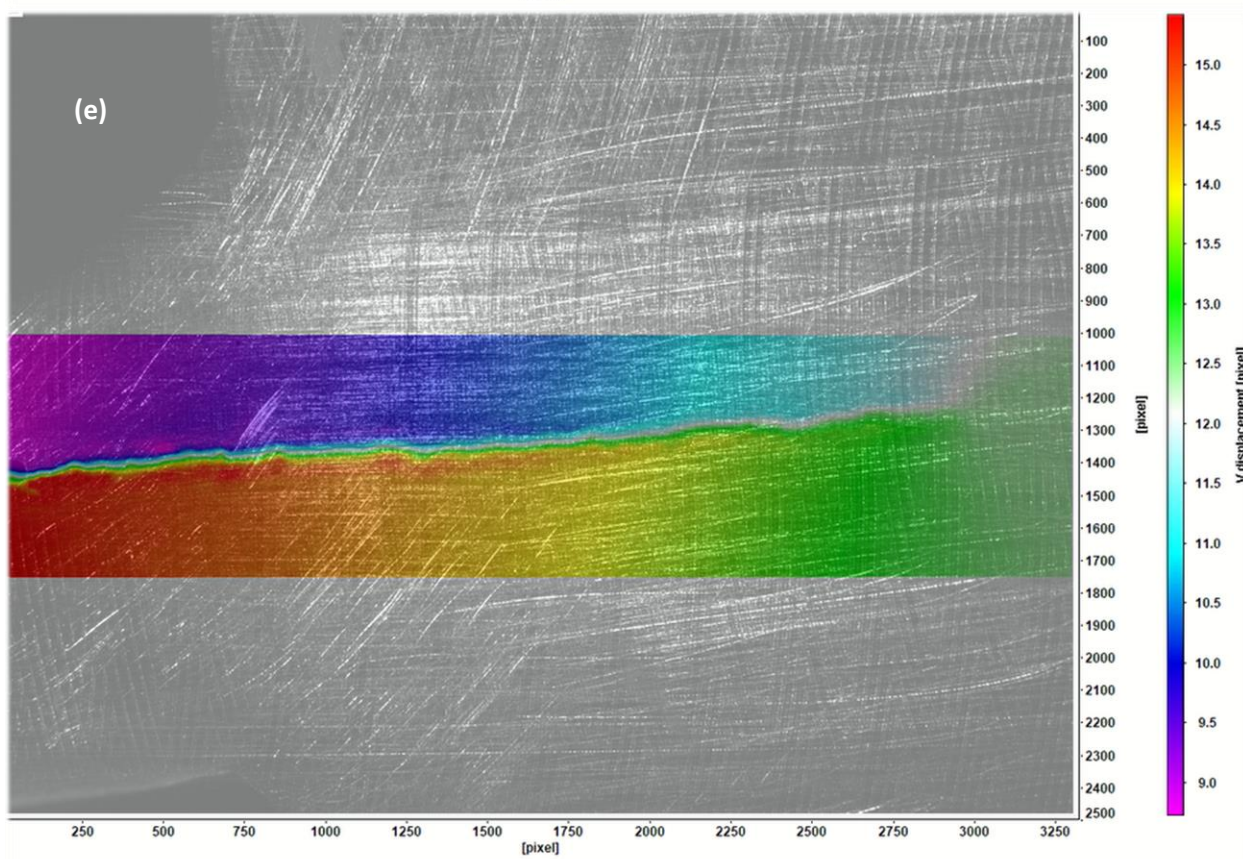
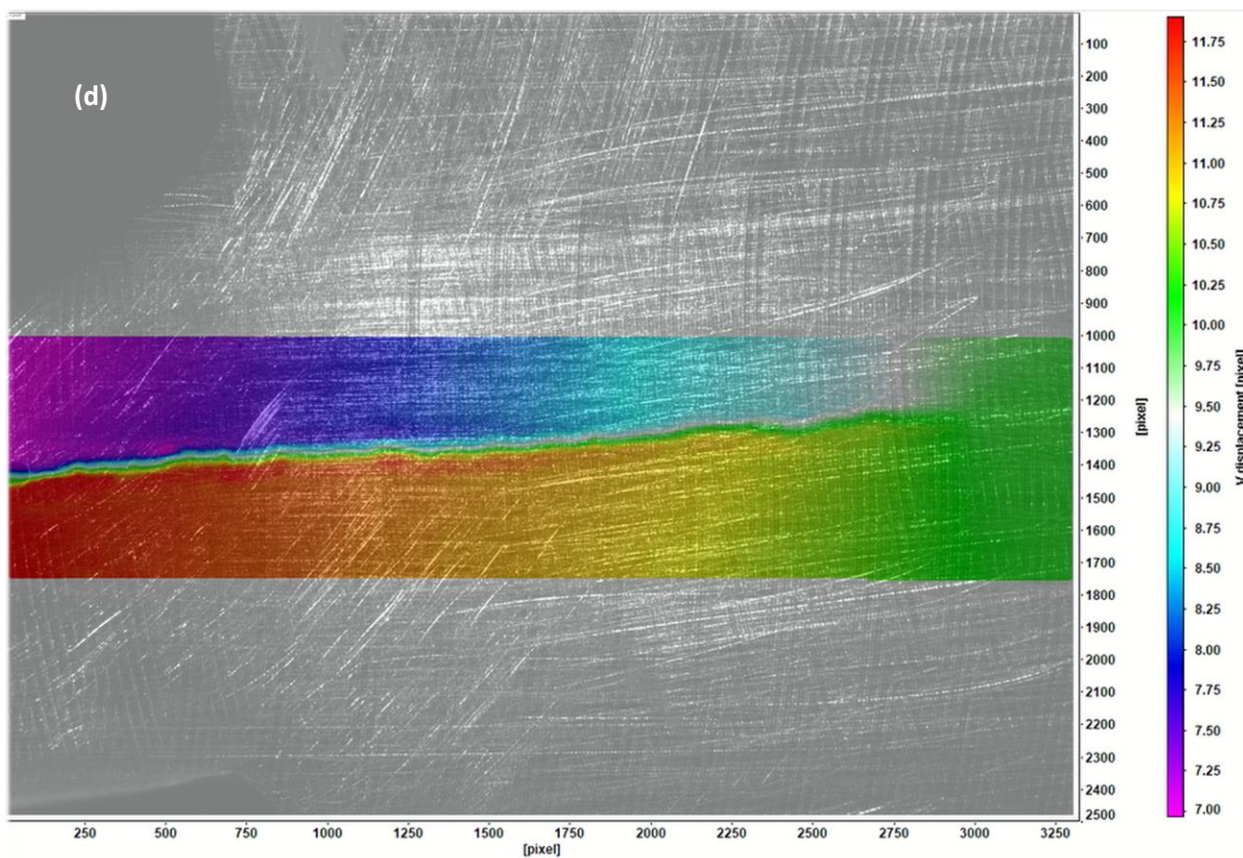
Figure 4.28: Variation of the crack tip opening displacement as a function of applied load during cycle 1.

Figure 4.28 shows the evolution of the COD at the crack tip versus the applied load for this cycle. The plot delivers an opening load value of approximately 668 N, which is within the range given in the previous plot. The value also fits the prediction of the opening load being much lower at this level, as it is a little over half the average value of the $\Delta K = 15 \text{ MPa}\cdot\sqrt{\text{m}}$ set. Average values for each data set will be given and discussed in the analysis and verification section.

4.3.2 Cycle 2







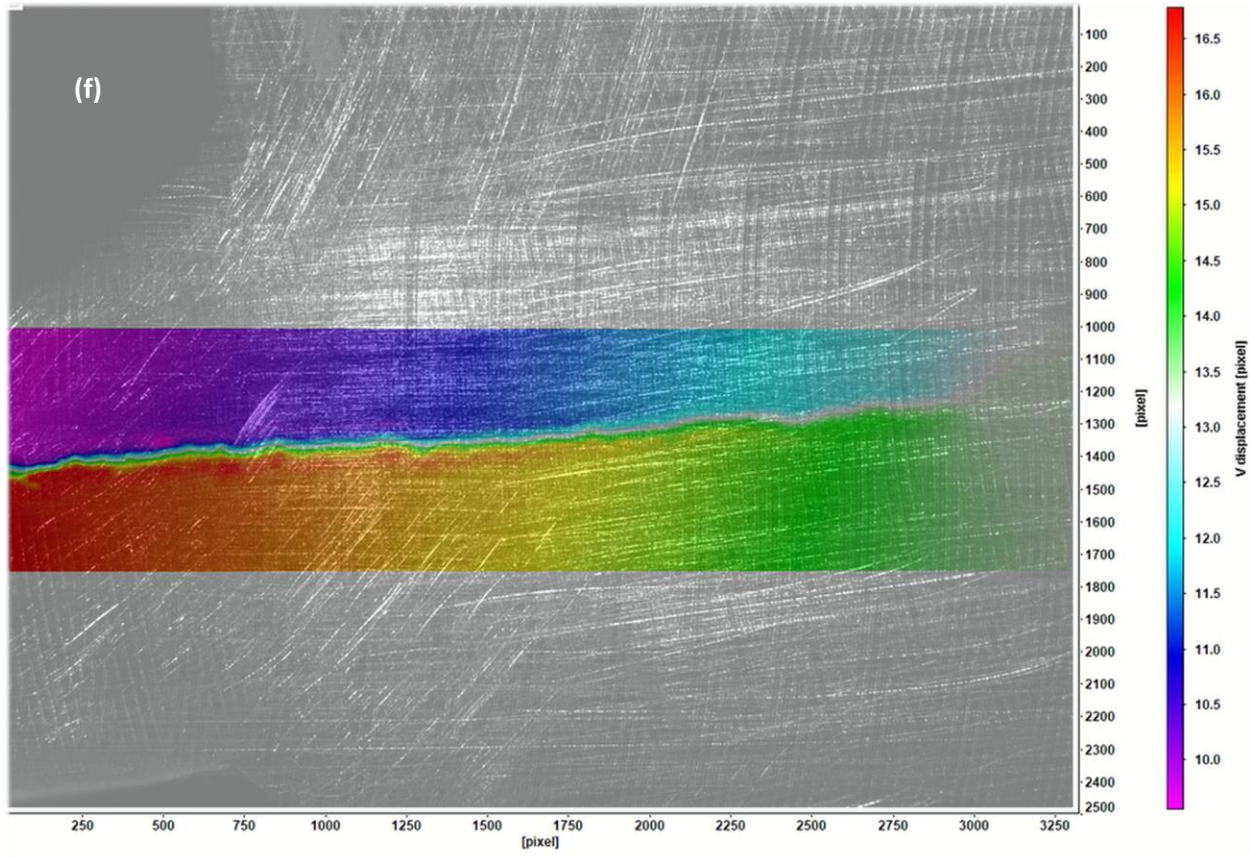


**Figure 4.29: Series of colored images showing progression of the vertical displacement of pixels in the near crack tip region at $\Delta K=20$ MPa $\sqrt{\text{m}}$ Cycle 2 from minimum to maximum load
(a) \sim 814 N, (b) \sim 1071 N, (c) \sim 1329 N, (d) \sim 1843 N, (e) \sim 2357 N, (f) \sim 3000 N**

From this cycle and the one before, it can already be seen that experience with the method had developed by this point to produce very clear images of the fracture. Therefore, images for this data set are the cleanest of all data sets. This is also aided by the advanced state of the crack in this data set, making the crack opening generally much more visible much sooner in each cycle.

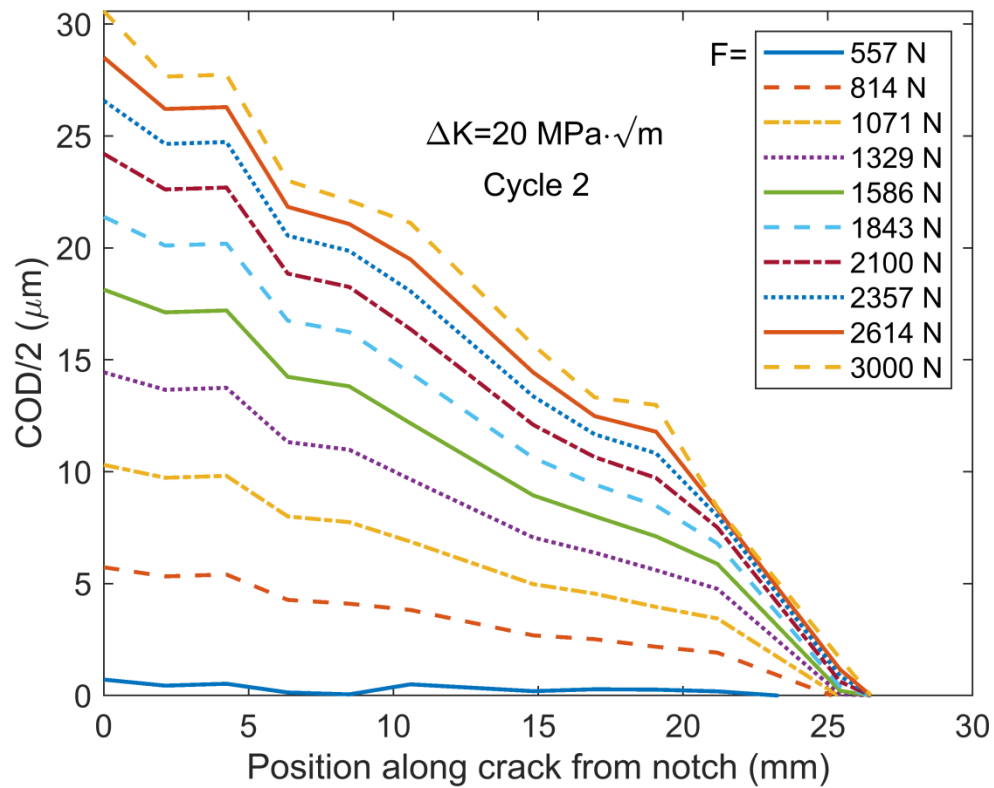


Figure 4.30: Half of the crack opening displacement (COD) evolution during the loading in cycle 2. The observed crack tip is located at horizontal position $x = 25.45 \text{ mm}$.

From Figure 4.30, it appears that the crack isn't quite as open at lower load levels, but it is open for a greater portion of the total length of the fracture at 557 N than in the previous cycle, which is expected. The squashed shape of the 557 N line is of concern, however, as the trend indicates it should not lie so close to the x axis at this point.

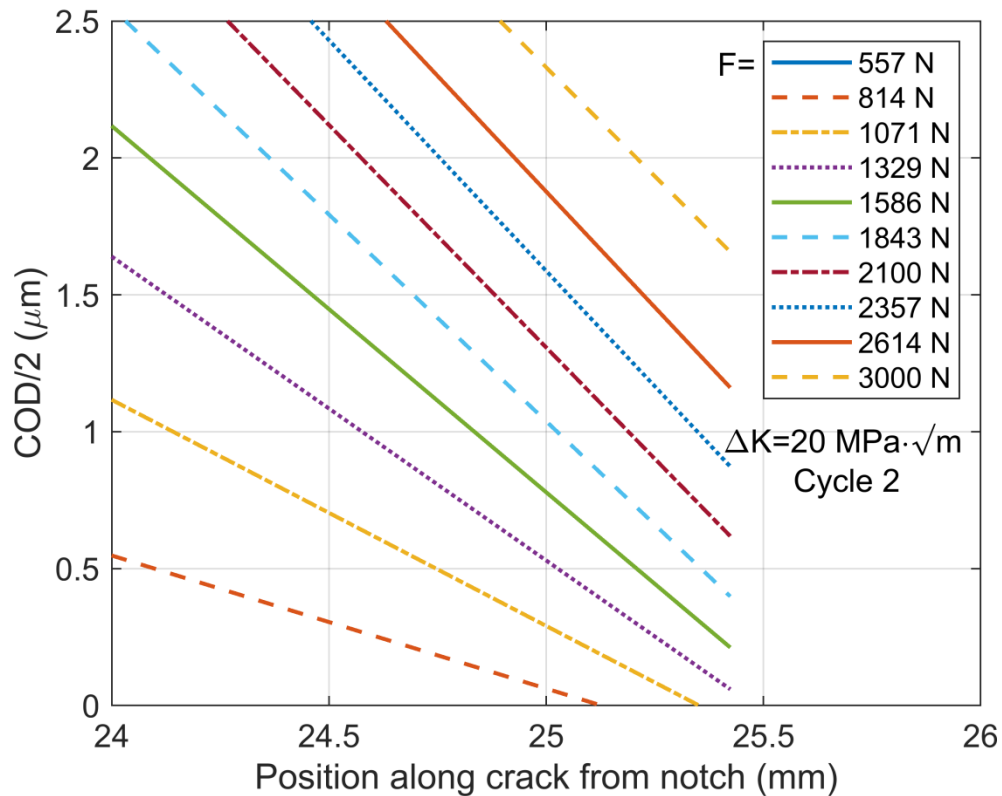


Figure 4.31: Crack tip focus for approximate opening load range identification.

Figure 4.31 is a zoomed image of the previous plot. This cycle breaks the trend displayed in the previous data set of opening load range decreasing with each subsequent cycle, with a visible range of 1071 N to 1329 N. This puts the opening load for this cycle more in line with the $\Delta K=10 \text{ MPa}\cdot\sqrt{\text{m}}$ or $\Delta K=15 \text{ MPa}\cdot\sqrt{\text{m}}$ data sets. It is possible that an accidental compressive load was applied to the specimen between this cycle and the last, resulting in greater load required to open the crack completely. The vast difference between this result and the last one is of concern, and further investigation of the crack opening behavior should be performed at this ΔK level. With only three cycles to a data set, a vast difference between results of even two of the cycles should be analyzed and possible measurement uncertainty sources identified.

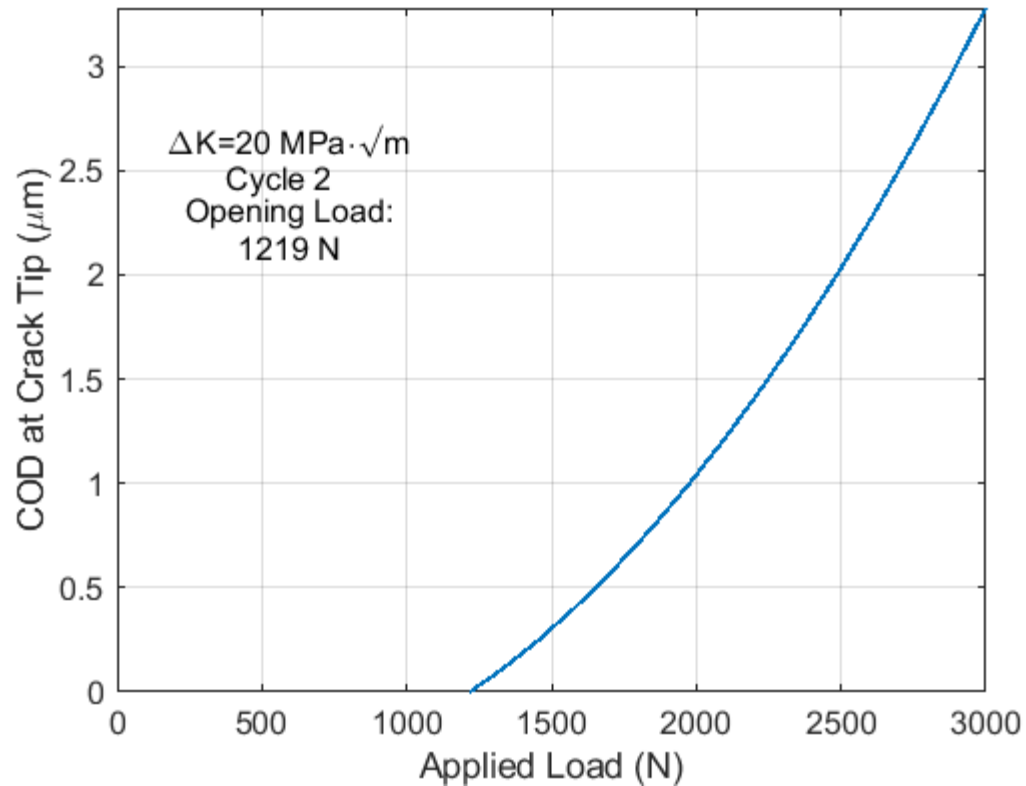
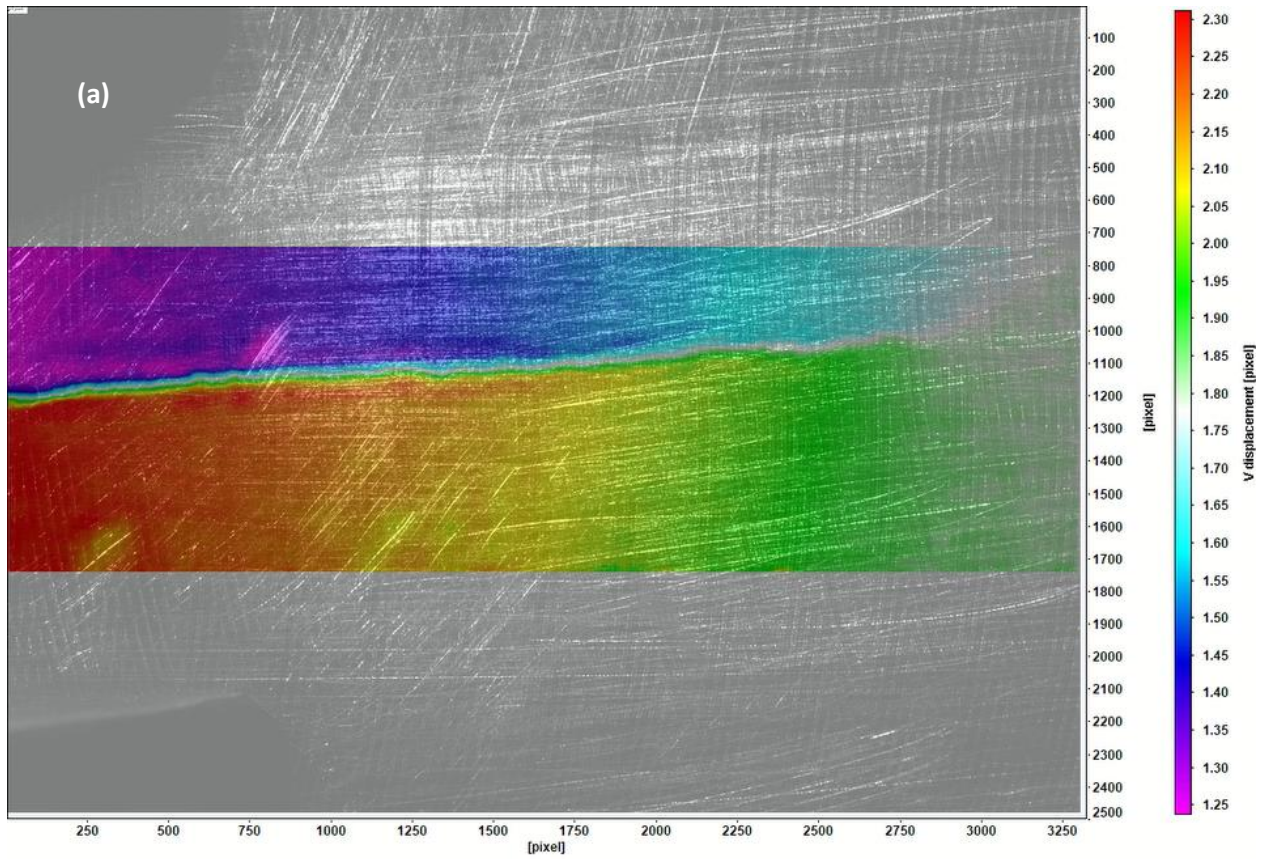
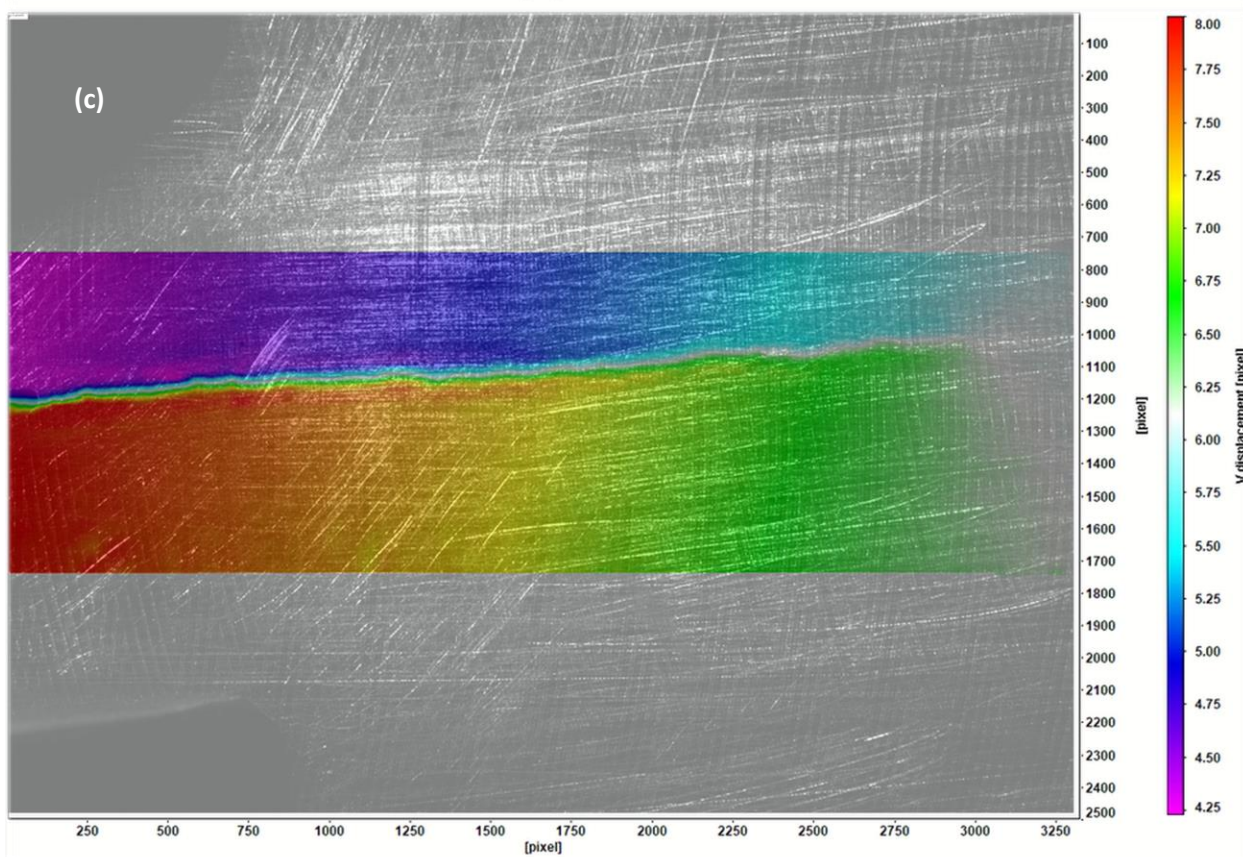
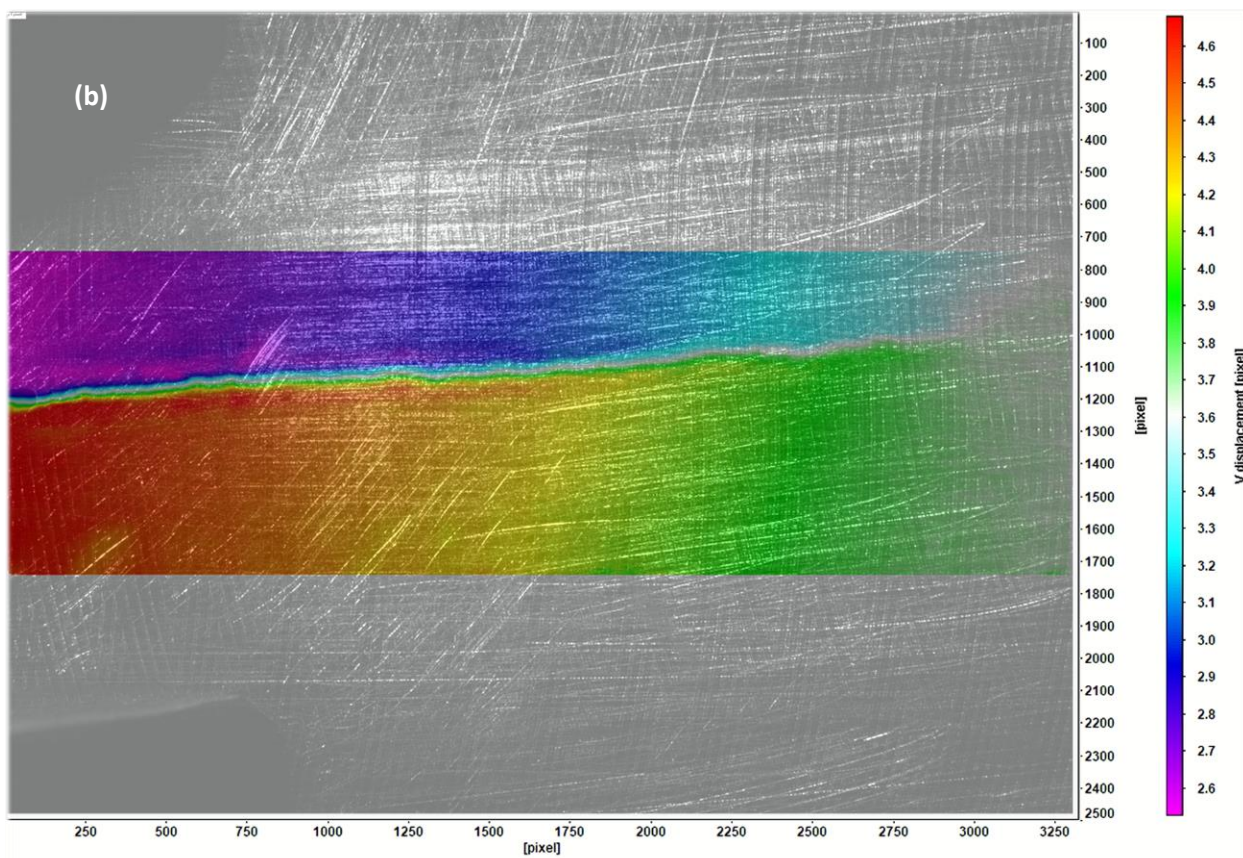


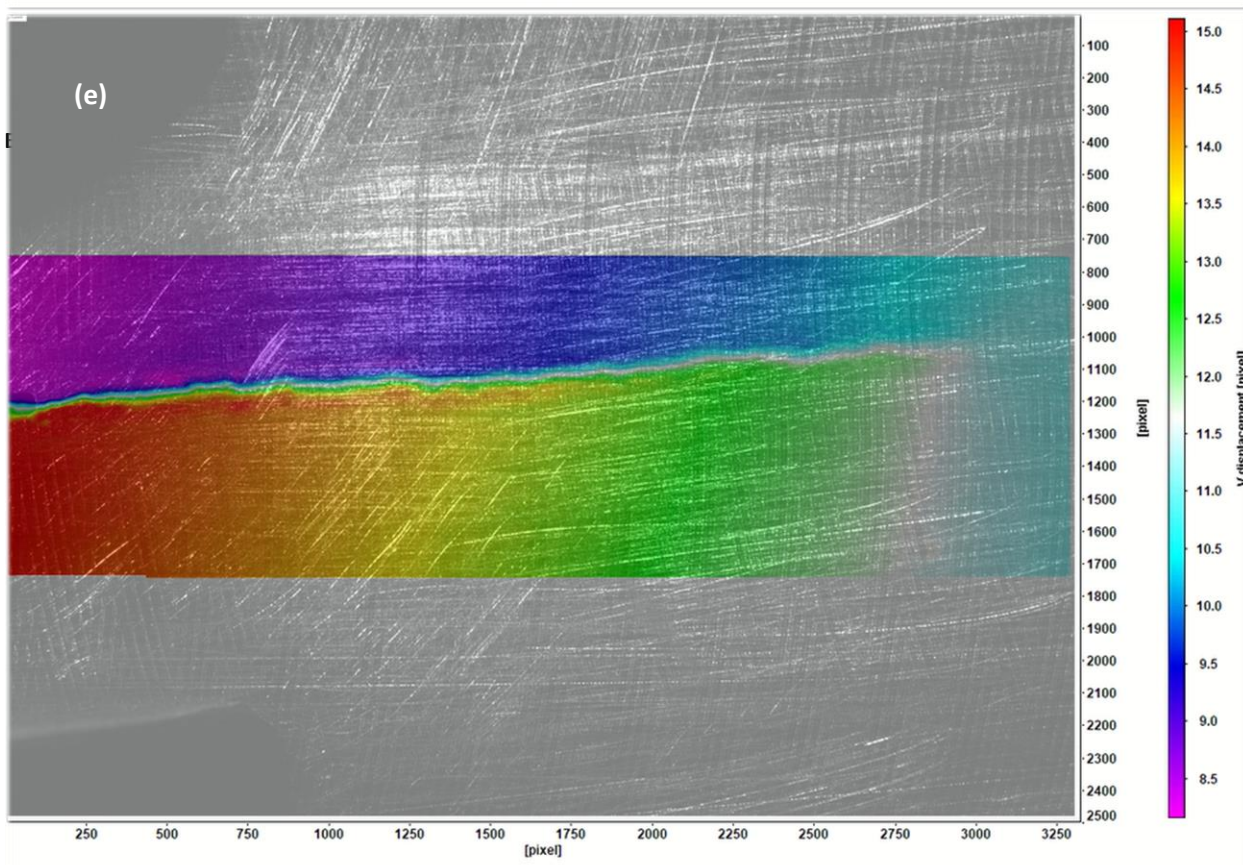
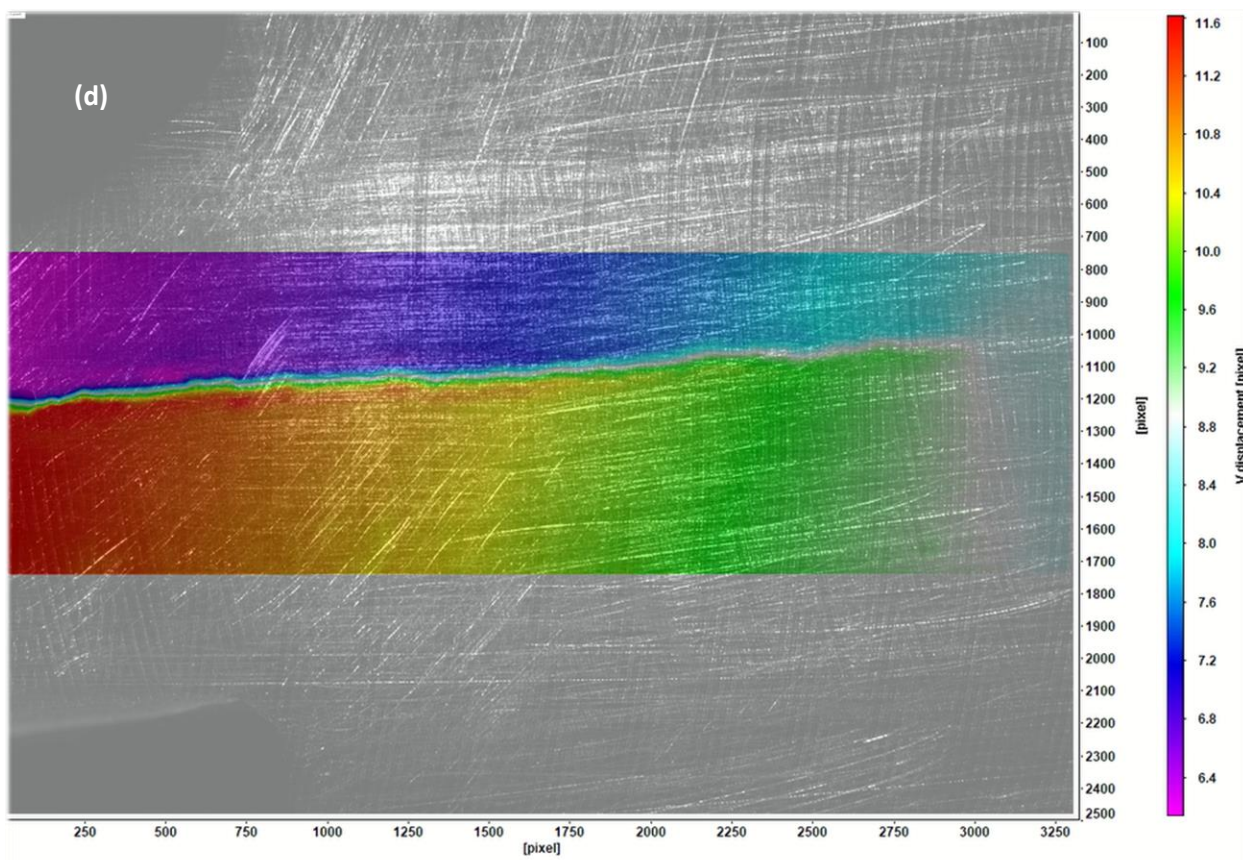
Figure 4.32: Variation of the crack tip opening displacement as a function of applied load during cycle 2.

Returning again to concave up behavior, this CTOD curve gives an opening load of about 1219 N, fitting within the range given for this cycle. Unfortunately, this is in fact dramatically different from the previous opening load. While the shape of this curve is better than the previous opening load curve, it is again not the shape we are concerned about in this project, but the x intercept. It seems likely at this point that this data set is not stable enough to be considered viable; however, it was included in this document for completeness and future investigations.

4.3.3 Cycle 3







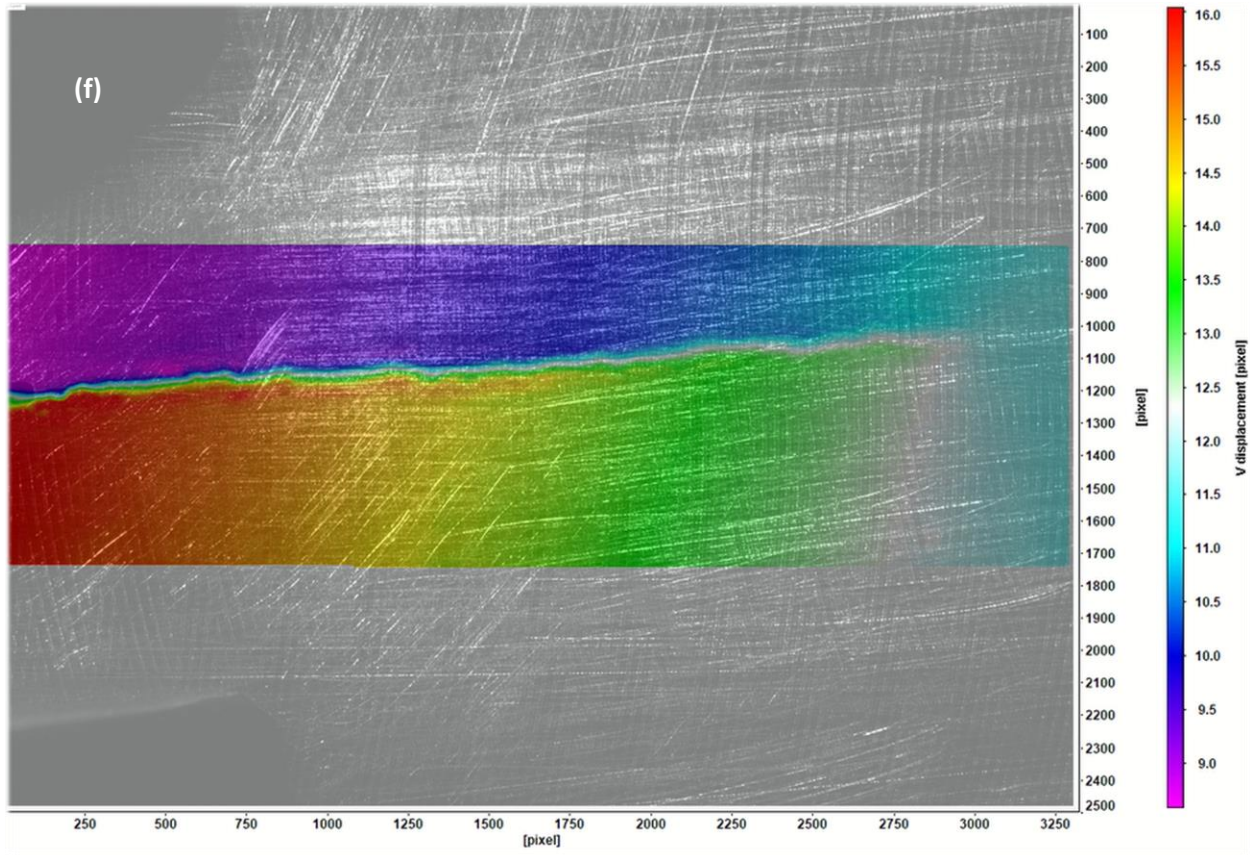


**Figure 4.33: Series of colored images showing progression of the vertical displacements of the pixels at of $\Delta K=20$ MPa- \sqrt{m} Cycle 3 from minimum to maximum load
(a)=~557 N, (b)=~814 N, (c)=~1329 N, (d)=~1843 N, (e)=~2357 N, (f)=~3000 N**

This cycle was performed as a replacement for a previous cycle that produced results inconsistent with the measurements at the lower ΔK levels. Therefore, this cycle was collected a full day after the previous two, which could result in changes to the fracture that could impact the values. Already of note in these images is the fact that this cycle is the only one in this data set where the crack tip does not exist entirely near the colorless region.

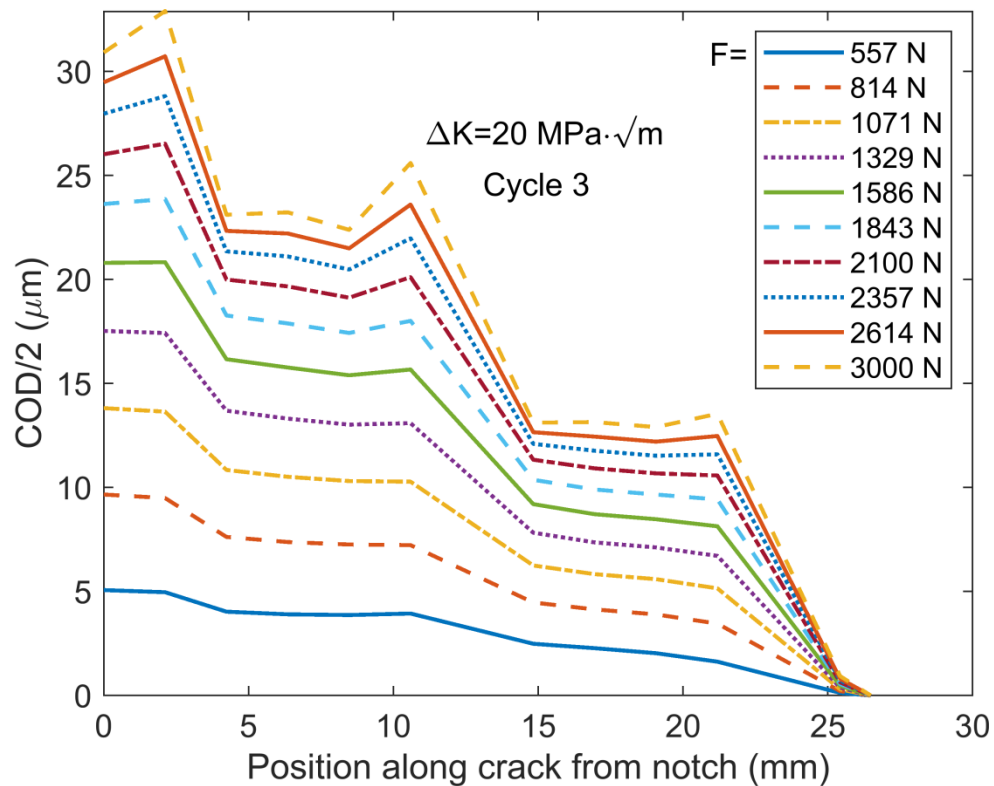


Figure 4.34: Half of the crack opening displacement (COD) evolution during the loading in cycle 3. The observed crack tip is located at horizontal position $x = 25.45 \text{ mm}$.

The crack is clearly much more open, much earlier, than it was in previous cycles, with the 557 N curve being open for far longer than previous cycles. This indicates that a dramatically lowered opening load will be given from this data. Also of concern is the dramatic spiking evident in the shape of these load lines. No other cycle has exhibited such a sharp inconsistency in the path of its load lines. This should be further investigated.

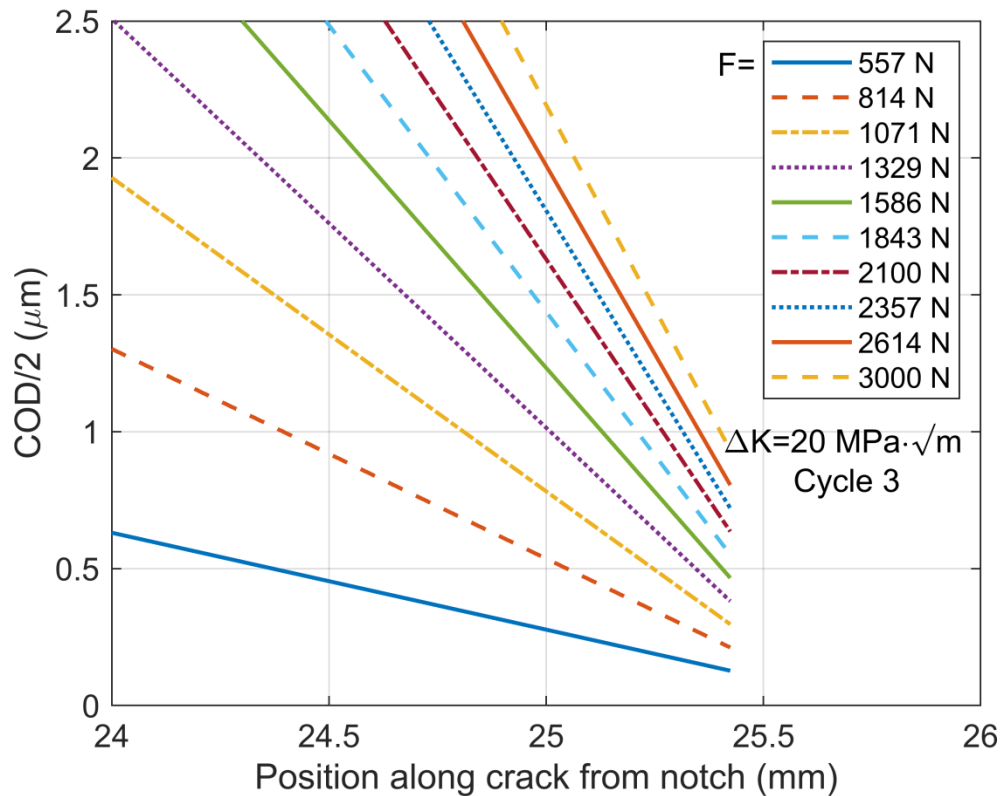


Figure 4.35: Crack tip focus for approximate opening load range identification.

The zoomed Figure 4.35 indicates, as predicted, that the opening load range for this data set is the lowest for the entire project, showing a range of 0 to 557 N. It is possible this is due to changes in the specimen between the collection of this cycle and the previous cycle, or perhaps just uncertainties in the data collection. With no cycle in this data set producing consistent opening load ranges, it seems the whole data set should be considered questionable for consideration when looking at trends in the crack's development.

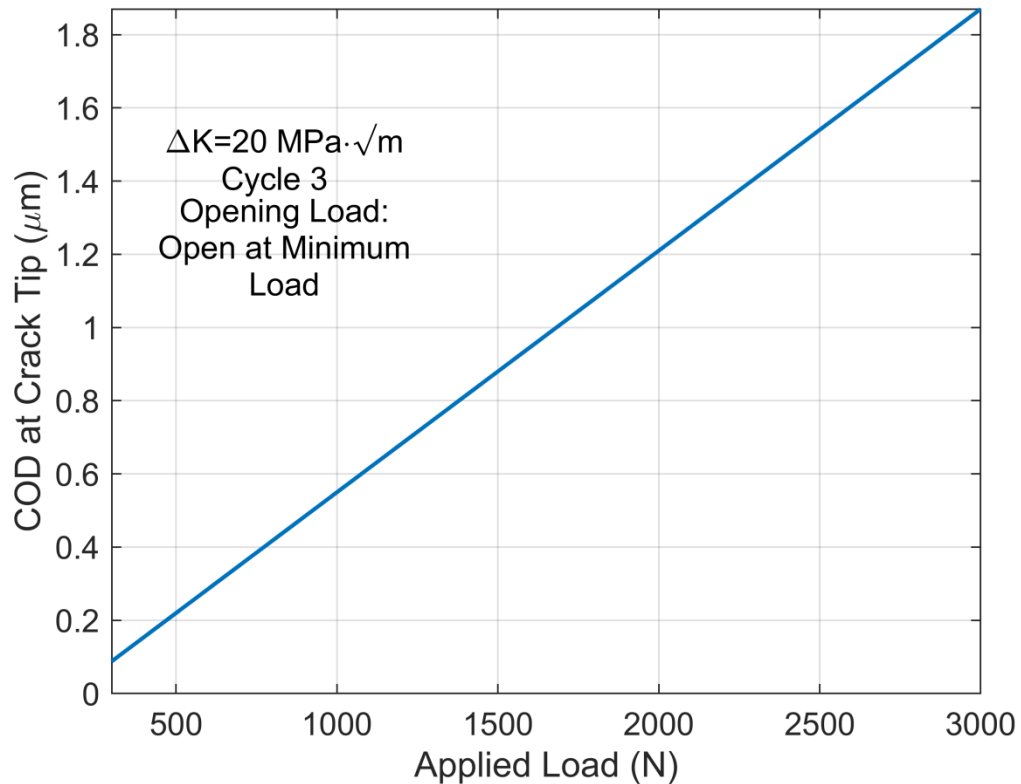


Figure 4.36: Variation of the crack tip opening displacement as a function of applied load during cycle 3.

The COD at the crack tip versus applied load curve for this data, as shown in Figure 4.36, exhibits a nearly linear trend, and it gives the opening load as the minimum load in the cycle. The curve does not even impact the x axis within the loading range of the cycle. The vast difference between values in this data set makes it impossible to identify a valid trend for the opening load from this data. At this point, it is assumed that the wide range of values determined for $\Delta K=20 \text{ MPa}\cdot\sqrt{\text{m}}$ is due to errors in the data collection and analysis process.

Chapter 5. Analysis & Verification

5.1 Compliance Curves

Compliance curves were developed for each ΔK level, and used to verify the opening load values determined by the DAC method. Given that the purpose of this project was to demonstrate that the DAC method is capable of functioning and delivering results independently of existing methods such as the clip gage, these plots were only consulted once the opening load was identified from the DAC data. Before constructing the compliance curves, it is valuable to know the average values for the three core data sets analyzed in this document. These are given in table 5.1 below.

Table 5.1: Identified Opening Loads and Average Opening Loads for all Data Sets at each ΔK Level and for each Loading Cycle. The applied fatigue loading during a cycle varied between approximately $F_{min} = 300$ N and $F_{max} = 3000$ N. The average measured opening loads are presented with 95% confidence level.

Data Set	Cycle 1 Opening Load	Cycle 2 Opening Load	Cycle 3 Opening Load	Average Opening Load
$\Delta K=10$ MPa· \sqrt{m}	1223 N	1265 N	1181 N	1223 N +/- 38.8 (95%)
$\Delta K=15$ MPa· \sqrt{m}	1181 N	1125 N	1055 N	1120.3 N +/- 58.3 (95%)
$\Delta K=20$ MPa· \sqrt{m}	668 N	1219 N	300 N	729 N +/- 427 (95%)

In the following compliance curves, opening load from the clip gage can be determined by identifying the y axis value corresponding to the inflection point in the curve. This generally is difficult to determine exactly, with a range of roughly acceptable values existing over a gradual change in curve direction.

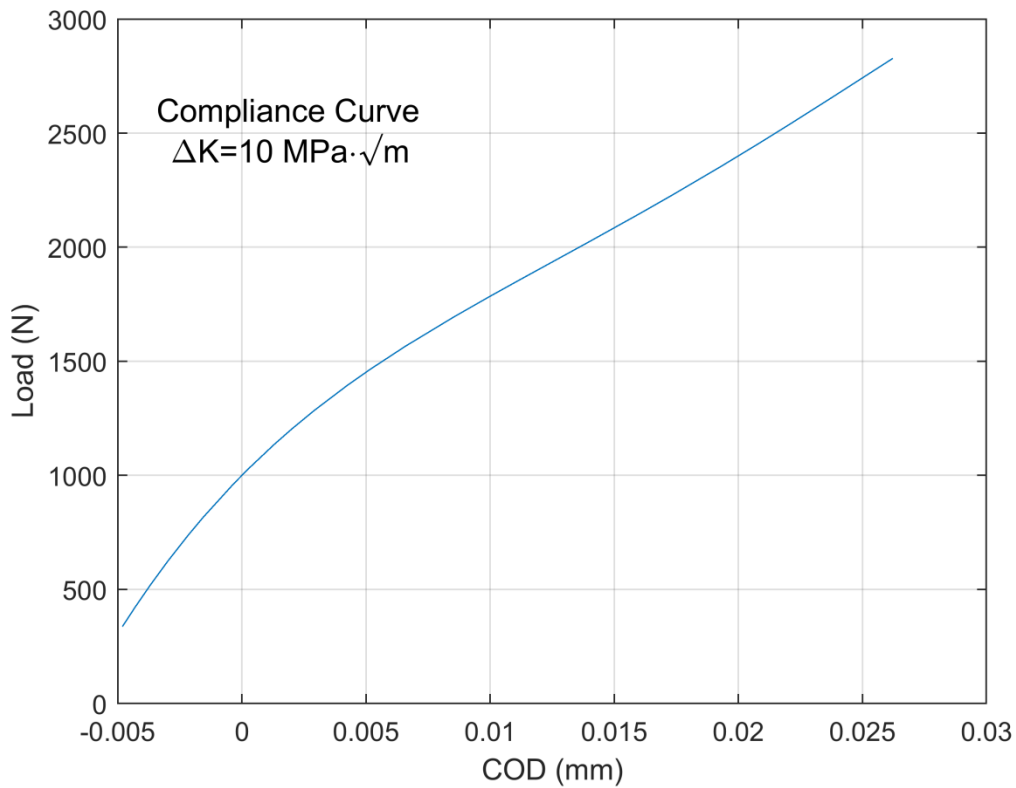


Figure 5.1: Load-displacement compliance curve measured at the load line using a clip gage for $\Delta K = 10 \text{ MPa}\cdot\sqrt{\text{m}}$.

Figure 5.1 shows the evolution of load versus COD measured at the load line using a clip gage. This curve appears to change from a non-linear curve to a linear one in the range between 1100-1400 N. The average opening load value for $\Delta K=10 \text{ MPa}\cdot\sqrt{\text{m}}$ measured with the DAC method according to table 5.1 was $F_{open} = 1223 \text{ N}$, which is within the range given by the clip gage. Therefore, it can be concluded that for this ΔK level, the two methods are similar enough to be in agreement.

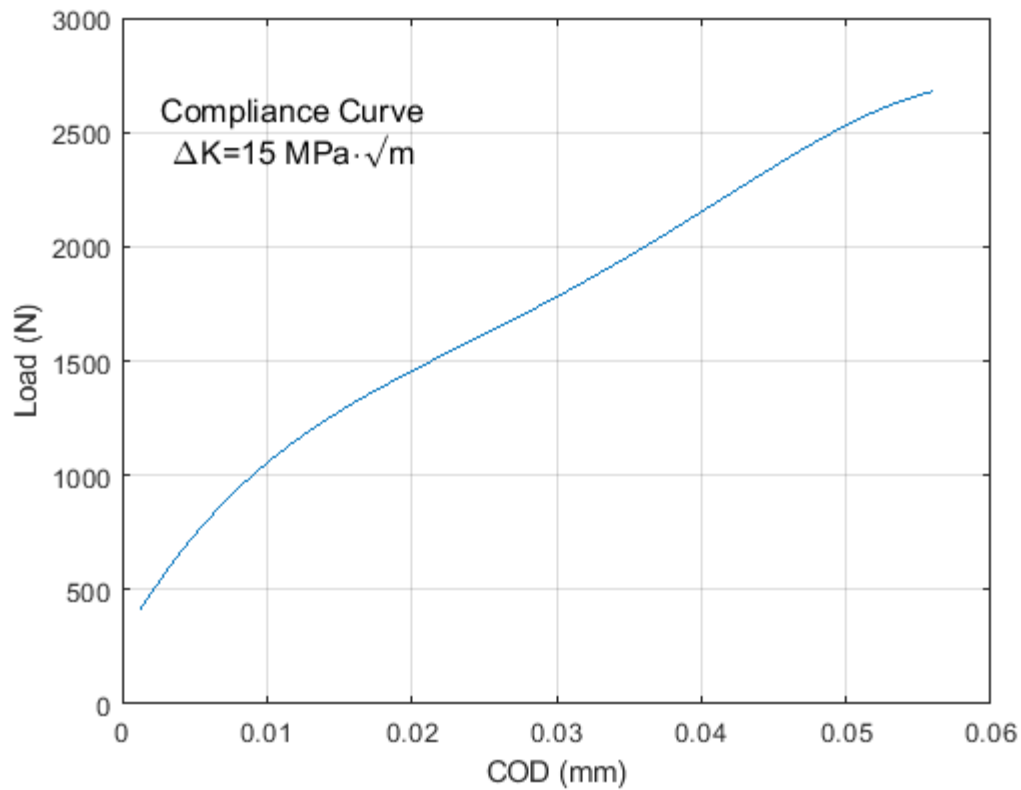


Figure 5.2: Load-displacement compliance curve measured at the load line using a clip gage for $\Delta K = 15 \text{ MPa}\cdot\sqrt{\text{m}}$.

Figure 5.2. shows the evolution of the load versus COD at the load line for $\Delta K = 15 \text{ MPa}\cdot\sqrt{\text{m}}$. The range of acceptable opening values is a bit lower for this compliance curve, at between 1000-1200 N. A more exact approximation is roughly 1137 N. Therefore, the average opening load value in table 5.1 of $F_{open} = 1120.3 \text{ N}$ identified for $\Delta K = 15 \text{ MPa}\cdot\sqrt{\text{m}}$ from the DAC method once again agrees with the clip gage measurement.

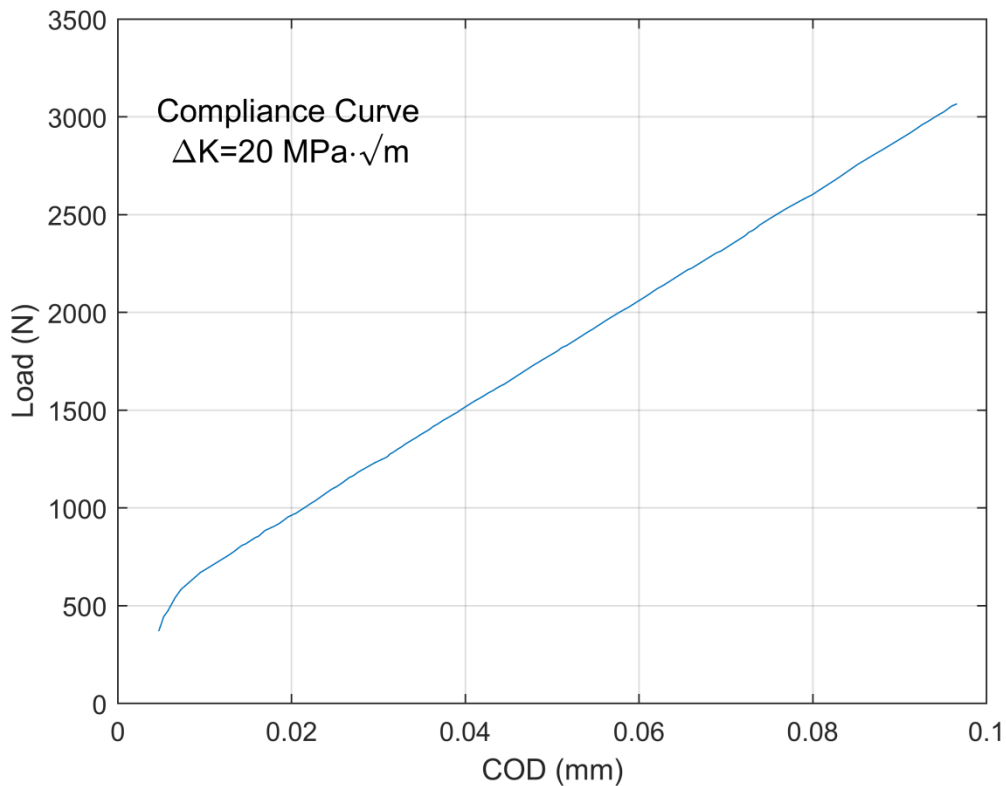


Figure 5.3: Load-displacement compliance curve measured at the load line using a clip gage for $\Delta K = 20 \text{ MPa}\cdot\sqrt{\text{m}}$.

Figure 5.3 shows the evolution of the load versus COD at the load line for $\Delta K = 20 \text{ MPa}\cdot\sqrt{\text{m}}$. As was displayed in the DAC data, the opening load for $\Delta K=20 \text{ MPa}\cdot\sqrt{\text{m}}$ is much lower than that for $\Delta K = 10 \text{ MPa}\cdot\sqrt{\text{m}}$ and $\Delta K = 15 \text{ MPa}\cdot\sqrt{\text{m}}$. The inflection point of this curve appears to be between 600 and 700 N. Closer inspection of the curve gives an approximate value of 670 N. This value is very close to the opening load measured in Cycle 1 at $\Delta K = 20 \text{ MPa}\cdot\sqrt{\text{m}}$, which was recorded at $F_{open} = 668 \text{ N}$. On the other hand Cycles 2 and 3 indicate opening loads varying widely from the opening load measured during Cycle 1 and the value computed with the DAC system.

The variability of opening load values during Cycles 2 and 3 in the $\Delta K=20 \text{ MPa}\cdot\sqrt{\text{m}}$ set means that even though the average is near the range as well, further investigation on the possible sources of error in the measurements for this ΔK level is warranted.

5.2 Method Comparison

Following completion of the $\Delta K=10 \text{ MPa}\cdot\sqrt{\text{m}}$ data set, it was decided that it is important to compare COD at the notch, i.e., load line as given by the DAC method to the displayed value measured by the

clip gage, as well as to an analytical method that uses the assumption that the plastic deformations around the crack tip can be neglected and the specimen behaves fully elastically. Before comparing the results from the three methods, the analytical equations used will be presented.

According to ASTM E2760: Standard Test Method for Measurement of Fatigue Crack Growth Rates [21], Equation 5.1 gives the COD at the load line in the CT specimen.

$$\delta_2 = \frac{P}{E'} V_2(a/b) \quad (5.1)$$

In this equation, used to map COD at the load line, P is the load applied, E' is an adjusted elastic modulus, and $V_2(a/b)$ relates crack length a to the distance from the load line to the far edge of the specimen beyond the crack b . E' is given by Equation 5.2.

$$E' = E/(1 - \nu^2) \quad (5.2)$$

In this equation, E is the known elastic modulus of the material, take as $E = 193.1$ MPa, and ν is the Poisson's ratio taken as $\nu = 0.3$. Finally, $V_2(a/b)$ is given by Equation 5.3.

$$V_2 = \left(\frac{1+a/b}{1-a/b} \right)^2 \left[2.1630 + 12.219(a/b) - 20.065 \left(\frac{a}{b} \right)^2 - 0.9925 \left(\frac{a}{b} \right)^3 + 20.609 \left(\frac{a}{b} \right)^4 - 9.9314(a/b)^5 \right] \quad (5.3)$$

In addition to the analytical approach, data from the clip gage was taken directly from the load frame display, and one cycle of DAC data was performed observing the load line region at both $\Delta K=15$ MPa $\cdot\sqrt{m}$ and $\Delta K=20$ MPa $\cdot\sqrt{m}$. Data from all three sources was superimposed onto a plot for each ΔK condition, shown below.

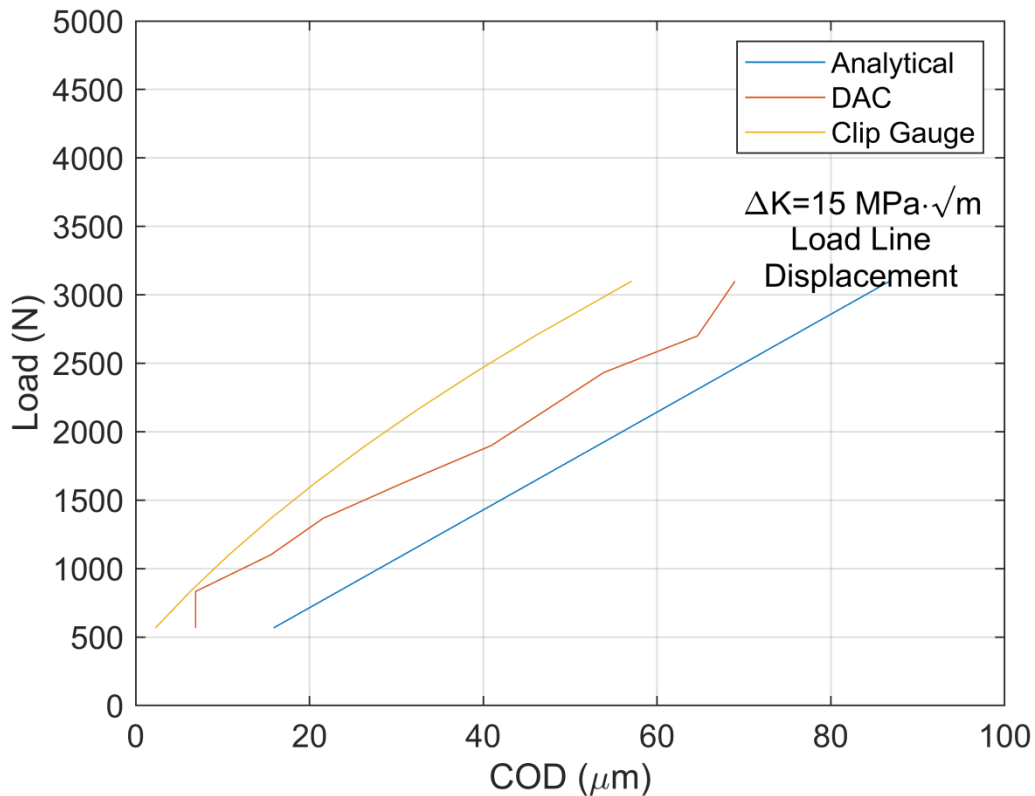


Figure 5.4: Comparison of the compliance curves obtained from the analytical, clip gage, and DAC COD methods for $\Delta K=15 \text{ MPa}\cdot\sqrt{\text{m}}$.

Figure 5.4 shows a comparison of the load versus COD at load line results from the three methods at $\Delta K=15 \text{ MPa}\cdot\sqrt{\text{m}}$. It can be seen in this graph that the DAC data runs in the middle, with the clip gage above, and the analytical method below. However, it initially climbs at a lower rate than either of those, before appearing to begin evening out at the maximum evaluated load of 3100 N. The agreement between the three methods, while not exact is in general satisfactory. This validates the DAC measurement process as viable method of monitoring COD at load line, whenever clip gage measurements are difficult or impossible to perform, such in the case of high temperature crack growth.

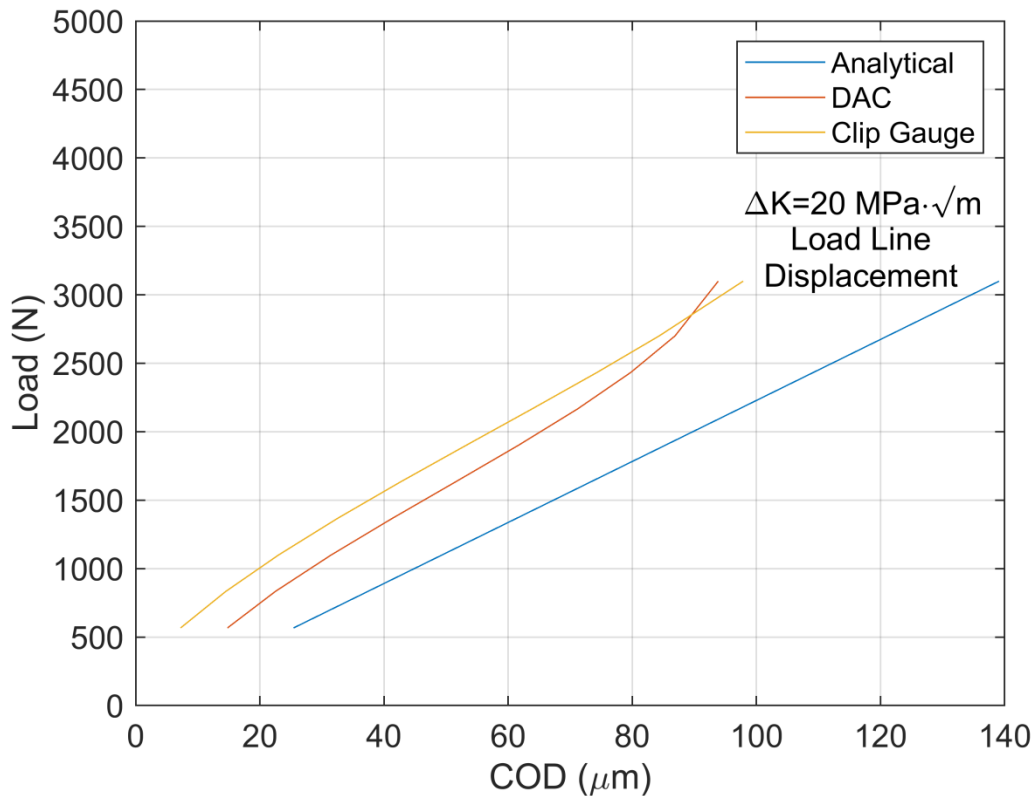


Figure 5.5: Comparison of the compliance curves obtained from the analytical, clip gage, and DAC COD methods for $\Delta K=20 \text{ MPa}\cdot\sqrt{\text{m}}$.

Figure 5.5 shows a comparison of the load versus COD at load line results from the three methods at $\Delta K = 20 \text{ MPa}\cdot\sqrt{\text{m}}$. As in the previous plot, the DAC curve is between the curves obtained using the analytical method and the clip gage measurement. It appears to follow the same approximate slope as that of the clip gage curve for the majority of its run, before beginning to climb toward the end. The consistency of the behavior demonstrated by the DAC method between these two plots, as well as its existence in the middle ground between the two established methods, serves to support its validity.

Chapter 6. Discussion

From the results presented in the previous sections it can be concluded that the DAC method shows great promise in measuring the opening and closing of the crack not only at the load line but also near the crack tip. The method of using the DAC to collect data on fracture development, and using software to analyze the data, has clear applicability not only at room temperature but also in extreme environments, such as high temperature, if visual access to the region of interest in the specimen can be ensured. Therefore, the next research efforts should focus on high temperature data collection. A high temperature clip gage extensometer can be used to gather data, and then that data can be compared to data gathered by a DAC in the same cycles, to identify any differences and determine if the DAC can be considered a more viable method than the clip gage method in such conditions. Of course, work will have to continue on refining and improving the accuracy of the data collection from the DAC method, as more is learned about improving conversion of raw data to plots, and conditions in which images are collected change. For instance, if the window into the furnace necessitates special positioning and settings on the camera to collect quality images, work will need to be done to determine the best solution.

A lot has been learned from the use of this method so far. First and foremost, great care must be taken in analyzing the colored images developed in the DaVis software. A great deal of error in data collection can be removed by spending more analysis time in the software itself. In this stage of the method's use, data was processed in the software, and then extracted and processed visually elsewhere. After data was collected for this project, the author learned that the software can deliver exact displacement values for a given cursor location on a processed image in the software. It is recommended that future data sets are built in the lab with the software itself, for improved accuracy. In this way, not only could more accurate data be developed along the full length of the fracture, but minute differences in displacement from point to point along a smaller, critical area of interest could be mapped. The significance of the increase in accuracy and reliability of data extraction by this change in method cannot be overstated; data points should be pulled directly from the software whenever possible.

When it comes to the actual image collection method, the consistency of the process would benefit from a lower cycle frequency. While the test used in this research was run at a frequency of 0.1 Hz as a compromise between loading too fast to control at high frequency and too slow such that it would have generated an enormous amount of images, it seems that lowering the frequency, perhaps to

0.05 Hz to start with, would be worth the increased processing time in exchange for improved accuracy of the method. This could become especially important as more variables are introduced to the data collection process, such as high temperature testing and the resulting need to work around a furnace.

Finally, it seems that it is more reliable to focus on just the crack tip region when identifying opening load values. Mapping a given point's opening displacement against load applied allows for the more precise determination of opening load for any given point along the crack plane, rather than just a range of potential values in which the load should exist. The realization that a focused area of the crack plane region could be mapped by pulling data with minute differences from the software directly could come into play for the purpose of focusing on the crack tip. Instead of just looking at a single point at the end of the fracture, a cluster of points surrounding that point could be mapped, and an even clearer picture of the crack tip throughout the cycle could be developed, allowing for more accurate assessment of opening load and even potentially development of the fracture beyond what can be seen clearly on the data set.

The measurements at $\Delta K=20$ MPa $\cdot\sqrt{m}$ produced some inconsistent results. The variability of these values should be further investigated for large ΔK values. It is important to remember that the primary goal of this project was to develop a DAC method and begin the process of establishing it as a method for tracking fracture data in future experiments. $\Delta K=10$ MPa $\cdot\sqrt{m}$ was the first set of data, and as much as it appeared more rough than later sets, it delivered viable results, and laid the groundwork for $\Delta K=15$ MPa $\cdot\sqrt{m}$. Measurements at $\Delta K=15$ MPa $\cdot\sqrt{m}$ delivered even better results, with opening loads coming out in agreement with expected trends in more ways than one. However, measurements at $\Delta K=20$ MPa $\cdot\sqrt{m}$, even though benefited from the foundation laid out by the previous data sets, produced some variability in results. It is likely that this is due to where the specimen was in its lifespan at that point, with the crack substantially through the specimen.

While there is value in speculating as to why $\Delta K=20$ MPa $\cdot\sqrt{m}$ didn't work out, more value can be found in directing that energy a bit further and trying to identify solutions. Two ideas come to mind toward this end. First, lowering cycle frequency would allow for greater care to be taken at advanced crack stages. More data would be collected for each cycle, and more control could be exerted on the collection process with a slower climb to maximum load. The second idea should be considered a last resort, as it would limit the potential of the method: it may turn out that the method simply works

better at lower ΔK values. However, more data should be collected at higher values and efforts should be made to improve the data collection process at higher ΔK values.

Chapter 7. Conclusion

In conclusion, the DAC method described in this document has the potential to solve the stated problem of unreliable data collection in extreme conditions. It has been demonstrated that the method can produce data which delivers information about the fracture development that is in agreement with known and reliable room temperature methods. Results collected were generally in agreement with the known tendency of opening load to decrease with increasing ΔK values, and average opening load values for the $\Delta K=10$ MPa $\cdot\sqrt{m}$ and $\Delta K=15$ MPa $\cdot\sqrt{m}$ data sets were similar to those identified on the corresponding compliance curves. Given the non-invasive nature of the data collection method, and therefore the unchanged functionality of the system in unusual testing conditions, it is concluded that the method can be used to develop similarly reliable results for more extreme experiments, such as high temperature tests. Next, a summary of possible future work is presented. First, the DaVis software is capable of delivering displacement data with much higher precision and reliability than was capable with the visual observation of processed images in this project. In addition to the use of precise displacement reporting in the software itself, it is also possible to export data from the software into a text file, allowing for an extremely well developed data set that can be utilized in Matlab code or other programs to generate plots and perform analysis. Additionally, with a more detailed set of data points, more attention can be paid to minute changes at the crack tip, allowing better mapping of crack development beyond the observed crack front, as well as improved analysis of opening load values. Another adjustment to the method that has been discussed is the averaging of values from each cycle. It is known that from cycle to cycle within each ΔK data set, the crack should not change to an extent that would impact results, and therefore each cycle should be very similar if not identical to the others in its data set. Therefore, it has been proposed that cycle displacement values should be averaged in future data sets, creating a unified set of plots across multiple cycles. From the averaged displacement values, key information such as data set opening load can be identified. In this way, variability in data sets can be eliminated, and a clearer picture of crack behavior can be developed. While averaging the displacement data may help with the issue of unusual opening load plot shapes, more work should be done to confirm that there is not an error in the method that produces such questionably curve shapes. Also, on the list of future work is a thorough uncertainty analysis of the method. While it does not seem feasible to develop a solid uncertainty analysis with only one specimen, it is recognized that such an analysis needs to be performed for this method to be reliably used to measure crack opening. To that end, another specimen should be tested under conditions identical to those used in this project, to ensure

repeatability of results, further refinement of the method, and help in building an understanding of method uncertainty. Future work with this method should include high temperature testing, to capitalize on the non-invasive nature of the method, as well as Creep-Fatigue Crack Growth testing and testing with different R ratios. Given its apparent potential for reliability, its application in difficult test environments, and its high potential for further development and improvement of results, it is recommended that this method be further pursued, toward the ultimate goal of improving the body of research surrounding crack growth.

References

- [1] A.T. Anderson, C.K. Michlovitz, & K. Hug. "Apollo 11 Lunar Photography." National Space Science Data Center, 1970.
- [2] "Data Acquisition & Cameras." University of Virginia School of Engineering and Applied Science. University of Virginia, 21 June, 2019. Web.
- [3] Min-ki Park & Soo-won Kim. "Development of an image data acquisition system using a multi-function front camera for automotive applications." 2015 International Symposium on Consumer Electronics (ISCE), Madrid, 2015, pp. 1-2, doi: 10.1109/ISCE.2015.7177812.
- [4] O.G. Philip, W.D. Schmidl, & Y.A. Hassan. "Development of a high speed particle image velocimetry technique using fluorescent tracers to study steam bubble collapse." Nuclear Engineering and Design, vol. 149, no. 1-3, pp. 375-385, 1994.
- [5] Serope Kalpakjian & Steven R. Schmid. Manufacturing Processes for Engineering Materials. 6th ed. N.p.: Pearson, 2017. pp. 118, 202-203.
- [6] Martin Taylor, Jose Ramirez, Indrajit Charit, Gabriel P. Potirniche, Robert Stephens, & Michael V. Galzoff. "Creep Behavior of Alloy 709 at 700°C." University of Idaho
- [7] Sam Sham. "Advanced Reactor Concepts Program ARC Materials Development - Accomplishments and Plans." Argonne National Laboratory, 2013.
- [8] Nippon Steel data sheet NF709, Nippon Steel Sumitomo Met. Corp., 2013.
- [9] Arturo Rojas. "Sodium-Cooled Fast Reactors as a Generation IV Nuclear Reactor." Stanford University. May 2018.
- [10] Jaewoon Yoo, Jinwook Chang, Jae-Yong Lim, Jin-Sik Cheon, Tae-Ho Lee, Sung Kyun Kim, Kwi Lim Lee, & Hyung-Kook Joo. "Overall System Description and Safety Characteristics of Prototype Gen IV Sodium Cooled Fast Reactor in Korea." Nuclear Engineering and Technology, 2016.
- [11] Nicholas Shaber, Robert Stephens, Jose Ramirez, Gabriel P. Potirniche, Martin Taylor, Indrajit Charit, & H. Pugesek. "Fatigue and Creep-Fatigue Crack Growth in Alloy 709 at Elevated Temperatures." University of Idaho

- [12] ASTM 1290: Test Method for determining Critical Crack Tip opening displacement (CTOD) from which the linear elastic fracture toughness (K_{IC}) can be determined
- [13] ASTM E647: Standard Test Method for Measurement of Fatigue Crack Growth Rates
- [14] PC Paris & F. Erdogan. "A critical analysis of crack propagation laws." *J. BasicEng-T ASME* 1963;85:528–33.
- [15] ASTM E1820: Standard Test Method for Measurement of Fracture Toughness
- [16] Jonathan A. Salem & Louis J. Ghosn. "Back-Face Strain for Monitoring Stable Crack Extension in Precracked Flexure Specimens." NASA, Glenn Research Center, 2010.
- [17] Omar Hatamleh, Royce Forman, Venkataraman Shivakumar, & Jed Lyons. "Strip Yield model Numerical Application to Different Geometries and Loading Conditions." NASA.
- [18] Gabriel P. Potirniche. "A closure model for predicting crack growth under creep-fatigue loading." *International Journal of Fatigue*, 2019.
- [19] Jose Ramirez, Gabriel P. Potirniche, Nicholas Shaber, Martin Taylor, H. Pugeseck, Robert Stephens, & Indrajit Charit. "The influence of plasticity induced crack closure on creep-fatigue crack growth in two heat resistant steels." *International Journal of Fatigue*, 2019
- [20] Hiroshi Tada, Paul Croce Paris, & George Rankin Irwin. *The Stress Analysis of Cracks Handbook*. 3rd ed. New York: ASME, 2000.
- [21] ASTM E2760: Standard Test Method for Measurement of Fatigue Crack Growth Rates
- [22] Ralph I. Stephens, Ali Fatemi, Robert R. Stephens, Henry O. Fuchs. *Metal Fatigue in Engineering*. 2nd ed., Wiley, 2001.